The Thesis Committee for Kyle William Meyer
Certifies that this is the approved version of the following thesis:

New insights into the carbon isotope composition of speleothem calcite: An assessment from surface to subsurface

APPROVED BY
SUPERVISING COMMITTEE:

Supervisor: _____
Daniel O. Breecker

Co-Supervisor: _____
Jay L. Banner

_____
MaryLynn Musgrove

New insights into the carbon isotope composition of speleothem calcite: An assessment from surface to subsurface

by

Kyle William Meyer, B.S.

Thesis

Presented to the Faculty of the Graduate School of

The University of Texas at Austin

in Partial Fulfillment

of the Requirements

for the Degree of

Master of Science in Geological Sciences

The University of Texas at Austin

May, 2012

Acknowledgements

I would like to acknowledge the tireless efforts of my advisors Dr. Daniel Breecker and Dr. Jay Banner and for their exceptional tutelage and guidance. I extend my gratitude to the management and staff at Inner Space Cavern and Natural Bridge Caverns for their consistent generosity and helpfulness. This research would not be possible without the assistance of my peers and fellow research group members both in the field and in the lab for their myriad contributions.

I want to provide my esteemed thanks to the faculty, staff, and students of the Jackson School of Geosciences and the University of Texas as a whole. I am humbled beyond words at the investment this institution has provided in terms of my education, personal development, and my future.

Lastly, I would like to thank my immediate family: My mother, father, and brother for supporting me in all things, including the decision to apply to and ultimately enroll in the University of Texas. I never thought I'd be fortunate enough to make it this far, and there isn't a day where I'm not thankful for the opportunity.

Abstract

New insights into the carbon isotope composition of speleothem calcite: An assessment from surface to subsurface

Kyle William Meyer, M.S. Geo. Sci.

The University of Texas at Austin, 2012

Supervisors: Daniel O. Breecker and Jay L. Banner

The purpose of this study was to provide new insights into the interpretation of speleothem (cave calcite deposit) $\delta^{13}C$ values. We studied two caves in central Texas, which have been actively monitored for over 12 years. We compared $\delta^{13}C$ values of soil CO_2 ($\delta^{13}C_s$), cave drip water ($\delta^{13}C_{DIC}$), and modern cave calcite ($\delta^{13}C_{cc}$). Measured average $\delta^{13}C$ values of soil CO_2 were -13.9 ± 1.4‰ under mixed, shallowly-rooted C_3-C_4 grasses and were -18.3 ± 0.7‰ under deeply-rooted ashe juniper trees (C_3). The $\delta^{13}C_{DIC}$ value of minimally-degassed drip water in Natural Bridge Caverns was -10.7 ± 0.3‰. The carbon isotope composition of CO_2 in equilibrium with this measured drip water is -18.1 ± 0.3‰. The agreement between juniper soil CO_2 and drip water (within ~0.2‰) suggests that the $\delta^{13}C$ value of drip water ($\delta^{13}C_{DIC}$) that initially enters the cave is controlled by deeply-rooted plants and may be minimally influenced by host-rock dissolution and/or prior calcite precipitation (PCP). At Inner Space Caverns, $\delta^{13}C_{DIC}$

values varied with vegetation above the drip site, distance from the cave entrance, and distance along in-cave flow paths.

Whereas CO_2 derived from deeply-rooted plants defines the baseline for drip water $\delta^{13}C_{DIC}$ entering the caves, kinetic effects associated with the degassing of CO_2 and simultaneous precipitation of calcite account for seasonal variability in $\delta^{13}C_{DIC}$ and $\delta^{13}C_{cc}$. We documented increases in $\delta^{13}C_{DIC}$ at a rate of up to 0.47‰/hour during the season of peak degassing (winter), suggesting that $\delta^{13}C_{DIC}$ variations may be controlled by total elapsed time of CO_2 degassing from drip water (T_{total}). We also observed seasonal shifts in the $\delta^{13}C$ values of modern calcite grown on glass substrates that are correlated with shifts in drip water $\delta^{13}C_{DIC}$ values and drip-rate. Therefore, we suggest that increased aridity at the surface above a given cave results in, slower drip-rates, higher $T_{total,}$ and therefore higher $\delta^{13}C_{DIC}$ values.

We propose that large variability (>2‰) in speleothem $\delta^{13}C_{cc}$ values dominantly reflect major vegetation changes, and/or increasing T_{total} by slowing drip-rates. Based on these findings, variability in speleothem carbon isotope records may serve as a proxy for paleoaridity and/or paleovegetation change.

Table of Contents

List of Tables

List of Figures

CHAPTER 1. OVERVIEW OF STABLE ISOTOPE GEOCHEMISTRY AS APPLIED TO SPELEOTHEM CALCITE AND PALEOCLIMATIC RECONSTRUCTION

1.1: INTRODUCTION

Speleothems (i.e., cave calcite deposits) serve as unique terrestrial proxy records of paleoenvironmental and paleoclimatic conditions (McDermott, 2004; Fairchild et al., 2006). Hendy and Wilson (1968) first evaluated the potential of speleothems to preserve relevant climatic information in the form of stable isotope ratios of oxygen ($\delta^{18}O$). With the development of uranium-series dating methods (Rosholt and Antal, 1962; Thompson, 1973; Edwards et al., 1986; Gascoyne, 1992; Musgrove et al., 2001; Richards and Dorale, 2003) researchers have been able to develop precise chronological constraints on changes of $\delta^{18}O$ values through time. Since then, variations in $\delta^{18}O$ values of speleothem calcite have shown highly-correlated relationships with other paleoclimate proxy records in depicting Heinrich events (Bar-Matthews et al., 1999), East-Asian monsoon intensity (Wang et al., 2001), and connections to marine isotope (Bar-Matthews et al., 2003) and ice-core records (Wang et al., 2001; Wang et al., 2008). In general, speleothem $\delta^{18}O$ values are controlled by the isotopic composition and temperature of the water entering a cave, with the possibility of influence from kinetic isotope effects (Hendy and Wilson, 1968; Hendy, 1971; Mickler et al., 2004, 2006).

In addition to the use of $\delta^{18}O$ values, numerous studies have sought to use carbon isotope ratios of speleothem calcite ($\delta^{13}C_{cc}$) to perform paleoclimate reconstructions. The interpretations of $\delta^{13}C_{cc}$ values are myriad, complex, and often region- or case-specific. Prominent examples of proposed mechanisms for the variability of speleothem calcite $\delta^{13}C$ values include: changes in

the $\delta^{13}C$ value of atmospheric CO_2 (Baskaran and Krishnamurthy, 1993), shifts in the relative proportions of C_3 and C_4 vegetation above caves (Dorale et al., 1992; Dorale et al., 1998), and changes in soil and vegetation productivity driven by changes in temperature and precipitation (Genty et al., 2006), and kinetic effects (Mickler et al., 2004; Spötl et al., 2005; Mickler et al., 2006).

The objective of this study is to better determine the factors that control the $\delta^{13}C$ values of speleothem calcite. We have taken a two-phase approach: (1) investigate soil and epikarst processes that influence the $\delta^{13}C$ value of dissolved inorganic carbon (DIC) in water before it enters caves and (2) assess processes occurring within the caves that influence the $\delta^{13}C$ value of drip water DIC and calcite.

1.2: Background

1.2.1 The formation of karst landscapes and the role of carbon

Cave development and karst formation arises from the dissolution of soluble host-rock (most commonly limestone). Palmer (1991) detailed the various possible mechanisms and resultant morphologies governing cave formation and speleogenesis. In this study, we are most concerned with late-stage speleogenesis, which is controlled by processes associated with vadose groundwater. This water is most often of meteoric origin and may be sourced proximally as precipitation, or distally and then transported to the cave via surface flow (e.g. large runoff events into the cave entrance) or as groundwater. This source water then travels through the soil horizon, into the epikarst (a highly weathered/fractured portion of the host-rock), the host-rock, and into caves (Figure 1). Fairchild et al. (2006) combined these zones into the dissolution region and the precipitation region. The dissolution region constitutes the soil horizon, epikarst, and

host-rock. This region is also where CO_2 is respired in the soil by plants and microbial communities, resulting in pCO_2 that is significantly higher than atmospheric levels (often in the range of several thousand ppmv). This respired CO_2 is dissolves in water travelling through the subsurface and speciates into DIC according to equations for carbonate equilibria as follows:

$$CO_{2\,(g)} \leftrightarrow CO_{2\,(aq)} \quad (1)$$
$$CO_{2\,(aq)} \leftrightarrow H_2CO_{3\,(aq)} \quad (2)$$
$$H_2CO_{3\,(aq)} \leftrightarrow HCO_3^-{}_{(aq)} \quad (3)$$
$$HCO_3^-{}_{(aq)} \leftrightarrow CO_3^{2-}{}_{(aq)} \quad (4)$$

where the production of carbonic acid (H_2CO_3) is chiefly responsible for lowering the pH of the groundwater in contact with the host-rock and therefore driving dissolution. The dissolution of host limestone increases concentrations of Ca^{2+}, Mg^{2+}, Sr^{2+} and other trace ions in solution. Water is transported by matrix, fracture, or conduit flow to open cavities in the subsurface. Matrix flow travels through the pore-spaces of the host-rock, fracture flow occurs in fractures that are typically a result of physical strain on the host-rock, and conduit flow represents the largest pore space aperture size, which forms by solution-enchancement (Atkinson, 1977; White and White, 2005). The precipitation region is defined by the entrance of vadose water into any void space within the subsurface with a lower pCO_2 than the epikarst, and where precipitation of the mineral calcite ($CaCO_3$) occurs by the reaction:

$$Ca^{2+} + 2HCO_3^- \leftrightarrow CaCO_{3\,(s)} + CO_{2\,(g)} + H_2O_{\,(aq)} \quad (5)$$

which is driven to the right by degassing of CO_2 from solution (Le Châtelier's principle). This process allows for various morphologies of calcite formation throughout the precipitation region

including: soda straws, flowstones, stalactites and stalagmites. Fairchild et al. (2006) summarized the approaches to evaluating geochemical information derived from each of these features and the complications that can arise from varying growth styles and geometries.

1.2.2. Surface and shallow-subsurface processes: Soil horizon through the epikarst

CO_2 concentrations typically increase with depth in a soil profile. CO_2 in the soil horizon represents a mixture between CO_2 from the atmosphere, plant-respiration, and SOM decomposition where each of these components exhibit a range of carbon isotope values. We must address each of these three CO_2 sources and how they influence the carbon isotope composition of soil CO_2 ($\delta^{13}C_s$). Starting with plant-respiration, plants follow one of three distinct photosynthetic pathways (C_3, C_4, and CAM) which controls the range of $\delta^{13}C$ values observed in its tissues and respired CO_2 (Farquhar et al., 1989; Ehleringer and Monson, 1993). Each pathway is named for the resulting acid first produced by the initial carboxylation reaction of photosynthesis, where C_3 vegetation produces a 3-carbon acid and C_4 and CAM vegetation produces a 4-carbon acid (Ehleringer and Monson, 1993). The typical range of carbon isotope values of C_3 plants is between -21‰ and -35‰, C_4 plants commonly exhibit compositions between -9‰ and -20‰, and CAM plants exist between these two ranges (Badeck et al., 2005). We should note that the $\delta^{13}C$ values of tissues from a given species of plant (and the respired CO_2 from each of these tissues) vary and follow distinct trends from leaves to roots (Figure 2; Badeck et al., 2005; Bowling et al., 2008; Wingate et al., 2010). In the soil horizon, we are most concerned with respired CO_2 from root tissues which is generally ~4‰ lower than the $\delta^{13}C$ value of the roots themselves (Bowling et al., 2008). Breecker et al. (submitted) have determined that

deeply-rooted C_3 vegetation strongly biases the CO_2 that enters the caves we studied and that this CO_2 is transported into the cave dominantly in the gas phase.

We can now turn to processes involving the decomposition of SOM. Plant litter (dead, largely undecayed plant matter), SOM, and humus (SOM that is considered fully-decomposed) follow a general trend of increasing $\delta^{13}C$ values with depth (Figure 2; Jessup et al., 2003; Crow et al., 2006; Boström et al., 2007). Respired CO_2 from SOM decomposition follows an identical trend, but with even higher $\delta^{13}C$ values than the bulk SOM (Boström et al., 2007). The offset between the carbon isotope composition of 'microbially-respired' CO_2 and SOM is consistent with similar offsets in complex, large-body organisms between tissues and respired CO_2 (Ayliffe et al., 2004). Ultimately, the initial decomposition of plant litter and recent SOM should commonly result in CO_2 isotopically similar to root respiration. With increasing depth, CO_2 $\delta^{13}C$ values from SOM decomposition should be significantly higher than values from shallower in the same profile.

While it is clear that soil-respired CO_2 represents contributions from both plant root-respiration (autotrophic) and the decomposition of SOM (heterotrophic), efforts to determine the proportion of these two contributions have been varied in approach and success. Most studies are concerned with a surficial assessment of soil-respired CO_2 with the goal of better defining fluxes in global carbon cycling (Hanson, 2000; Sulzman et al., 2005; Trombore et al., 2006; Davidson and Janssens, 2006). These studies acknowledge that the proportion of these two contributions vary seasonally and regionally, with soil-respired CO_2 being composed of anywhere between 10% - 90% root respiration (in some cases >90%; mean values include 45.8% for forest vegetation and 60.4% for non-forest vegetation; Hanson, 2000; Sulzman et al., 2005).

We must also consider the effect of mixing from atmospheric CO_2 on the carbon isotope composition of soil CO_2. This effect is described by an endmember mixing model between soil-respired CO_2 and atmospheric CO_2 (Figure 3; Cerling, 1984; Cerling et al., 1991; Amundson et al., 1998). The $\delta^{13}C$ value of respired CO_2 can be calculated by substracting 4.4‰ (a constant that arises from the contrasting diffusivities of $^{13}CO_2$ and $^{12}CO_2$) from the y-intercept of this plot (Cerling et al., 1991; Amundson et al., 1998). When we calculate $\delta^{13}C_r$ for a single measurement, the diffusion constant can be larger than 4.4‰ (particularly at pCO_2 < 1000 ppmv), which is determined by diffusion modeling with known soil CO_2 concentrations (Cerling, 1984; Cerling et al., 1991; Davidson, 1995; Amundson et al., 1998).

1.2.3. Sub-surface processes and associated geochemical evolution: epikarst to calcite precipitation

Groundwater becomes progressively more acidic with increasing *p*CO2. This acidity allows for the dissolution of limestone ($CaCO_3$) host-rock into its constituent ions Ca^{2+} and CO_3^{2-}. The incorporation of host-rock carbonate (CO_3^{2-}) into solution has been previously proposed to contribute to the carbon isotope composition of DIC ($\delta^{13}C_{DIC}$; Hendy, 1971; Fairchild 2006). The average carbon isotope composition of marine carbonates is between -2‰ and 8‰ (Veizer et al., 1999). These high $\delta^{13}C$ values are problematic for speleothem climatic interpretations, because they have potential to significantly influence the $\delta^{13}C$ value of DIC that has equilibrated with soil CO_2. Hendy and Wilson (1968) reported that the average contribution from the host-rock is between 30% - 50% (though not exceeding 50%; Hendy, 1971) as determined by radiocarbon (^{14}C) analyses of cave water. We can gauge the degree of host-rock contribution to drip water by evaluating the percent modern carbon (pMC) of a groundwater or

drip water sample. Whereas measuring drip water provides constraints on host-rock contributions in a modern setting, we hypothesize that using simultaneous U-series and ^{14}C dating may allow for an assessment of host-rock contributions in speleothem calcite less than 35 ka. Discrepancies where the ^{14}C-age is significantly older than an age determined by U-series methods may suggest that significant host-rock carbon was present in the drip water DIC at the time of speleothem formation. However, we must also consider the exchange of CO_2 produced in the soil horizon and epikarst with water in the subsurface. An open system allows for complete exchange between continually renewed soil-respired CO_2 and the groundwater in the epikarst which would overwhelm the $\delta^{13}C$ signal from the host-rock (Hendy, 1971; Fairchild 2006). We should also note that the oxidation of old OM in the soil horizon has been observed to 'dampen' drip water pMC (Genty et al., 1998).

Perhaps the most significant factor controlling the carbon isotope composition of groundwater and/or drip water is the kinetic isotope effect from rapid and continued degassing of CO_2. It is acknowledged that in temperate and subtropical caves the gradient between the pCO_2 of drip water and cave-air varies seasonally, also resulting in seasonal variations in the rate of calcite precipitation (Spötl et al., 2005; Guilfoyle, 2006; Banner et al., 2007; Mattey et al., 2010; Frisia et al., 2011; Tremaine et al.; 2011). It is generally observed that cave-air (and drip water) temperatures remain relatively constant throughout the year (due to insulation by the host-rock), whereas surface temperatures fluctuate over seasonal timescales (Spötl et al., 2005; Banner et al., 2007). Commonly, in the summer, surface air temperatures are high relative to temperatures within the cave, and surface air and cave-air are subject to little mixing. During the winter surface temperatures are low relative to cave-air temperatures and the cave undergoes density-

driven ventilation by surface air of relatively low pCO_2. Other factors such as the cave morphology, passage tortuosity, and entrance position/orientation can also affect the magnitude and duration of ventilation. Ventilation promotes a high rate of degassing and a concomitantly high rate of calcite precipitation (Banner et al., 2007). However, rapid degassing is acknowledged to kinetically fractionate carbon isotopes, whereby $^{12}CO_2$ preferentially escapes from solution relative to $^{13}CO_2$ (Hendy, 1971; Mickler et al., 2004; Guilfoyle, 2006; Spötl et al., 2005; Mickler et al., 2006; Fairchild et al., 2006; Polag et al, 2010; Lambert and Aharon, 2011). Guilfoyle (2006) conducted a number of studies on collected drip water and modern calcite samples from the caves in this study. Guilfoyle (2006) identified kinetic isotope effects in measured $\delta^{18}O$ and $\delta^{13}C$ values in both cave drip water and calcite, which interpreted as the result of rapid degassing of CO_2 from solution. Mickler et al. (2004) also identified kinetic isotope effects based on measured $\delta^{18}O$ and $\delta^{13}C$ values of modern calcite samples precipitated on glass substrates. They modeled carbon isotope evolution by the process of continued degassing from drip water and the simultaneous precipitation of calcite as a Rayleigh distillation process.

From the model of Mickler et al. (2004), we can demonstrate that along a continuous flow-path calcite that is precipitated at later intervals will be progressively enriched with respect to ^{13}C as a consequence of the light fraction of carbon being selectively degassed from the remaining DIC pool. However, the continued precipitation of calcite under equilibrium conditions would be expected to preferentially remove more ^{13}C as opposed to ^{12}C from solution and should result in progressively lower $\delta^{13}C_{DIC}$ down the flow path. This process is referred to as prior calcite precipitation (PCP). Any void space or region in the epikarst that groundwater or

drip water is able to degas into allows for PCP and carbon isotope evolution, therefore, it is critical to quantify this influence at the first entry of water to the cave. Studies of trace element ratios of various cations (Mg^{2+}/Ca^{2+}, Sr^{2+}/Ca^{2+}, Ba^{2+}/Ca^{2+}) that commonly form carbonate minerals have allowed for quantification and interpretations of PCP (Fairchild et al., 2000; Wong et al., 2011; Sinclair, 2011; Sinclair et al., 2011). Whereas there are a number of factors that can ultimately affect these trace element ratios, PCP is generally documented when covariation of these ratios is observed (particularly between Mg^{2+}/Ca^{2+} and Sr^{2+}/Ca^{2+}). Precipitation of calcite will first selectively remove Ca^{2+} from solution, resulting in elevated trace element ratios in solution and subsequently precipitated calcite (Fairchild et al., 2000; Wong et al., 2011; Sinclair, 2011; Sinclair et al., 2011). Therefore, we would expect rapid degassing and calcite precipitation to produce highly-correlated changes in trace element ratios and carbon isotope ratios over seasonal timescales. This hypothesis still needs to be explored, and we hope to address this at a later time.

A final consideration for carbon isotope variability involves the equilibrium carbon isotope fractionations between CO_2 gas, DIC species, and calcite. Vogel et al. (1970) first determined the temperature sensitivity of the equilibrium carbon isotope fractionation between $CO_{2(g)}$ and $HCO_3^-{}_{(aq)}$. The fractionation factor was later refined by additional experimental results (Mook et al., 1974; Zhang et al., 1995). For example, for a solution at 25˚C, the fractionation between $CO_{2(g)}$ and $HCO_3^-{}_{(aq)}$ is 7.23‰ and increases to 10.02‰ at 5˚C (Zhang et al., 1995). The equilibrium isotope fractionation between $HCO_3^-{}_{(aq)}$ and $CaCO_{3(s)}$ is not as well-constrained and has had numerous experimental approaches to determine its nature. Romanek et al. (1992) described the HCO_3^- - $CaCO_3$ fractionation as invariant with temperature and fixed at 1‰,

however, recent work suggests that the fractionation factor may indeed be temperature-sensitive (Figure 4; Polag et al., 2010).

1.2.4. Geologic and hydrologic setting of the Edwards Plateau

We conducted this study in and above two commercially-developed show caves of central Texas: Inner Space Cavern and Natural Bridge Caverns. Both caves are situated at the intersection of the prominent Balcones Fault Zone (BFZ) and the Edwards Plateau (Maclay and Small, 1983; Dorsey and Slagle, 1987; Hanson and Small, 1994; Small et al., 1996). The BFZ consists of dominantly NE-SW trending, high-angle normal faults believed to be generated by sediment loading along the Texas coastal plains. This region also defines the extent of the Edwards aquifer and its recharge zone (particularly where faults and fractures in the Edwards Limestone are surficially expressed, allowing for direct communication of surface flow into the aquifer), one of the most productive karst aquifers in the country (Hanson and Small, 1994; Small et al., 1996).

Inner Space Cavern (IS) is located approximately 2 miles south of Georgetown, Texas adjacent to Interstate Highway 35 (I-35). The cave is 4,851 m in total surveyed length, and 24 m at its deepest point (Elliot and Veni, 1994). The cave spans several members of the Edwards Group, which is characterized primarily by Cretaceous limestones as well as dolomites, mudstones, shales, and marls of the Kainer and Person Formations (Figure 5; Maclay and Small, 1983; Dorsey and Slagle, 1987; Elliot and Veni, 1994; Small et al., 1996). The Edwards Group and the Georgetown Formation represent the primary hydrologic units of the Edwards aquifer (Small et al., 1996). In one chamber that is prone to very high pCO_2 seasonally (>1.5%), a fan has been installed to provide artificial ventilation, but is rarely used. Study sites included in-cave

sites (Figure 6) and corresponding surface sites with installed soil gas wells proximal to specific vegetation (Elliot and Veni, 1994).

Natural Bridge Caverns (NB) is located 15 miles west of New Braunfels, Texas along Farm-to-Market Road 3009. The site consists of two separate caves, the North Cave and the South Cave, which were separated by collapse and may still be connected in terms of cave-air circulation, but exhibit different ranges in annual CO_2 concentrations (Banner et al., 2007; Wong et al., 2011). In select chambers and passages that are prone to very high pCO_2 seasonally (>1.5%), fans have been installed to provide artificial ventilation, but are rarely used. The caves are 3,354 m in total surveyed length and 76 m at its deepest point (Elliot and Veni, 1994). The cave has developed in the uppermost members of the Glen Rose Formation, which stratigraphically underlies the Edwards Group (Figure 5; Elliot and Veni, 1994; Small and Hanson, 1994). We established study sites in the North Cave (Table 3; Figure 7) primarily in a chamber named the Castle of White Giants (CWG; Elliot and Veni, 1994).

Both caves have extensive urban development on the surface in the form of parking lots, amusement areas, highways, and visitor's centers (Banner et al., 2007; Wong et al., 2011). In-cave temperatures remain largely constant throughout the year with average cave-air and drip water temperatures at each location falling in the range of 20.1˚C – 22.2˚C (Appendix B; Banner et al., 2007). Average precipitation and surface temperatures at IS and NB are determined by NOAA 30-year regional climatology records (1981-2010) (http://www.nws.noaa.gov/climate/local_data.php?wfo=ewx). For IS, mean annual temperature (MAT) is 20.8˚C and mean annual precipitation (MAP) is 87.0 cm/yr, while at NB MAT is 20.8 ˚C and MAP is 82.0 cm/year.

1.2.5. Vegetation and biotic setting of the Edwards Plateau

The ecosystem of the Edwards Plateau and BFZ is defined as a subtropical savanna characterized by patchy, mixed grassland and woodland vegetation documented throughout central and southern Texas (Jessup et al., 2003; Bai et al., 2009; Bai et al., 2012). Soils in the region are dominantly lithic arguistolls and lithic haplustolls (of the Mollisol soil order) and are between 0- 45 cm thick (California Soil Resource Lab, http://casoilresource.lawr.ucdavis.edu). The region provides habitat to native and non-native species of C_3, C_4, and CAM vegetation, and has been undergoing extensive woodland (C_3) encroachment since early settlement in the area (Jessup et al., 2003; Bai et al., 2009; Bai et al., 2012). Southern live oak (*Quercus virginiana*) and ashe juniper (*Juniperus ashei*) are the dominant tree species responsible for this encroachment and, in the case of the juniper, have been treated as an invasive species despite being native to the region (Jessup et al., 2003). Jessup et al. (2003) surveyed and inventoried tissue samples of representative plant species across the Edwards Plateau and reported the carbon-isotope composition of leaf and stem material corresponding to each of these species (Table 1). This particular biome allows for stark variations in the proportions of C_3, C_4, and CAM plant types evidenced by field observations and aerial documentation/remote-sensing (Figure 7). The vegetation on the surfaces above both caves is dominated by *Q. virginiana* and *J. ashei* (woodlands), and King Ranch bluestem (*Bothriochloa ischaemum*; C_4) and Cedar Sedge (*Carex planostachys*; C_3) (grasslands). Large patches of Texas prickly pear (*Opuntia engelmanii*; CAM) and other mixed C_3-C_4 grasses are present (Table 1).

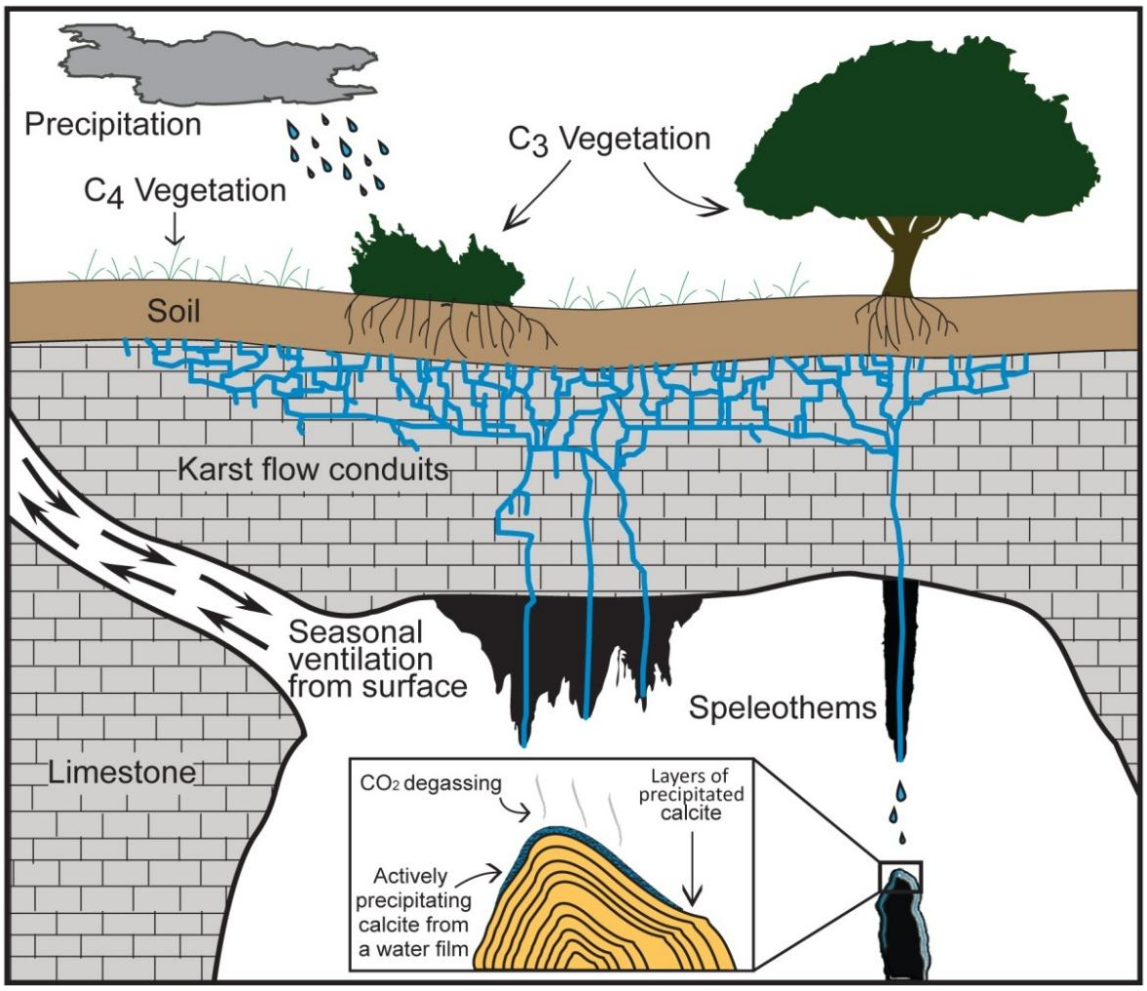

Figure 1. Summary schematic of karst landscape and speleothem formation. CO_2 from the atmosphere, root-respiration, and decomposition of soil organic matter (SOM) is dissolved into groundwater and speciates into carbonic acid (H_2CO_3) and bicarbonate (HCO_3^-). H_2CO_3 is responsible for the dissolution of limestone and the incorporation of Ca^{2+}, CO_3^{2-} and additional HCO_3^- into solution. The water subsequently percolates into a cave, which ventilates seasonally, and CO_2 is degassed from solution into low-pCO_2 cave-air driving the precipitation of calcite ($CaCO_3$).

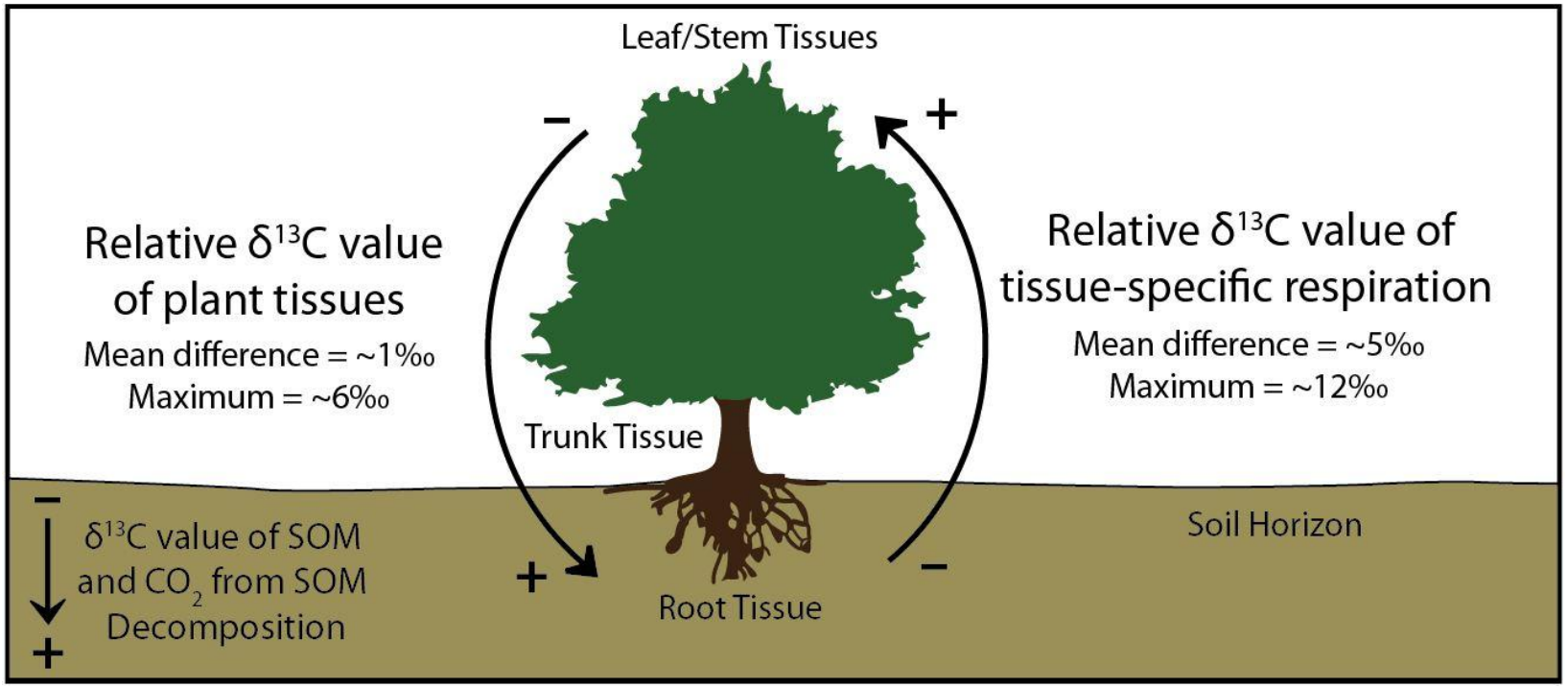

Figure 2. Summary schematic of the relative carbon isotope compositions of plant tissue, tissue-specific respiration, soil organic matter (SOM), and the CO_2 associated with decomposition of SOM. Plant tissues are typically enriched with ^{13}C moving from aboveground to below ground, while the respiration from these tissues follows the opposite trend. $\delta^{13}C$ values for SOM and respiration from decomposition increase with depth, while SOM is typically depleted in ^{13}C relative to this CO_2.

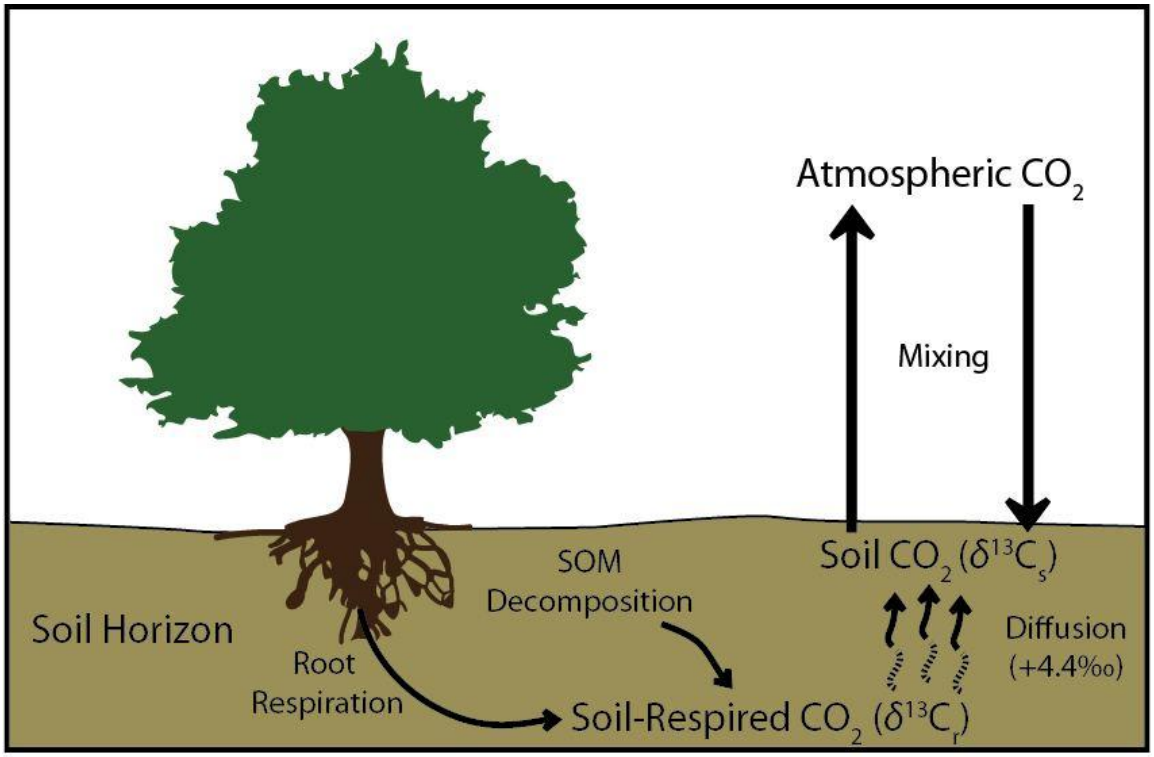

Figure 3. Summary schematic used to convey the endmember-mixing relationship between soil-respired CO_2 and atmospheric CO_2. Soil-respired CO_2 ($\delta^{13}C_r$) is a product of the combined CO_2 fluxes of root respiration and SOM decomposition. Soil CO_2 ($\delta^{13}C_s$) is the resultant reservoir of CO_2 in the soil horizon after soil-respired CO_2 has undergone diffusion (causing an equilibrium carbon isotope fractionation resulting in $\delta^{13}C_s$ values being 4.4‰ higher than $\delta^{13}C_r$) and mixing with atmospheric CO_2 in soil pores.

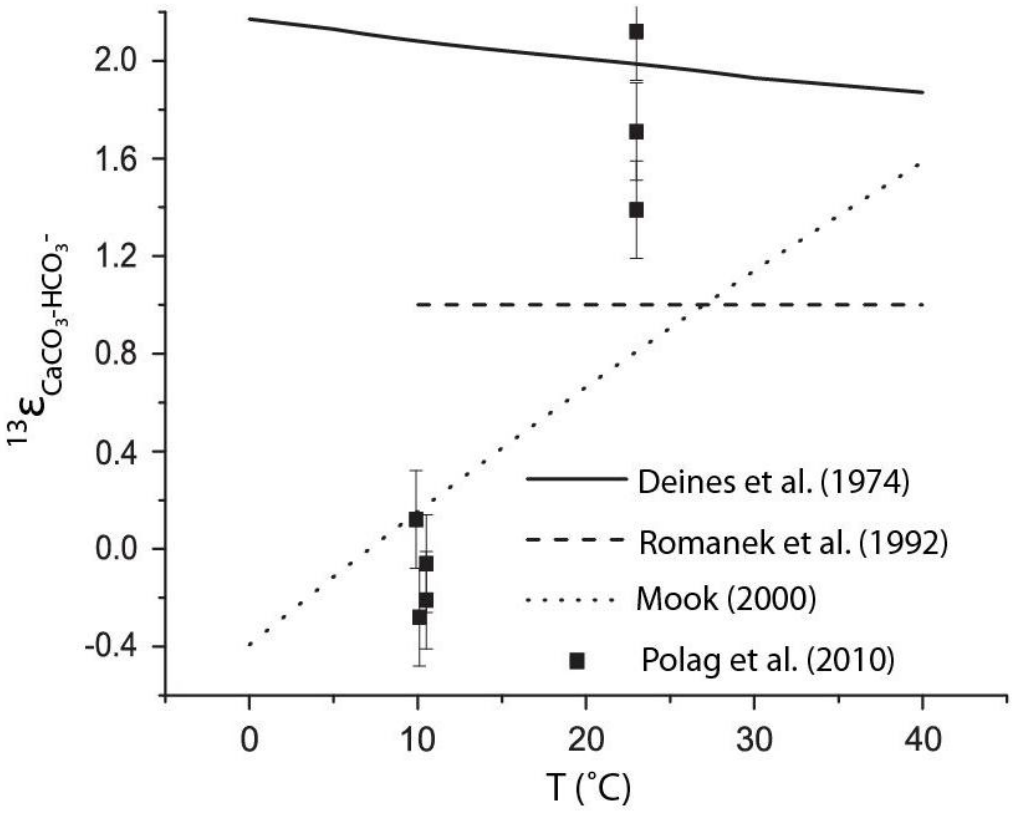

Figure 4. Experimental results of equilibrium carbon isotope fractionation between HCO_3^- and $CaCO_3$ adapted from Polag et al. (2010). The various experimental approaches show little agreement, which emphasizes the need to constrain this fractionation factor. The enrichment factor, ε, is defined as: $\varepsilon = (\alpha - 1)*1000$.

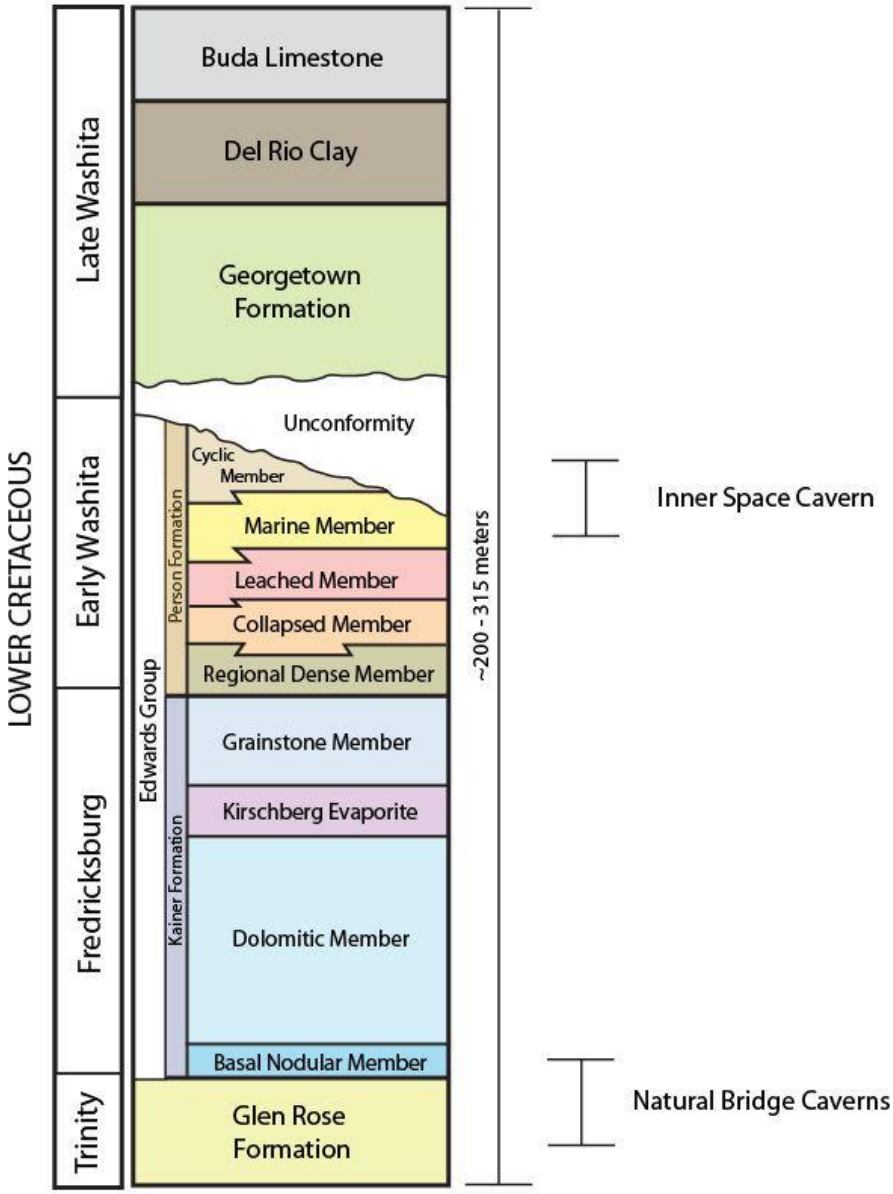

Figure 5. Representative stratigraphic section of the central Texas Edwards Plateau adapted from Cowan (2010) and Maclay and Small (1983). Relative unit thickness, total section thickness and the units which the caves span are approximate (Kastning, 1983; Cowan, 2010).

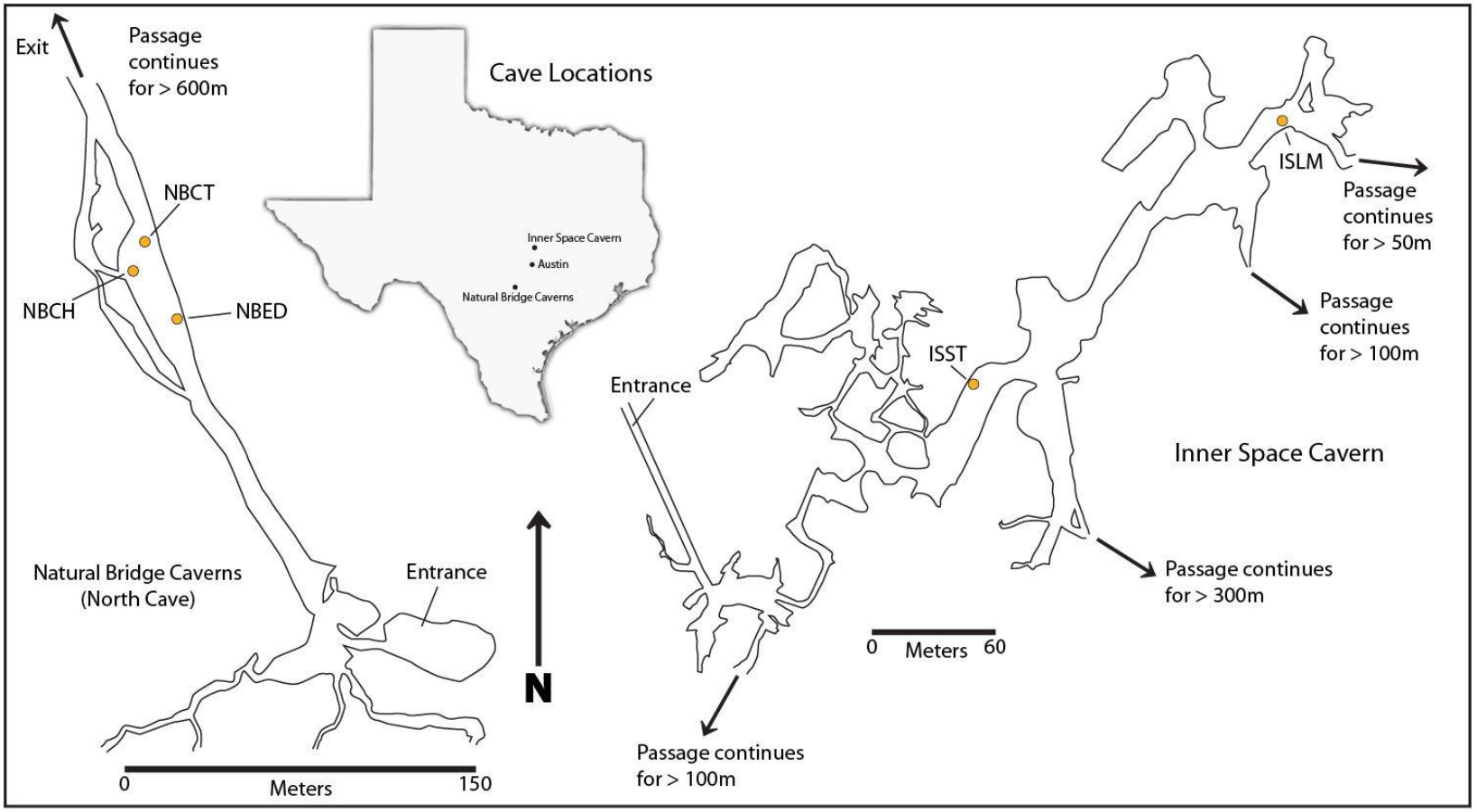

Figure 6. Map of Natural Bridge Caverns and Inner Space Cavern adapted from Veni and Elliot (1994). Sampling locations relevant to this study are marked on each cave. Full site descriptions are listed in Appendix A.

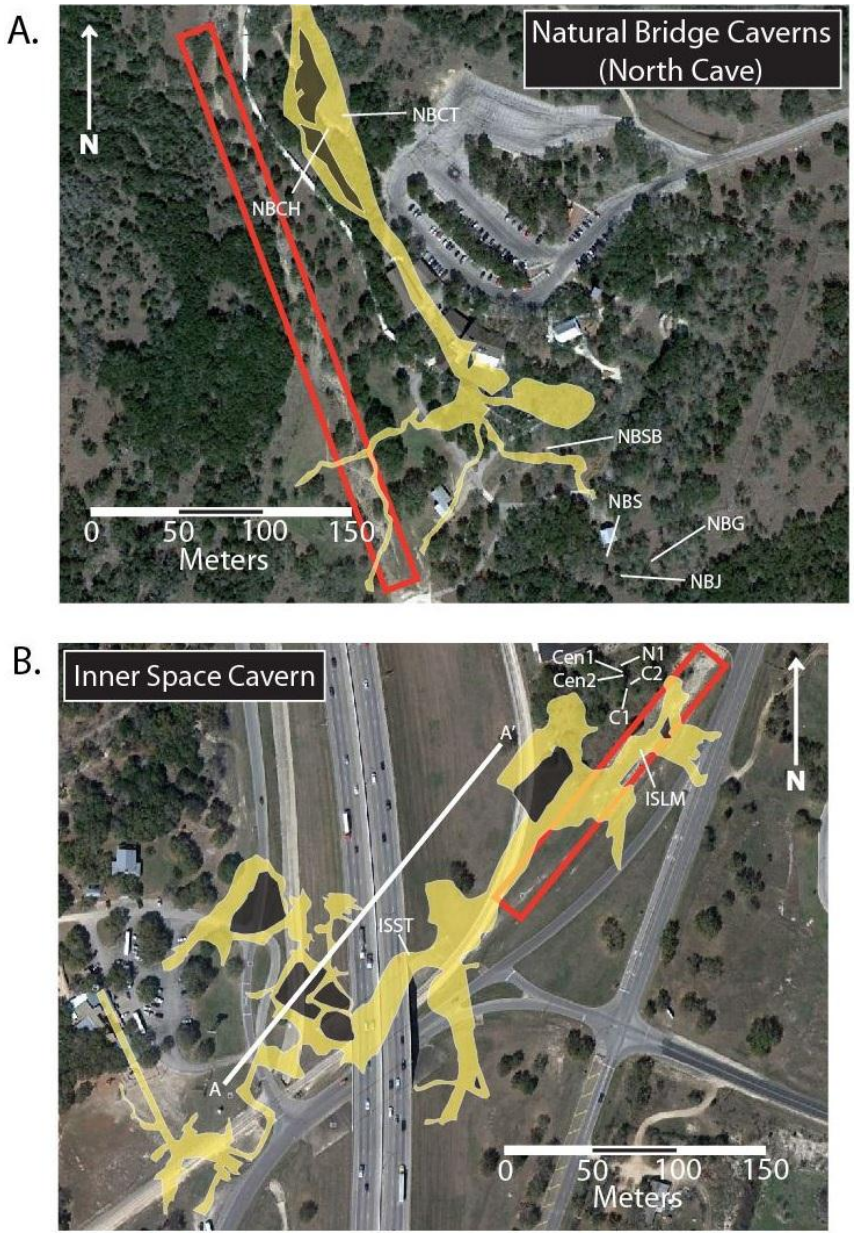

Figure 7. Composite images of Natural Bridge Caverns (A) and Inner Space Cavern (B) adapted from Veni and Elliot (1994) and Google Earth™. At Natural Bridge Caverns we have only depicted the North Cave. NB drip sites (NBCH, NBCT) and soil gas wells (NBSB, NBG, NBS, NBJ) are shown. At Inner Space Cavern, line A – A' is the approximate transect we followed for transient soil gas well sampling. IS drip sites (ISST, ISLM) and the location of permanent soil gas wells (C1, C2, Cen1, Cen2, and N1) are also depicted. These are the same sampling locations as used in Breecker et al., (submitted). The locations of prominent surface karst features are outlined in red and described in Appendix A. Full site descriptions are also listed in Appendix A.

Table 1. Plant tissue, root-respiration and SOM $\delta^{13}C$ values modified from Jessup et al. (2003).

Plant Species/SOM Type	Mean $\delta^{13}C$ value (‰ vs. VPDB)	Standard error (± ‰)
Plant Tissue		
C_3 vegetation		
Quercus Virginiana (Southern live oak)	-27.1	0.3
Juniperus ashei (Ashe juniper)	-26.7	0.2
Carex planostachys (Cedar sedge)	-28.0	0.3
C_4 vegetation		
Botriochloa ischaemum (King Ranch bluestem)	-14.9	1.0
CAM vegetation		
Opuntia engelmanii (Texas prickly pear)	-13.5	0.2
Root-respired CO_2*		
Juniperus ashei		
Incubated 8 Days	-23.6	0.1
Incubated 18 Days	-24.9	0.9
SOM		
Quercus Virginiana		
Mean litter composition	-26.7	0.2
Mean value at 20-30 cm	-16.7	0.3
Juniperus ashei		
Mean litter composition	-27	-
Mean value at 20-30 cm	-15.9	0.7
C_3-C_4 Grasslands		
Litter (proximal to oak woodlands)	-20.8	1.3
Mean value at 20-30 cm	-13.2	0.1
Litter proximal to juniper woodlands	-22.8	0.4
Mean value at 20-30 cm	-13.7	-

*Represents data from this study.

CHAPTER 2. FIELD AND LABORATORY METHODS FOR DETERMINING CARBON ISOTOPE COMPOSITION OF SOIL CO_2, DRIP WATER, AND CALCITE

2.1: FIELD SAMPLING METHODS

2.1.1. Soil CO_2 sampling

We constructed soil gas wells from ¼" O.D. (outside diameter) stainless steel tubing cut to different lengths and slotted or drilled above a sealed and tapered point at the end of the tube. The open end of the tubes were then sealed with a rubber septum and Swagelok® fittings similar to those developed by Breecker and Sharp (2008). We collected soil gas samples at approximately 4-6 week intervals from wells installed above each cave and proximal to specific vegetation represented throughout the field area (Figure 7). The same soil gas wells were used by Breecker et al. (submitted) for monitoring soil CO_2 above the caves. Sampling was conducted using 5 mL Luer-Lock™ syringes outfitted with 25G needles, and we collected 3 mL soil gas samples and 5 mL atmospheric air samples. For each sample we primed the syringe by flushing it with gas from the well several times. Samples were then immediately injected into He-flushed, septum-capped 12 mL Labco Exetainer® vials. We typically collected one replicate per sample. We also collected rootlets trenched from under an ashe juniper at the NB field area. The rootlets were cleaned of any soil and extra debris with forceps and a rinse of deionized (DI) water. We then placed the rootlets in He-flushed, septum-capped 12 mL

Labco Exetainer® vials and allowed the roots to incubate at 25˚C. We sampled the headspace of these vials with a 1 mL Luer-Lock™ syringe after 8 and 18 day intervals.

At NB we installed soil gas wells at 4 sites with 4 wells per site and at depths ranging from 6 – 34 cm to construct a vertical profile of the soil horizon for each representative form of vegetation (Table 2; Figure 7). At IS, where the cave is located beneath I-35, the Texas Department of Transportation (TxDOT) cleared a significant portion of roadside vegetation including nearly all deeply-rooted trees and shrubs. Given the regular maintenance schedule of TxDOT road crews, we could only install transient wells (removing the wells immediately after sampling) with the exception of 5 permanent wells that were installed in a small grove of largely undisrupted live oak woodland overlying site ISLM (Figure 7).

2.1.2. Drip water and cave air sampling

Drip water samples were collected on the same day as soil gas samples at approximately 4-6 week intervals from active drip sites within each cave (primarily targeted for proximity to surface soil gas wells; Figure 7). The drip sites we studied are listed in greater detail in Table 3, and more complete descriptions can be found in Banner et al. (2007) and Wong et al. (2011). Drip water was collected by two different methods: 1) in narrow-mouthed 20 mL HDPE Nalgene® bottles from the source of the drip within the cave and from intervals along natural flowstones, 2) from constructed artificial flow-paths. One style of flow-path was designed from 1” diameter PVC pipe attached to a funnel for drip water collection and slotted to allow for sampling along the length of the

pipe (~1.6 m). We also designed a flow-channel from 1/8" Lexan® sheets custom-outfitted with universally adaptable Gorillapod® legs for mounting on features of any shape and orientation (which we refer to as the 'Lexan® flow channel'). The Lexan® flow-channel was also slotted for placing 10 cm x 10 cm glass plates on the length of the channel for collecting modern calcite samples (Figure 8). We then transferred 0.4 mL of drip water by 1 mL Luer-Lock™ syringes outfitted with 25G needles within 30 seconds of initial collection and injected into He-flushed, septum-capped 12 mL Labco Exetainer® vials in the same fashion as soil gas samples. We collected three replicates for mass spectrometric analysis per drip water sample. Each value reported for drip water $\delta^{13}C_{DIC}$ is the average (and standard deviation) of these 4 total samples. These samples were then placed immediately under refrigeration for storage before analysis. Separate drip water aliquots were collected in 20 mL and 100 mL HDPE Nalgene® bottles for trace element analysis, field and lab alkalinity titrations, and pH and water temperature measurements.

We sampled both natural and artificial flow-paths of varying flow-rates and rates of total water flux. Additionally, we performed in-cave degassing experiments with ~5 mL aliquots of drip water from the ISST and NBCH sites in 30 mL HDPE Nalgene® bottles where the collected drip water was then allowed to degas CO_2 into the cave atmosphere, which varied in pCO_2 between 540 and 740 ppmv over the duration of the experiment. These samples were collected approximately every 1/2 hour for 4 ½ hours of total degassing time in-cave (T_{total}). Additionally, given that the average in-cave flow-path film thickness on the features we sampled was ~0.5 – 3 mm, we repeated this

experiment by collecting 30 mL of drip water in 14 cm diameter glass petri dishes to serve as a more analogous film thickness (~1 mm) to that of natural cave features, and provide a more open-air environment for the drip water to degas. For this iteration we collected drip water at NBCH where pCO_2 ranged between 673 and 765 ppmv during the sampling interval, which was conducted every 1/2 hour for 2 ½ hours.

We collected drip water from a variety of drip sites inside the caves (Table 3; fig. 6) and have classified these sites as either: 1) 'directly-sourced' (stalactites/soda-straws by which water enters the cave from the epikarst and is exposed to the cave atmosphere for a negligible amount of time, typically < 30 seconds, before collection), or 2) 'indirectly-sourced' (water travels along an in-cave flow-path for some unknown and longer period of time before collection, i.e. drip water at the distal end of a flowstone). We made this distinction in order to account for the effects of in-cave degassing on the $\delta^{13}C_{DIC}$ values of drip water.

Cave-air and surface atmospheric CO_2 concentrations and air temperatures were determined by Telaire® 7001 CO_2 Meters, Vaisala® GM70 Handheld CO_2 Meters, and analog mercury/ethanol thermometers. Cave-air samples were collected in the same fashion as soil CO_2 samples.

2.1.3. Modern calcite growth and sampling

We emplaced 10 cm X 10 cm glass plates under active drip-sites within the cave, allowing us to collect modern calcite precipitated over ~4 - 6 week intervals by methods after Mickler et al. (2004) and Banner et al. (2007). The collection of calcite samples has

been underway in both caves for over 10 years. We collected and analyzed calcite samples over the same sampling interval as the drip water and soil gas samples at the following sites: $ISST_{indirect}$, $ISST_{direct}$, ISLM, and NBCT (Table 3). For the directly-sourced ISST site ($ISST_{direct}$) we installed a Lexan® flow-channel and collected plates from three slots along the length of the channel (Figure 8). Calcite growth rates and total accumulation vary seasonally (Banner et al., 2007) and as a consequence of the severe central Texas drought through 2011-2012 the indirectly-sourced ISST drip site ($ISST_{indirect}$) was completely dry for the first time in 12 years of consistent monitoring during the drought, which resulted in a lapse of temporal coverage of collected plate calcite.

2.2: LABORATORY SAMPLE PREPARATION, METHODS, AND ANALYSIS

2.2.1. Soil CO_2, drip water, and calcite sample preparation

All samples were processed for analysis on a Thermo Scientific MAT 253 stable isotope ratio mass spectrometer (IRMS). Soil gas samples, if not ready for immediate analysis, were diluted. We diluted samples by transferring aliquots with a valved syringe into additional He-flushed Exetainer® vials. Drip water samples were injected with 103% H_3PO_4 to drive DIC from solution into the headspace of the vial as gaseous CO_2. For precise determination of the carbon isotopic composition and total DIC of these samples they equilibrated at 25˚C for a 12-40 hour time period post-injection (Salata et al. 2000). Additional samples were acidified and stored under refrigeration for future analysis by inductively-coupled plasma mass spectrometer (ICP-MS) at a later date. Precipitated

plate calcite was scraped in various locations across the plate to map carbon isotope variability from the center to edge of the plate (Mickler et al., 2006; Guilfoyle, 2006; Feng et al., 2012; Feng et al., in prep). We typically collected 200 – 500 μg of calcite per sample, which were then placed in 12 mL Exetainer® vials and then flushed with UHP helium. Calcite samples were also injected with 103% H_3PO_4 and reacted for 2 hours at 50˚C.

2.2.2. Sample analysis by continuous-flow GC-IRMS

The carbon isotope compositions of CO_2, DIC and calcite were measured using a Thermo Scientific MAT 253 GC-IRMS on continuous-flow mode through a Thermo Scientific Gasbench II and PAL autosampler. Soil samples were cryo-focused to a single pulse by directing the sample through a liquid nitrogen cold trap before introduction to the mass spectrometer. A CO_2-in-air standard calibrated to the VPDB scale in the Stable Isotope Laboratory at CU-INSTAAR in Boulder, Colorado was used to calibrate an internal laboratory CO_2-in-air standard for use in determining the carbon isotope composition of the soil CO_2 samples. Drip water samples were measured in comparison to an internal laboratory $NaHCO_3$ standard (as a solid and as an aqueous solution) and calcite samples were measured in comparison to an internal laboratory marble standard. Both $NaHCO_3$ and marble standards were calibrated relative to samples of Carrara marble, NBS-18, and NBS-19.

We determined CO_2 concentrations and total [DIC] of soil CO_2 and drip water samples, respectively, by producing calibration curves relating the mass 44 peak area

(V·sec) measured by the mass spectrometer to the moles of carbon in CO_2-in-air standards and aqueous $NaHCO_3$ standard solutions. For the CO_2-in-air standard, we determined absolute pCO_2 from the CU-INSTAAR standard to within ±0.7%. Measured mass 44 peak area (V·sec) corresponded linearly to the several measured volumes of the CU-INSTAAR standard diluted in 12 mL vials flushed with UHP helium (generating a calibration curve for the peak area size associated with a given concentration of CO_2) with an average R^2 = 0.989. For the $NaHCO_3$ standard, we prepared 0.5 L standard solutions (using a predetermined mass of $NaHCO_3$ dissolved in DI water) with calculated alkalinity values ranging from 1 to 10 meq/L as HCO_3^-, which we precisely determined by titration with 0.1 N HNO_3. We extracted 0.4 mL of each standard solution (the same volume as all drip water samples collected in the field), which were injected into 12 mL He-flushed Exetainer® vials, and acidified the samples with 103% H_3PO_4 in the same fashion as the drip water samples. The calculated alkalinity and total [DIC] were then linearly correlated to the measured mass 44 peak area (V·sec) with an average R^2 = 0.981.

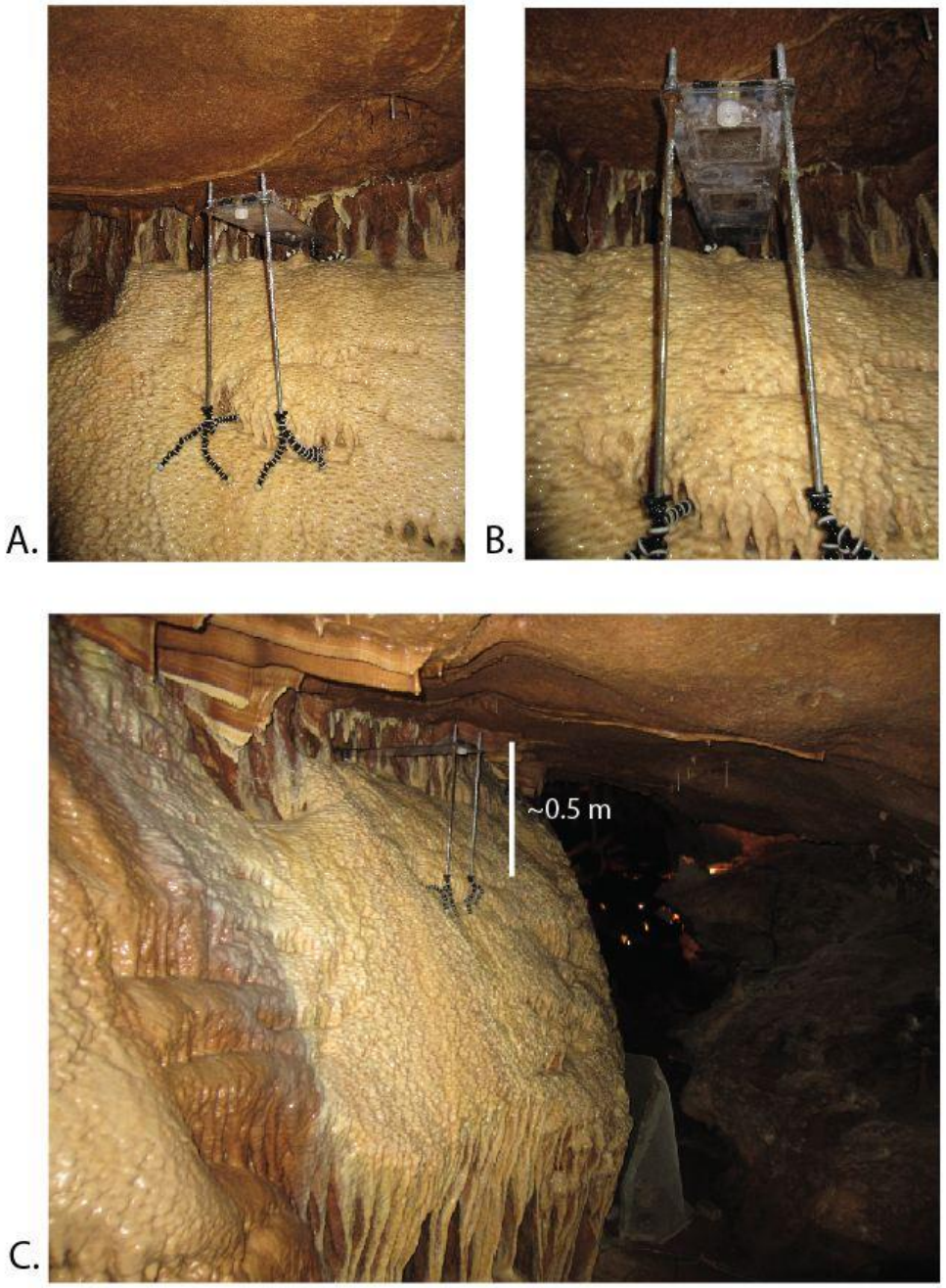

Figure 8. Images of the Lexan® flow channel used for monitoring studies at ISST. Depicted above: (A) the flow channel is outfitted with three Gorillapod® legs to attach to virtually any surface, (B) the channel is constructed from two Lexan® sheets which were cut to hold 10 cm X 10 cm glass plates for collecting modern calcite precipitates, and (C) the flow channel is emplaced under site $ISST_{direct}$, above the wire mesh protecting site $ISST_{indirect}$.

CHAPTER 3. RESULTS OF CAVE AND SURFACE MONITORING, DISCUSSION OF FINDINGS, AND THE IMPLICATIONS FOR INTERPRETING SPELEOTHEM CARBON ISOTOPE COMPOSITIONS

The following sections detail the results of the various sampling methods, and discuss the interpretation of these findings. We begin with the results of soil gas sampling, which indicated soil-respired and root-respired $\delta^{13}C$ values were nearly identical. The soil CO_2 values ($\delta^{13}C_s$) at NB indicate that the average $\delta^{13}C_{DIC}$ values of drip water are in equilibrium with CO_2 in soils beneath juniper trees and not the CO_2 under grasslands. We also detail the effect of heterogeneous distributions of vegetation above IS on cave drip water $\delta^{13}C_{DIC}$ values and how these results compare to those at NB. Within the caves, we observed that drip water $\delta^{13}C_{DIC}$ varied with the length of time the water remained under low pCO_2 conditions before sampling. In all cases calcite $\delta^{13}C$ values ($\delta^{13}C_{cc}$) closely followed $\delta^{13}C_{DIC}$ values, and appear subject to small-magnitude variations (~0 - 2‰) associated with disequilibrium conditions.

3.1: RESULTS

3.1.1. Carbon isotope composition of soil gas and respired CO_2 in the study region

The mean $\delta^{13}C$ values of soil CO_2 ($\delta^{13}C_s$) and soil respired CO_2 ($\delta^{13}C_r$; Davidson 1995) under mixed C_3-C_4 grasses are -13.9 ± 1.4‰ (n = 6) and -19.7 ± 0.9‰ (n = 6) resepectively. For soil under ashe juniper trees (the dominant deeply-rooted plant of the region) measured $\delta^{13}C_s$ = -18.3 ± 0.7‰ (n = 6) and $\delta^{13}C_r$ = -23.8 ± 0.6‰ (n=6; Table 2).

The $\delta^{13}C$ value of CO_2 respired during laboratory incubation of juniper roots after eight days was -23.6 ± 0.1‰ and after 18 days was -24.9 ± 0.9‰ (Table 1).

Soil CO_2 concentrations increased with depth in all soils above NB (Figures 8 and 9; Table 2). At NB, $\delta^{13}C_s$ values decreased with depth to ~30cm, below which they were constant with depth (Table 2). Soil CO_2 concentrations, $\delta^{13}C_s$ values, and $\delta^{13}C_r$ values also varied temporally during the period of study. $\delta^{13}C_r$ varied only slightly (< 1‰; Table 2), while $\delta^{13}C_s$ varied seasonally with the highest values measured during the summer (Figure 9, Figure 10). $\delta^{13}C_r$ values calculated using Davidson's (1995) equation were indistinguishable from values calculated from Keelng plot y-intercepts (Figure 11).

3.1.2. Carbon isotope composition of directly- and indirectly-sourced cave drip water

The mean dripwater $\delta^{13}C_{DIC}$ at NBCH was -10.7 ± 0.3‰ and the mean at $ISST_{direct}$ was -9.9 ± 0.3‰ (Figure 12; Table 3). Table 3 summarizes the seasonal ranges in drip water $\delta^{13}C_{DIC}$ for all sites. Using the calibration reported by Zhang et al. (1995) and mean annual drip water temperatures of 22.7 ± 0.6˚C (NB) and 21.7 ± 0.8˚C (IS), the mean $\delta^{13}C$ values for CO_2 in equilibrium with drip water are -18.1 ± 0.3‰ (NBCH) and -17.3 ± 0.3‰ ($ISST_{direct}$). The $\delta^{13}C_{DIC}$ values of directly-sourced drip water sampled on the same day at IS from sites proximal to the cave entrance (ISST = -10.0 ± 0.1‰) and those more distally located (ISLM = -12.7 ± 0.3‰) were significantly different. On the surface above the cave, vegetation is also different at these two sites (Table 3).

During the in-cave degassing experiments, $\delta^{13}C_{DIC}$ values increased at a rate of 0.24‰/hr with a film thickness measured at ~1.5 cm, and 0.47‰/hr with a film thickness measured at ~1 mm (Figure 13). In order to determine the relative contributions to drip water $\delta^{13}C_{DIC}$ values from host-rock dissolution and prior calcite precipitation, we collected drip water aliquots for ^{14}C-analysis (AMS) and trace-metal analysis (ICP-MS). These samples will be analyzed at a later time. ^{14}C-analysis will constrain the percent modern carbon (pMC) of the drip water, which has traditionally been interpreted as a two-endmember mixture between host-rock (in this case Cretaceous limestone) and modern values. However, contributions from old SOM also should be evaluated as a significant component of the radiocarbon age of these samples.

3.1.3. Modern calcite carbon isotope composition

The $\delta^{13}C_{DIC}$ and $\delta^{13}C_{cc}$ values at each site were well correlated (Figure 13; Table 5). For both directly- and indirectly-sourced drip water, $\delta^{13}C_{cc}$ values followed $\delta^{13}C_{DIC}$ values, but exhibited a greater range than was predicted by equilibrium fractionation between HCO_3^- and $CaCO_3$ (NBCT $\Delta^{13}C_{m\text{-}e}$ = -0.3‰ to +0.3‰; $ISST_{direct}$ $\Delta^{13}C_{m\text{-}e}$ = +0.3 to +0.9‰). In all cases $\delta^{13}C_{cc}$ values were more positive than associated drip water $\delta^{13}C_{DIC}$ values (Table 5).

3.2: DISCUSSION

3.2.1. Assessment of carbon isotope compositions of soil CO_2 and soil respired CO_2.

Measured $\delta^{13}C_s$ values are consistent with two-endmember mixing between atmospheric CO_2 (regional measured average $\delta^{13}C_{surface}$ = -9.0 ± 0.1‰ and pCO_2 = 397 ppm) and soil-respired CO_2 (where $\delta^{13}C_r = \delta^{13}C_s$ - 4.4‰; Figure 11). If the soil CO_2 concentration is above ~4000 ppm, then the atmospheric component would represent less than 10% of soil CO_2 and have a small effect (based on our data ~0.5 to 1‰) on $\delta^{13}C_s$. Given that CO_2 concentrations increase with depth, we observed threshold points (we refer to as 'CO_2 thresholds') in the soil horizon below which atmospheric CO_2 became negligible in terms of $\delta^{13}C_s$. This depth varied between 20 cm in the winter and 40 cm in the summer, and is likely due to seasonal changes in plant productivity. Water percolating past this depth will therefore reflect soil-respired CO_2 (modified by diffusion) and not atmospheric CO_2.

The $\delta^{13}C$ value of CO_2 produced during juniper root incubations (-23.6 ± 0.1‰) was in close agreement with the calculated $\delta^{13}C_r$ value determined from soil gas samples collected in the field (-23.8 ± 0.6‰). Bostrom et al. (2007) observed that both SOM and CO_2 from SOM decomposition are significantly enriched in ^{13}C compared to live plant matter and recent plant litter. Therefore, the similarity between the observed $\delta^{13}C$ values of root-respired and soil-respired CO_2 can be explained by several scenarios: 1) deep in a soil profile microbial respiration is minimized and effectively overwhelmed by root respiration; 2) freshly decomposing roots and other plant matter in the epikarst produce CO_2 that is nearly identical in carbon isotope composition to root-respired CO_2; 3) the

results of the Bostrom et al. (2007) study do not apply to this region and the carbon isotope composition of CO_2 produced from the decomposition of SOM is nearly identical to root-respired CO_2. The Bostrom et al. (2007) study was conducted on samples from a Norwegian spruce forest, which do not serve as an analogous biome to the savanna of central Texas. It may be possible to resolve the proportion of CO_2 from SOM decomposition that contributes to $\delta^{13}C_r$ by conducting soil incubation experiments under a range of conditions (e.g. different SOM contents). We seek to test these hypotheses at a later date. For the remaining soil gas well sites the value of $\delta^{13}C_r$ is also complicated by inputs from vegetation that correspond to mixtures of C_3, C_4, and CAM plants in a variety of proportions.

3.2.2. Cave drip water $\delta^{13}C_{DIC}$: The 'vegetation baseline,' and kinetic isotope effects

We expected seasonal differences in drip water $\delta^{13}C_{DIC}$ values from varying inputs to the DIC pool (e.g. host-rock dissolution, PCP), but found variability in $\delta^{13}C_{DIC}$ of directly-sourced sites could not be distinguished from analytical uncertainty (Figure 12). From the $\delta^{13}C_{DIC}$ values of directly-sourced drip water at NB we calculated the average $\delta^{13}C$ value of CO_2 in equilibrium with this water (-18.1 ± 0.3‰). The average $\delta^{13}C_s$ of measured soil gas collected from under juniper trees at NB was nearly identical at -18.3 ± 0.7‰. Results indicate that ashe juniper trees appear to dominate the carbon isotope composition of cave drip water collected throughout the year. This was also true for the indirect sites (NBCT and NBED) during summer months, when cave ventilation, drip

water degassing, and the rate of calcite precipitation/accumulation are all at a minimum for these sites (Figure 12).

When we contrast the values of juniper $\delta^{13}C_s$ with predicted equilibrium CO_2 $\delta^{13}C$ values (calculated from directly-sourced $\delta^{13}C_{DIC}$), we find a small difference during the central Texas summer (Figure 9, Figure 10). With the persistence of severe drought conditions through these months soil pCO_2 was significantly lower, likely as a result of decreased plant productivity and significant plant death (Figure 9, Figure 10). During this low-pCO_2 season, the relative contribution of atmospheric CO_2, to total soil CO_2 increased and the depth where soil CO_2 only records biologic CO_2 shifted to greater depths in the soil profile (Figure 9, Figure 10). With the return of precipitation and lower surface temperatures subsequent to drought conditions, there was a strong response in the amount of live vegetation present, increased soil pCO_2, and convergence of $\delta^{13}C_s$ and equilibrium drip water CO_2 values (Figures 8, 10). Given that soil profiles in central Texas are thin (typically 30-45 cm thick), our deepest soil gas well was 34 cm. However, we hypothesize that $\delta^{13}C_s$ values would continue to approach $\delta^{13}C_r$ + ~4.4‰ with depth below the soil zone (approximately -18.3‰ for juniper trees and presumably the dominant carbon isotope composition within the epikarst overlying the NB sites). We also suggest that downward percolating water would equilibrate with soil CO_2 that is minimally influenced by atmospheric CO_2 before it enters the cave. Jackson et al. (1999) documented juniper roots at NB that extended at least 9 m into the subsurface and oak roots as deep as ~25 m. Sampling sites within the cave are located in a chamber approximately 40 m below the surface, which would allow a large distance for vadose

groundwater to equilibrate with plant root respired CO_2 (modified by diffusion) before it enters the cave (Figure 14).

To contrast our work with $\delta^{13}C_{DIC}$ values of drip water in other caves, we compiled the maximum range of available drip water $\delta^{13}C$ values from studies in Gibraltar, Italy, Austria, and Florida (Figure 16; Mattey et al., 2010; Frisia et al., 2011; Spötl et al., 2005; Tremaine et al., 2011). In order to minimize PCP or kinetic effects we only evaluated the range of values corresponding to the period of minimum cave ventilation documented in each study. In all cases, including those with mixed C_3-C_4 vegetation, the drip water values fell in the range we would predict from equilibrium isotope exchange with CO_2 from C_3 plants (Figure 16). C_4 vegetation is more favorably adapted to a warm, arid climate and low atmospheric pCO_2, and only currently represents ~3% of the nearly 250,000 documented species of terrestrial vegetation (Ehleringer et al., 1997; Sage, 2004). This demonstrates how C_4-dominance is constrained to only particular regions. For example, Teeri and Stowe (1976) assessed 27 studies across North America and found that C_4 plants only dominated (consisted of >50% of total grass species) grass floras in 7 of the studies. These studies were not exclusively conducted on grassland biomes, and C_4 plants may have constituted an even smaller proportion of total vegetation in a given study area. Also, only a small fraction of C_4 species are trees or shrubs, which further limits cases where deeply-rooted C_4 plants would be prone to dominating surface vegetation coverage (e.g. grasslands). Ehleringer et al. (1997) describe the 'transition temperatures' at which C_4 plants predominate over C_3 plants in modern settings for 16 regions across North America, Africa, Europe, Australia, and Asia with the average being

25.5˚C. It is important to note that this average transition temperature exceeds the MAT of central Texas. Ehleringer et al. (1997) also modeled the change in transition temperatures as a function of pCO_2, which at 200 ppm (roughly the atmospheric pCO_2 during the Last Glacial Maximum) would decrease by ~8-10˚C. For example, Clark et al. (2001) describe the highest estimated prevalence of C_4 grasses in the Northern Plains of North America, under maximum aridity conditions during the Holocene (~8000 – 4000 B.P.) , as ~40% of total grasses in the record. Therefore, in cases with mixed C_3-C_4 vegetation and the presence of trees or shrubs, we would expect C_3 plants to bias the $\delta^{13}C_{DIC}$ of drip water except in extreme cases of elevated MAT, high aridity, and/or low atmospheric pCO_2 (e.g. during glacial intervals).

The flux of soil $CO_{2(g)}$ throughout the epikarst would imply that the subsurface above the cave functions as an open system (Fairchild et al., 2006; Breecker et al., submitted). An open system has significant bearing on the effect of host-rock dissolution and PCP on $\delta^{13}C_{DIC}$. Host-rock dissolution must occur to provide Ca^{2+} in solution, and therefore we would predict an equivalent contribution of limestone CO_3^{2-} and HCO_3^-, which has been previously proposed to account for as much as 50% of the total DIC pool (Hendy and Wilson, 1968; Hendy, 1971). However, with more positive values of limestone in the region, any measurable contribution from the limestone would result in $\delta^{13}C_{DIC}$ values higher than those in equilibrium with soil CO_2 under juniper trees. Similarly, PCP that has occurred at any point in the epikarst prior to entry within the cave should yield a higher $\delta^{13}C_{DIC}$ value. In contrast, at directly-sourced drip sites, we observed consistent values of $\delta^{13}C_{DIC}$ throughout the year (NBCH, $ISST_{direct}$), implying that

equilibrium carbon isotope fractionation occurs between soil CO_2 and $HCO_{3\,(aq)}^-$ without alteration by either of these processes. PCP has been previously documented in these caves (Wong et al., 2011) including one of the sites we evaluated in this study (NBCT). Guilfoyle (2006) also documented seasonal variability in trace element ratios at various locations around site ISST, which may represent active PCP at these sites. The Guilfoyle study showed no apparent seasonal variability at site ISLM, which would suggest PCP is not occurring at this site. An open system for CO_2-HCO_3^- exchange in the epikarst would allow for the 'overprinting' of a host-rock or PCP signal in the carbon isotope composition of drip water entering the cave, despite the occurrence of host-rock dissolution and PCP. This would also suggest that there is a large reservoir and/or flux of $CO_{2(g)}$ throughout the entire epikarst, which is consistent with dominantly gas-phase advective transport of CO_2 into the cave (Breecker et al., submitted). The rate of CO_2 production in the soil horizon and/or epikarst must also be sufficiently high to overwhelm host-rock and PCP inputs. Therefore, in these caves we hypothesize that the primary control on the carbon isotope composition of drip water is respiration from the dominant deeply-rooted vegetation in the region and any subsequent change in $\delta^{13}C_{DIC}$ must occur via processes within the cave.

In each of these cases we have only considered directly-sourced drip water or drip water collected during the season of minimum CO_2 degassing and calcite precipitation. Indirectly-sourced drip water $\delta^{13}C_{DIC}$ values collected during 2004-2006 at both caves demonstrated high-magnitude (~1-5‰) seasonal variability (Guilfoyle, 2006; Figure 12) and drip water $\delta^{13}C_{DIC}$ values from the same sites collected over 2011-2012 show

variability of approximately equal magnitude (Figure 12). Additionally, 2011 was a year of severe drought conditions across the state of Texas, whereas 2004-2006 spanned both drought and non-drought conditions (http://www.ncdc.noaa.gov/sotc/drought/). Considering the nature of indirectly-sourced drip sites and the relationship demonstrated herein between T_{total} and drip water $\delta^{13}C_{DIC}$ (+0.24‰/hr to +0.47‰/hr), disequilibrium effects from CO_2 degassing are likely the primary factor responsible for positive isotope excursions from the vegetation-controlled values of drip water DIC (Guilfoyle, 2006; Feng et al., in prep.). Since measured carbon isotope values did not decrease below those defined by the input from deeply-rooted vegetation, we refer to these values as the 'vegetation baseline' for carbon isotope composition. All subsequent departures from this baseline are likely the result of in-cave processes.

3.2.3. Calcite $\delta^{13}C$ values and interpretations of a 10-year modern calcite record

For dripwater sites with associated samples of modern calcite growth, calcite sampled from glass plates (near the site of drip water impact) closely followed the carbon isotope composition of the drip water (Table 6; Figure 13). Calcite samples collected from near the edge of a plate (away from the site of drip water impact) were not considered as these samples are subject to the highest degree of kinetic effects (Guilfoyle, 2006; Feng et al., in prep.). To conform with notation used by Feng et al. (in prep.), we use the term $\Delta^{13}C_{m\text{-}e}$ to describe the difference between measured $\delta^{13}C_{cc}$ values for modern calcite samples and the $\delta^{13}C_{cc}$ predicted for calcite formed under equilibrium conditions (from the fractionation factor used by Romanek et al., 1992). We observed

significant variability in modern calcite $\Delta^{13}C_{m\text{-}e}$ values, which ranged between -0.9‰ to +0.9‰. Whereas equilibrium fractionation between HCO_3^- and $CaCO_3$ during calcite formation predicts higher $\delta^{13}C_{cc}$ values than $\delta^{13}C_{DIC}$ values, there is significant disagreement in the overall magnitude and potential temperature sensitivity of the enrichment factor, $\varepsilon^{13}_{calcite\text{-}DIC}$ (where $\varepsilon = (\alpha - 1) * 1000$). Values for this enrichment factor at a temperature of 22˚C range from 0.7‰ to 2.0‰ (Figure 4; Deines et al., 1974; Romanek et al., 1992; Mook et al., 2000; Polag et al. 2010). Nonetheless, we observed values significantly lower than this range, which likely represents the influence of disequilibrium on carbon isotope fractionation between HCO_3^- and $CaCO_3$. Other studies have also suggested that rapid, disequilibrium calcite precipitation should result in $\delta^{13}C_{cc}$ values 'inheriting' the $\delta^{13}C_{DIC}$ values of drip water (Mickler et al., 2004; Feng et al., in prep). Ultimately, a reevaluation of the equilibrium fractionation factor and an assessment of kinetic fractionation between HCO_3^- and $CaCO_3$ are necessary to best account for these small and variable differences in $\varepsilon^{13}C_{cc\text{-}DIC}$. This small-scale variability may be effectively negligible when considering the other higher-magnitude carbon isotope variations in the context of record reconstructions.

Feng et al. (in prep) have generated a time-series of modern calcite samples from sites $ISST_{indirect}$ and ISLM (Table 3; Figure 17). $ISST_{indirect}$ is an indirectly-sourced drip site, whereas ISLM is a directly-sourced drip site. The $ISST_{indirect}$ site demonstrates high seasonal variability in $\delta^{13}C$ (up to ~4.5‰) and values that are significantly more positive than those at ISLM, which shows low seasonal variability (~1.5‰; Figure 17). For both $ISST_{indirect}$ and ISLM there is a distinct vegetation baseline (the lowest $\delta^{13}C_{cc}$ values;

$ISST_{indirect}$ = -8.2 ± 0.3‰ and ISLM = -11.1 ± 0.2). Directly above ISLM there is a small grove of live oak, grasses, prickly pear and a solitary juniper tree. Overlying ISST there is impervious cover from I-35 and mixed C_3-C_4 grasses at the roadside (Figure 7). Therefore, these two sites represent endmember cases for a drip site corresponding to savanna woodland (ISLM), and a site representing grassland devoid of deeply-rooted plants (ISST). These two distinct vegetation baselines in the modern calcite record are offset from one another by approximately 3‰ (Figure 17). The vegetation baseline of ISST still falls in the range of dominantly C_3-influenced $\delta^{13}C_{cc}$ values, which is unsurprising given that the savanna grasses of central Texas are mixed C_3-C_4 species (Jessup et al., 2003; Table 1). However, Breecker et al. (submitted) found that $\delta^{13}C_s$ values above this site were typically ~4‰ higher than the equilibrium CO_2 $\delta^{13}C$ values we calculated from drip water at this site ($ISST_{direct}$ = -17.3 ± 0.3‰) The dominance of C_3 $\delta^{13}C$ values imparted to drip water and calcite at this site may represent a greater proportion of C_3 grasses in this area. Another possibility would be the presence of deep C_3 plant roots from before the brush and trees were removed that are still respiring or undergoing decomposition and that would maintain $\delta^{13}C_s$ near values associated with deeply-rooted plants in the area. It is also possible that root-respired CO_2 or groundwater that has equilibrated with the root-respired CO_2 of these plants has undergone advective transport to the ISST site. Prominent surficial karst features proximal to the surface expression of the ISST and ISLM sites are noted on Figure 7.

The contrasting magnitudes of $\delta^{13}C_{cc}$ variability between the two sites demonstrate the effect of protracted CO_2 degassing from drip water in a low pCO_2 cave

atmosphere. The ISST site is an indirectly-sourced drip site and is closer to the cave entrance with significant seasonal variability in pCO_2, while ISLM is directly-sourced and further from the cave entrance. We attribute T_{total} of drip water as the driving mechanism for high-magnitude $\delta^{13}C_{cc}$ variability in the modern calcite record produced by Feng et al. (in prep) based on observations for seasonal drip water $\delta^{13}C_{DIC}$ variability. Assuming that $\delta^{13}C_{cc}$ simply follows the behavior of $\delta^{13}C_{DIC}$, kinetic effects associated with the degassing of CO_2 likely drive departures from the respective vegetation baselines of each site.

3.2.4. Implications for central Texas speleothem carbon isotope records

We have constrained two factors that have major roles in controlling the carbon isotope composition of speleothem calcite in central Texas: 1) the signal from deeply-rooted surface vegetation and 2) kinetic isotope effects based on the magnitude of T_{total}. While we propose that these are likely the two primary controls on $\delta^{13}C_{cc}$ values, there is an array of conditions that could produce $\delta^{13}C_{cc}$ variations by one or both of these particular factors. Marked changes in surface vegetation may account for large-scale (> 1‰) variability in a speleothem carbon isotope record. Using the ranges reported in Badeck et al. (2005), a transition from vegetation with values equivalent to the lowest reported C_3 value to the highest C_4 value could be as much as ~26‰. In a speleothem record of seasonal to century-scale resolution, we would anticipate changes in $\delta^{13}C_{cc}$ of this nature to be gradual given the slow rate (decadal to millennial) of ecotone migration (Overpeck et al., 1992; Boutton et al., 1998; Bai et al., 2009; Bai et al., 2012).

Additionally, if $\delta^{13}C_s$ is controlled by a large component of decomposing SOM, the consequent overturn of the SOM pool from a change in surface vegetation may also slow the rate of change in speleothem $\delta^{13}C$ values.

Changes in the duration of exposure of drip water to cave-air will also result in large-scale variability of $\delta^{13}C_{cc}$. This is achieved by significantly lengthening $T_{total,}$ which can occur by either slowing the drip-rate, or modifying a flow path in such a way that the in-cave residence time of water along the flow path is altered. In order for degassing to occur, the presence of a strong gradient between [DIC] in cave drip water and cave-air pCO_2 is required. It is important to note that this gradient would be strongest in temperate and subtropical cave systems, and may be more difficult to assess for speleothem records from the tropics (James and Banner, 2008). Tropical caves at low-latitudes (e.g. Jinapsin Cave, Guam) are subject to ventilation on a diurnal scale or from synoptic weather patterns, and the degree of annual variation in surface air temperatures and cave-air pCO_2 is much smaller than at higher-latitude caves (Banner et al., 2007; James and Banner, 2008).

Under conditions conducive to CO_2 degassing from drip water, any drip site where T_{total} is maximized should elicit a shift in $\delta^{13}C_{cc}$ (on the order of ~0.47‰/hour; Figure 15) temporally that would be measurable in a speleothem calcite record. One mechanism to increase T_{total} would be to modify the flow path that drip water follows after entering the cave and prior to falling onto a speleothem. This modification could be abrupt or gradual and would only require an increase in the residence time of drip water as a sheet flow or droplet. For example, the gradual transition of a soda straw to a

stalactite, resulting in a film of drip water adhering to the stalactite (a direct drip site becoming an indirect site), would cause an increase in the reservoir size of the drip water and also increase T_{total}. Alternatively, T_{total} would be increased by simply reducing the drip-rate of the water supplying a speleothem. We would expect decreased drip-rates to represent the simplest and most probable process to increase $T_{total.}$ Given the significant seasonal impact of drought conditions on drip water flux into the caves we have studied, (Banner et al., 2007; this study), changes in T_{total} for a site would generally result in significantly more abrupt changes (on the scale of months) in $\delta^{13}C_{cc}$ of a speleothem record than we might expect from major surface vegetation changes.

To further explore the influence of T_{total} on $\delta^{13}C_{DIC}$ we evaluated drip rate variability over the same interval of the modern calcite record produced by Feng et al. (in prep.), and found covariation between $\delta^{13}C_{cc}$ and drip-rate (Figure 18). We contrasted this observation with drip water data from St. Michaels Cave, Gibraltar (Mattey et al., 2010) and for at least one drip site observed a similar covariation between drip-rate and $\delta^{13}C_{DIC}$ values, which we would expect to be 'translated' into equal-magnitude variations in $\delta^{13}C_{cc}$ (Figure 19). For the other drip sites in the Mattey et al. (2010) study we saw a trend between drip-rate and the magnitude of carbon isotope variations. Mattey et al. (2010) concluded that drip water $\delta^{13}C_{DIC}$ values vary nearly independently of discharge rate, whereas we argue that these values appear to be significantly influenced by drip-rate. We also argue that since these results are apparent in two cave systems separated by approximately 8200 km, they may be applicable for many temperate and subtropical cave systems. We argue that variability in speleothem $\delta^{13}C$ values will occur under low pCO_2

conditions and will be modulated by drip-rate, which must be below a given threshold value (likely cave-specific) in order for these changes in $\delta^{13}C_{DIC}$ and $\delta^{13}C_{cc}$ to be observable.

A major shift in vegetation from C_3 to C_4 plants would reflect changes to environmental conditions more favorable for C_4 dominance which include: increased MAT, higher aridity, and/or lower atmospheric pCO_2. Depending on the resolution of a speleothem record, and the region the speleothem formed in, one or more of these factors may be more plausible than the others. Regardless, major vegetation shifts would be expected to transpire at the decadal to century-scale. By contrast, changes in drip-rate would indicate more arid conditions and could to occur on decadal or even sub-annual timescales. Generally speaking, a large-magnitude increase in speleothem $\delta^{13}C$ temporally may simply suggest the onset of more arid surface conditions.

We propose that coupled speleothem $\delta^{13}C$ and $\delta^{18}O$ values may help separate the possible mechanisms that would cause temporal changes in $\delta^{13}C_{cc}$ values. Changes in speleothem $\delta^{18}O$ values are generally interpreted to reflect changes in cave temperature, the oxygen isotope composition of precipitation, and the degree of vadose groundwater evaporation (Mickler et al., 2006). If we can establish a cave-specific context for temporal variations in speleothem $\delta^{18}O$ values, then we may be able to better interpret the likely mechanism behind $\delta^{13}C$ variations and vice-versa. For example, if we establish that large decreases in speleothem $\delta^{18}O$ values represent a temporal increase in cave temperature, we could expect to see a synchronous increase in speleothem $\delta^{13}C$ values.

There are several examples of correlated, high-magnitude, and anti-phased $\delta^{18}O$ and $\delta^{13}C$ excursions in published speleothem records (Bar-Matthews et al., 1999; Frumkin et al., 2000; Bar-Matthews et al., 2003; Mickler et al., 2006; Genty et al., 2006; Spötl et al., 2008). For example, Frumkin et al. (2000) interpreted a speleothem isotope record from Jerusalem as demonstrating arid conditions in the region during an interglacial interval (Figure 20). Across this event $\delta^{13}C$ and $\delta^{18}O$ values are correlated and anti-phased. Whereas Frumkin et al. (2000) attributed increased $\delta^{13}C$ values during this interval to vegetation changes, we suggest that decreased T_{total} could account for the same magnitude of change observed. Both of these proposed mechanisms would result in the same trend and support the inference of more arid climate. These examples also show different magnitudes of variability in what might be considered a vegetation baseline. Further constraints on factors such as the contributions of SOM to $\delta^{13}C_{s,}$ or on $\varepsilon^{13}_{\text{calcite-DIC}}$ may limit some of the 'noise' in this baseline. These baseline variations may also represent changes within the dominant C_3 plant communities which would require rigorous surveys of $\delta^{13}C_s$ values for given biomes. It may also be possible to contrast temporal changes in speleothem $\delta^{13}C_{cc}$ with biomarkers in speleothem calcite in order to further reconstruct past environments and biomes (Rushdi et al., 2011; Blyth et al., 2011). The use of compound-specific isotope analysis may be able to further constrain shifts between C_3 and C_4 vegetation, but the application of these methods is still only in the early stages of development (Rushdi et al., 2011).

Further work may allow for distinguishing between changes in surface vegetation or T_{total} as the cause of variation in speleothem calcite $\delta^{13}C$ values. Changes in surface

vegetation would likely manifest as gradual changes of $\delta^{13}C$ values in a high-resolution speleothem record (seasonal to century-scale), whereas changes in T_{total} would account for typically more abrupt high-magnitude changes to and from the vegetation baseline. If these factors can be sufficiently disentangled for a given speleothem record, perhaps by coupled speleothem $\delta^{18}O$ values, there is strong potential for $\delta^{13}C$ values as a paleovegetation indicator and/or for a sense of surface aridity.

3.3: CONCLUSIONS

Our results indicate that the root-respired CO_2 of deeply-rooted plants strongly biases the carbon isotope composition of vadose groundwater that enters NB and IS as drip water. Throughout the year, directly-sourced cave drip water $\delta^{13}C_{DIC}$ values retain a strong correspondence to $\delta^{13}C_s$ under deeply-rooted plants. This indicated that the epikarst region is likely functioning as an open system, allowing for equilibrium isotope exchange reactions between groundwater and CO_2 respired in the soil horizon (or epikarst). This open system setting effectively overwhelms the host-rock contributions to the DIC pool and the effect of PCP, which would both otherwise influence the $\delta^{13}C_{DIC}$ values.

The process of kinetic CO_2 degassing from cave drip water is an addition major control on $\delta^{13}C_{DIC}$ and thereby $\delta^{13}C_{cc}$. For all studied sites, calcite carbon isotope values closely track those of drip water, but the carbon isotope fractionation factors between HCO_3^- and $CaCO_3$ are variable. We have placed empirical constraints on the change in $\delta^{13}C_{DIC}$ with respect to time using an analogous water film thickness and under conditions

that would represent the highest possible rate of degassing in these central Texas caves. Therefore, we propose that large-scale variability in speleothem $\delta^{13}C$ records occurs by either 1) marked changes in surface vegetation or 2) changes in T_{total}. We postulate that speleothem climate records can be evaluated for processes that are associated with these two variables. Temperate/subtropical speleothem $\delta^{13}C$ records may be used as a means for tracking drastic vegetation turnover, or as a relative gauge of surface aridity. Future work will require further assessment of small-magnitude and large-magnitude variability as follows:

- Continued evaluation of variations in $\delta^{13}C_s$ and $\delta^{13}C_r$ as responses from surface vegetation from environmental and climatic stresses, and for differences among biomes of deeply-rooted plants.
- Assessments of SOM carbon isotope compositions coupled with SOM incubation experiments to understand the role of decomposition in this system and the variability it can provide.
- Quantification of PCP and host-rock dissolution effects by radiocarbon and trace element analyses to demonstrate the 'strength' of an open system at 'resetting' the carbon isotope composition of cave drip water.
- Further constraints on the relationship between time and kinetic CO_2 degassing of drip water particularly with varying cave-air pCO_2, [DIC], and film thickness (and other surface-area-to-volume relationships).

- Modeling the rate of shifts in speleothem $\delta^{13}C$ values to best distinguish the onset of a change in either of these two primary variables under an array of different conditions.
- Exploring the application of biomarkers and compound-specific isotope analysis in speleothem calcite to separate distinct biotic carbon isotope values (e.g. C_3 from C_4, or vegetation from microbial).

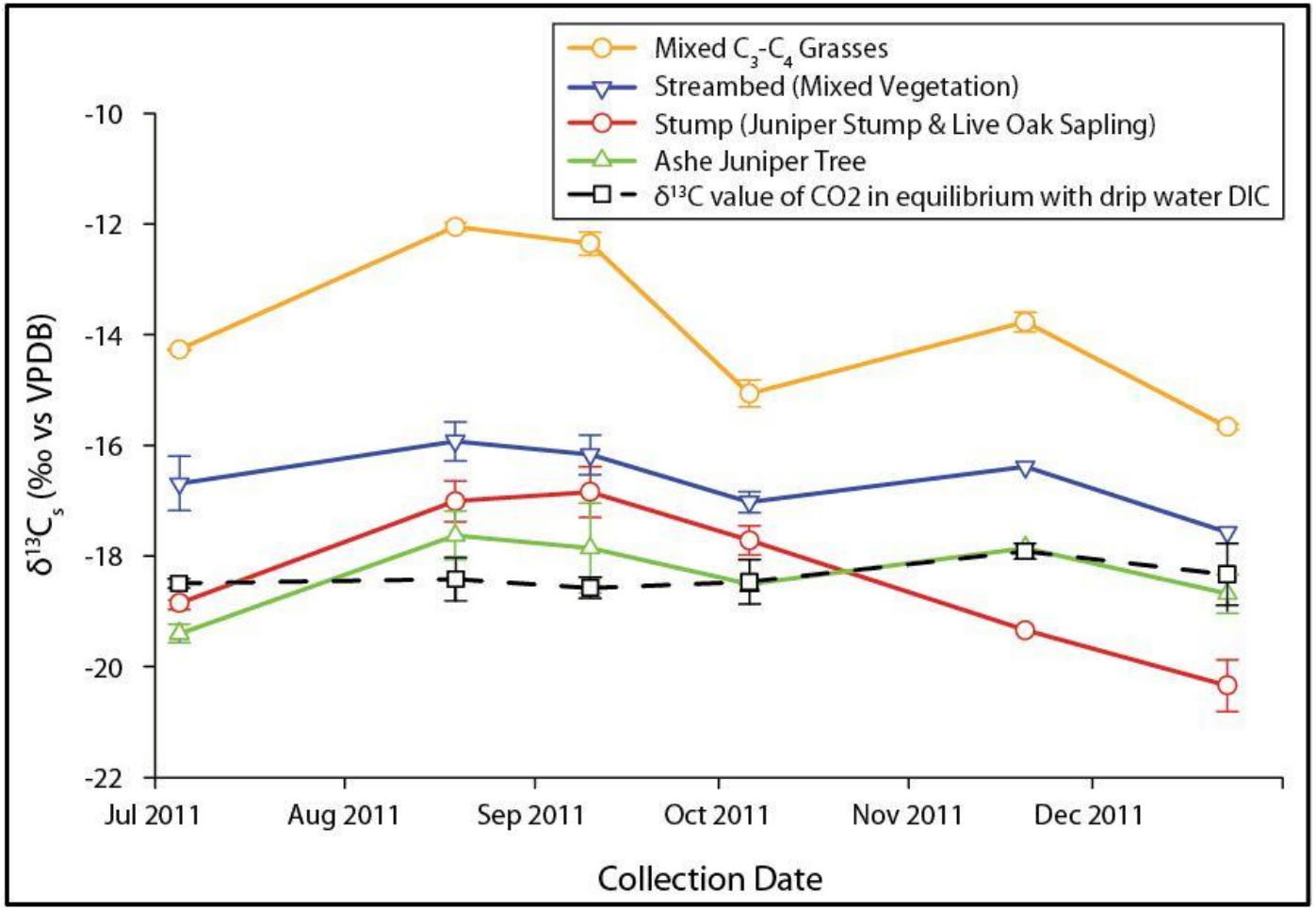

Figure 9. Time-series of $\delta^{13}C_s$ values at Natural Bridge Caverns. Each time-series corresponds to a different set of soil gas wells underlying a specific type of vegetation. The dashed line represents the calculated $\delta^{13}C$ value of soil CO_2 in equilibrium with measured drip water $\delta^{13}C_{DIC}$ (NBCH; 22.7˚C). Each line is the average of the two deepest wells in the profile.

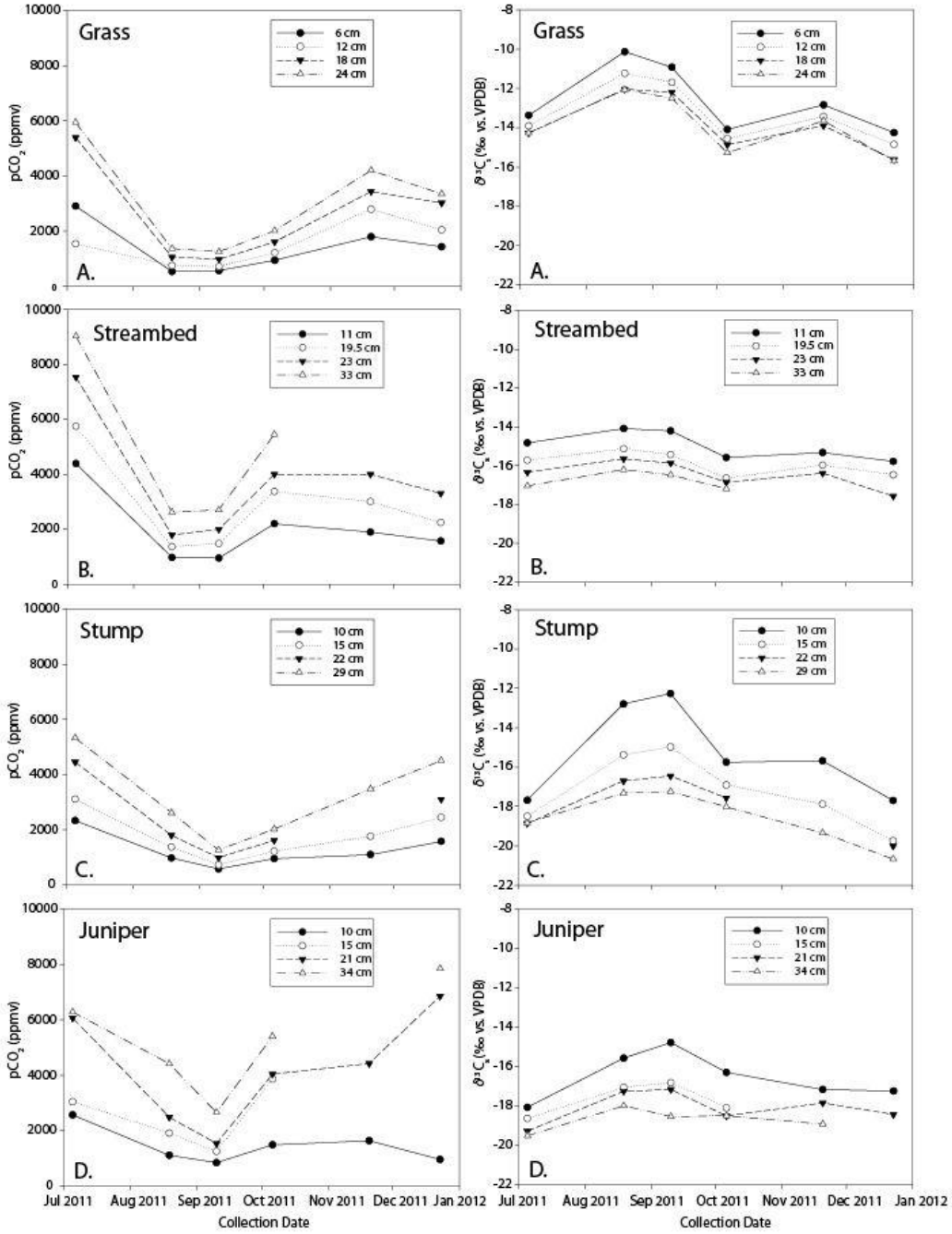

Figure 10. Natural Bridge Soil CO_2 and $\delta^{13}C_s$ time-series. Each line represents a well installed at a given depth in the soil profile. Each series of wells corresponds to a specific type of vegetation: mixed C_3-C_4 grasses (A), a streambed of mixed vegetation (B), an ashe juniper stump and live oak sapling (C), and an ashe juniper tree (D). When soil pCO_2 is low during the summer we can see the influence of atmospheric mixing on $\delta^{13}C_s$.

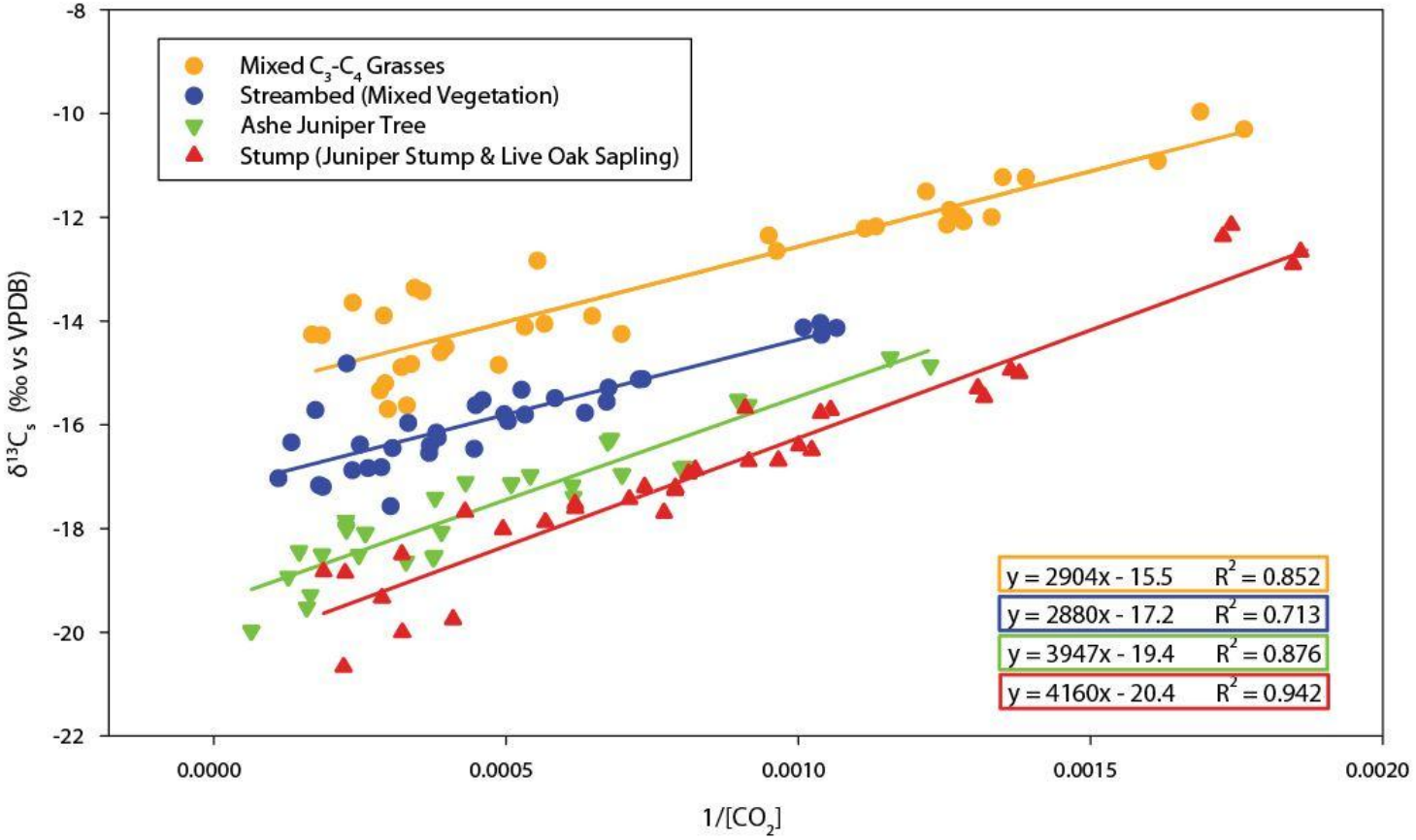

Figure 11. $\delta^{13}C_s$ and pCO_2 variations of soil gas from different vegetation at Natural Bridge Caverns. Straight lines on this plot represent two-endmember mixing between soil-respired and atmospheric CO_2. The y-intercept of each curve minus 4.4‰ corresponds to the value of $\delta^{13}C_r$.

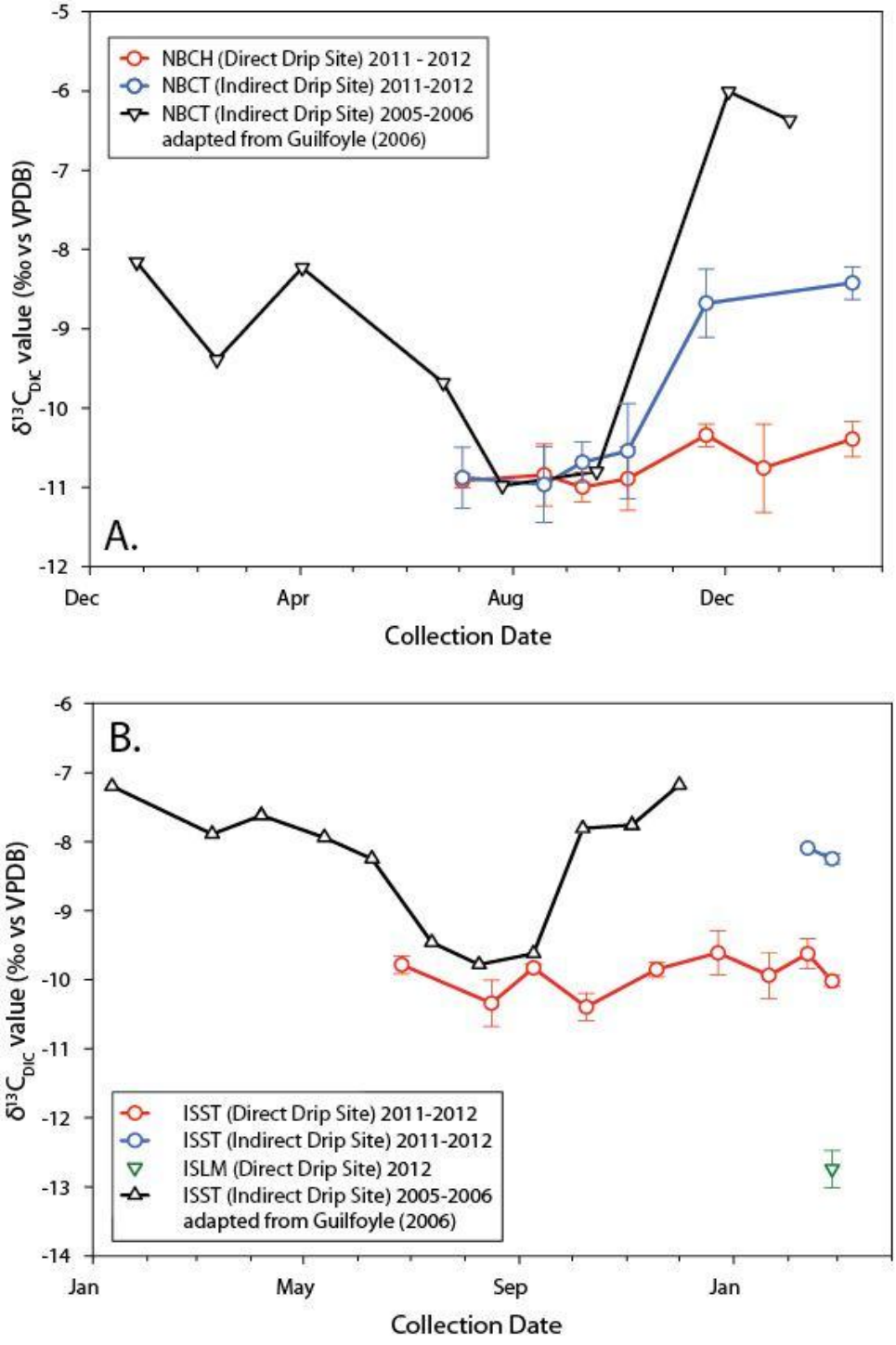

Figure 12. Drip water $\delta^{13}C_{DIC}$ time-series for Natural Bridge Caverns (A) and Inner Space Cavern (B). Data from this study is compared with the 2005-2006 data from Guilfoyle (2006) for the $ISST_{indirect}$ site.

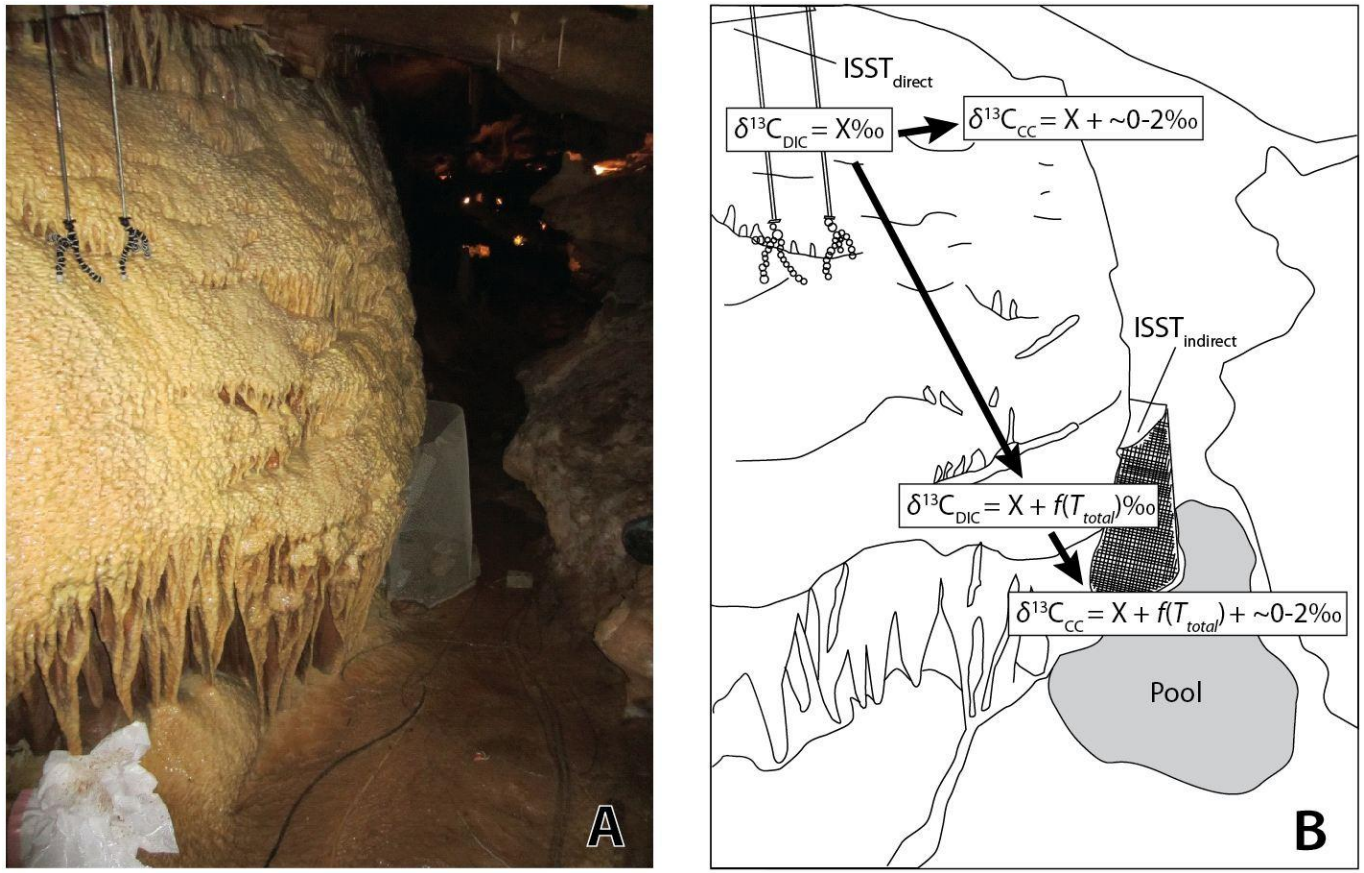

Figure 13. The relationship between drip water $\delta^{13}C_{DIC}$ and $\delta^{13}C_{cc}$. Depicted above are: (A) a photograph of the ISST drip sites and (B) a schematic of $\delta^{13}C_{cc}$ tracking $\delta^{13}C_{DIC}$. Starting with a drip water $\delta^{13}C_{DIC}$ composition of X‰, the calcite collected at the direct site would have a $\delta^{13}C_{cc}$ = X + ~0-2‰. For calcite collected from the indirect site with an initial source drip water $\delta^{13}C_{DIC}$ = X‰, where the drip water continued along a flow path for a given amount of time, $\delta^{13}C_{cc}$ = X + $f(T_{total})$ + ~0-2‰ (where $f(T_{total})$ is equivalent to the change in $\delta^{13}C_{DIC}$ as a function of T_{total}).

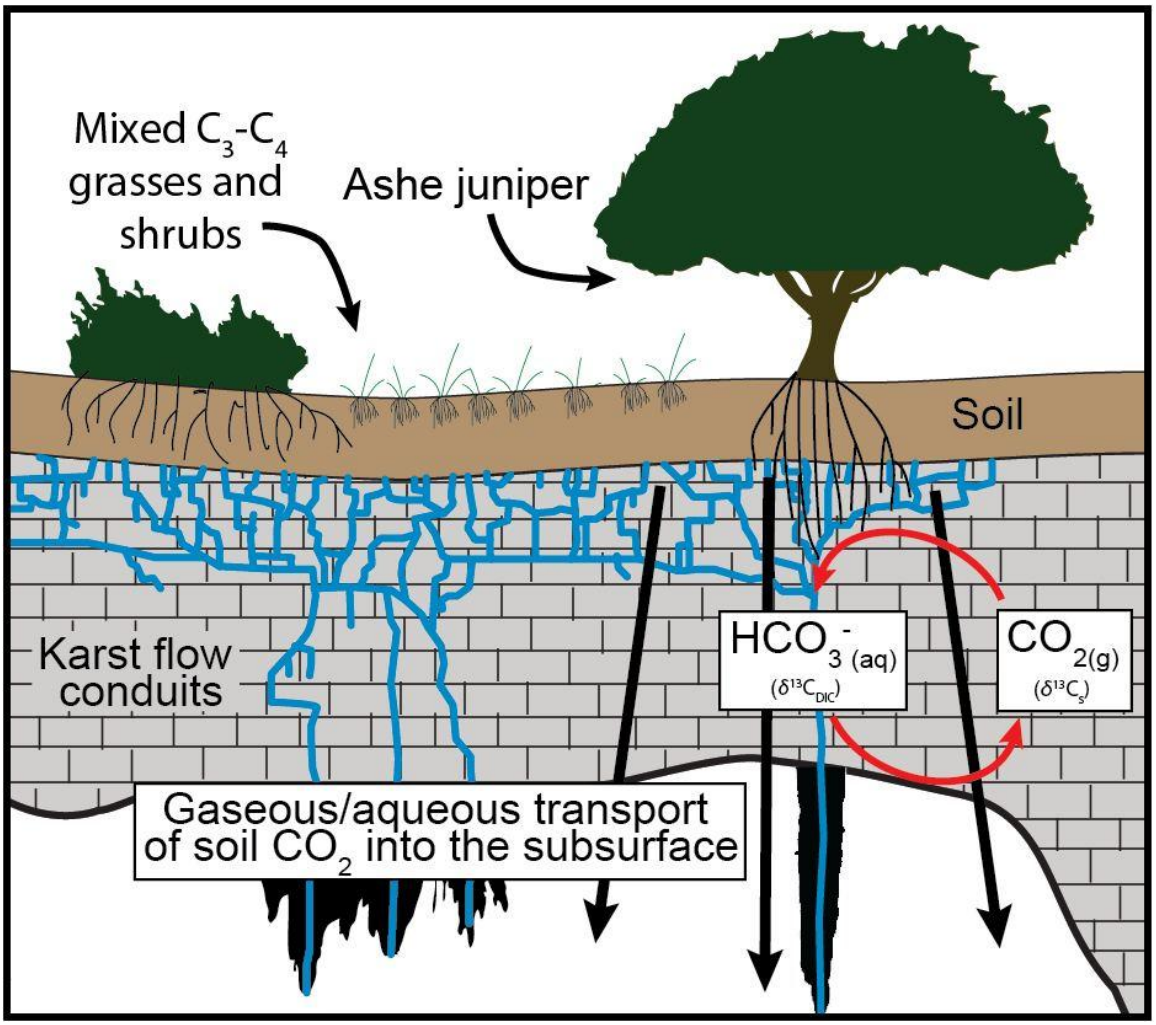

Figure 14. Schematic of open system $CO_{2(g)} – HCO_3^-{}_{(aq)}$ exchange in the soil and epikarst. Breecker et al. (submitted) have suggested that CO_2 enters a cave dominantly in the gaseous phase by advection and/or diffusion. Groundwater simultaneously percolates through the epikarst in contact with this CO_2 flux, which allows for continuous equilibrium carbon isotope exchange between DIC (HCO_3^-) and CO_2.

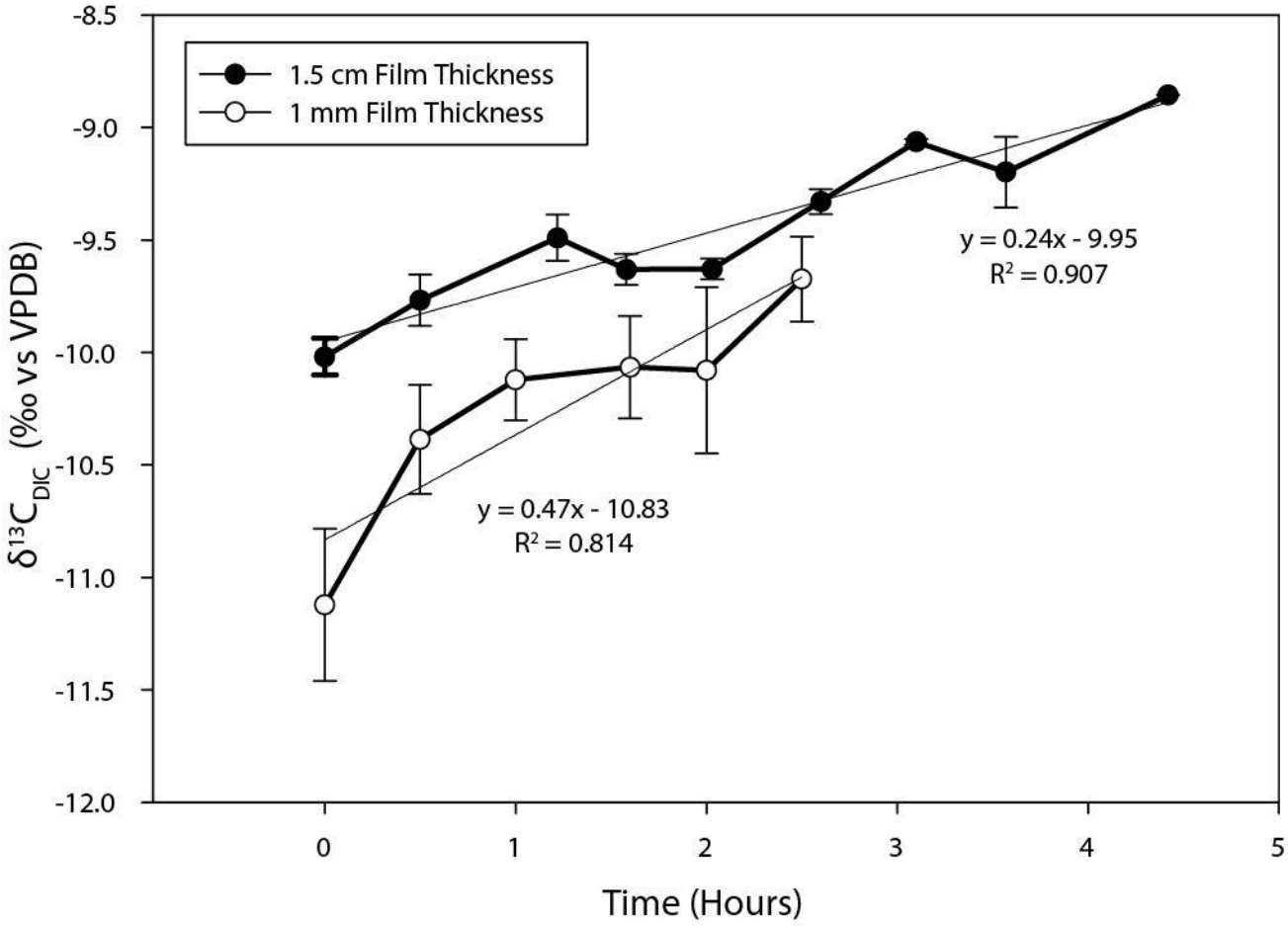

Figure 15. Drip water $\delta^{13}C_{DIC}$ as a function of time. The drip water from this experiment was sampled from $ISST_{direct}$ (1.5 cm) and at NBCH (1 mm). When we performed the degassing experiment with a higher exposed surface-area-to-volume (SA/V) ratio (1 mm film thickness SA/V = ~10; 1.5 cm film thickness SA/V = ~0.7), the rate of change in $\delta^{13}C_{DIC}$ increased.

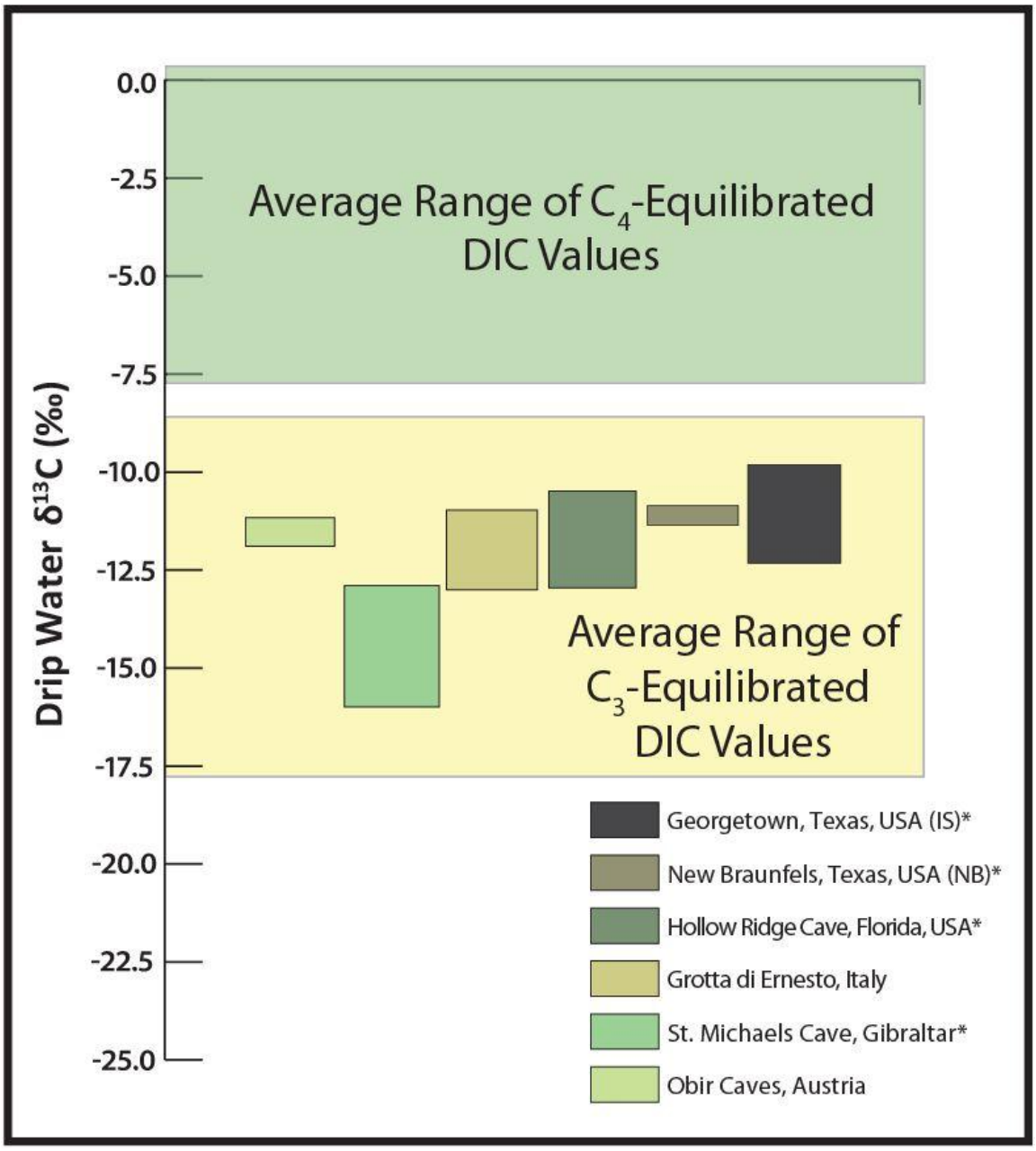

Figure 16. Comparison of drip water $\delta^{13}C_{DIC}$ values of subtropical and temperate caves around the world. In addition to the Texas caves (IS and NB) we have included Hollow Ridge Cave (Tremaine et al., 2011), Grotta di Ernesto (Frisia et al., 2011), St. Michaels Cave (Mattey et al., 2010), and Obir Caves (Spötl et al., 2005). The $\delta^{13}C_{DIC}$ values correspond to the season of high cave-air pCO_2 (minimum CO_2 degassing from drip water, low calcite precipitation). C_3 and C_4 ranges are reported in Badeck et al. (2005). *Denotes regions with mixed C_3-C_4 plant coverage.

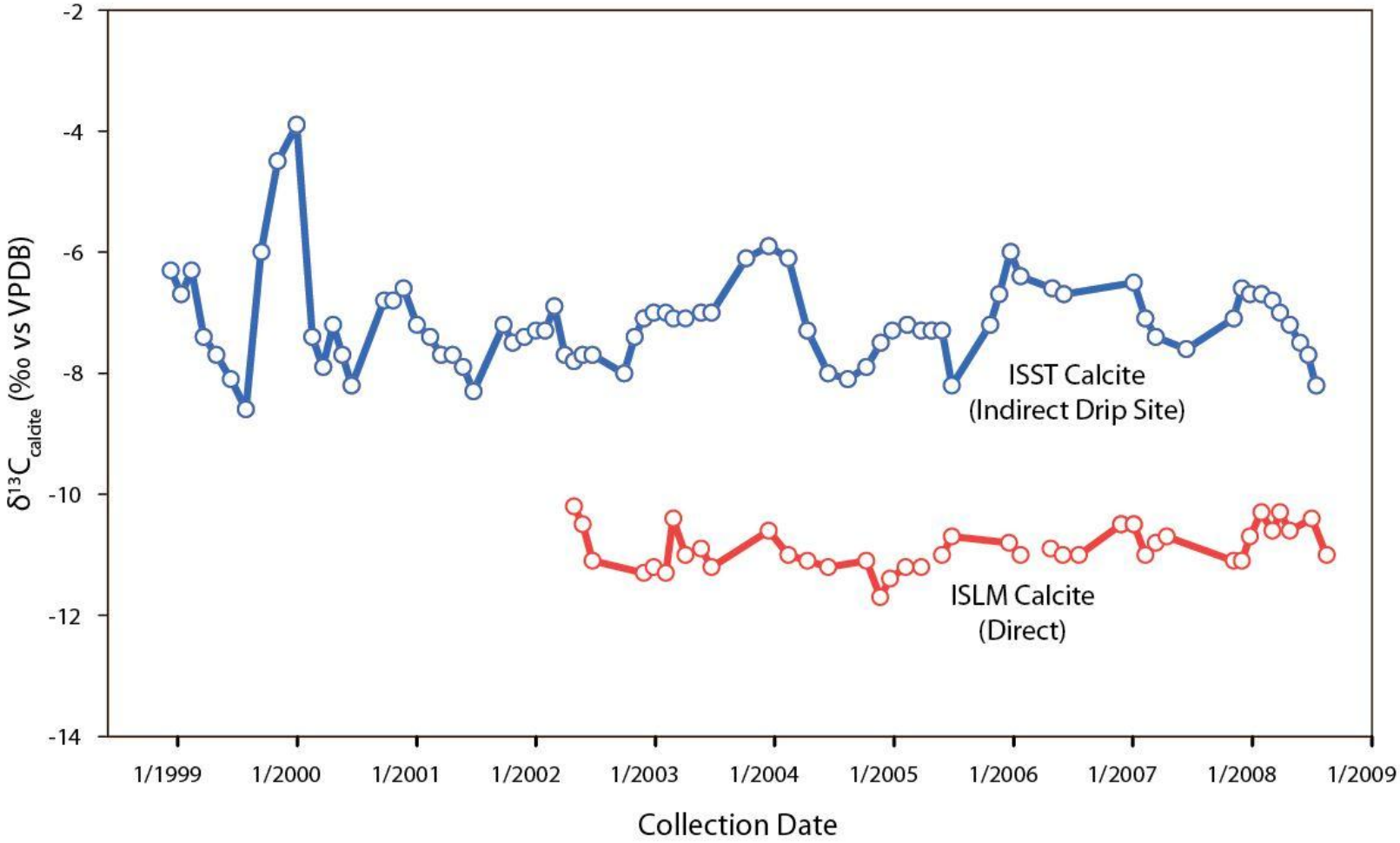

Figure 17. Modern calcite $\delta^{13}C$ time-series from Inner Space Cavern. The directly-sourced drip site (ISLM) demonstrates low-magnitude variability and corresponds to a grove of live oak trees at the study area which defines a vegetation baseline. The indirectly-sourced drip site (ISST) exhibits high-magnitude variability and corresponds to a vegetation baseline defined by cleared surface vegetation. ISST is also significantly closer to the cave entrance than ISLM. Modified from Feng et al. (in prep.).

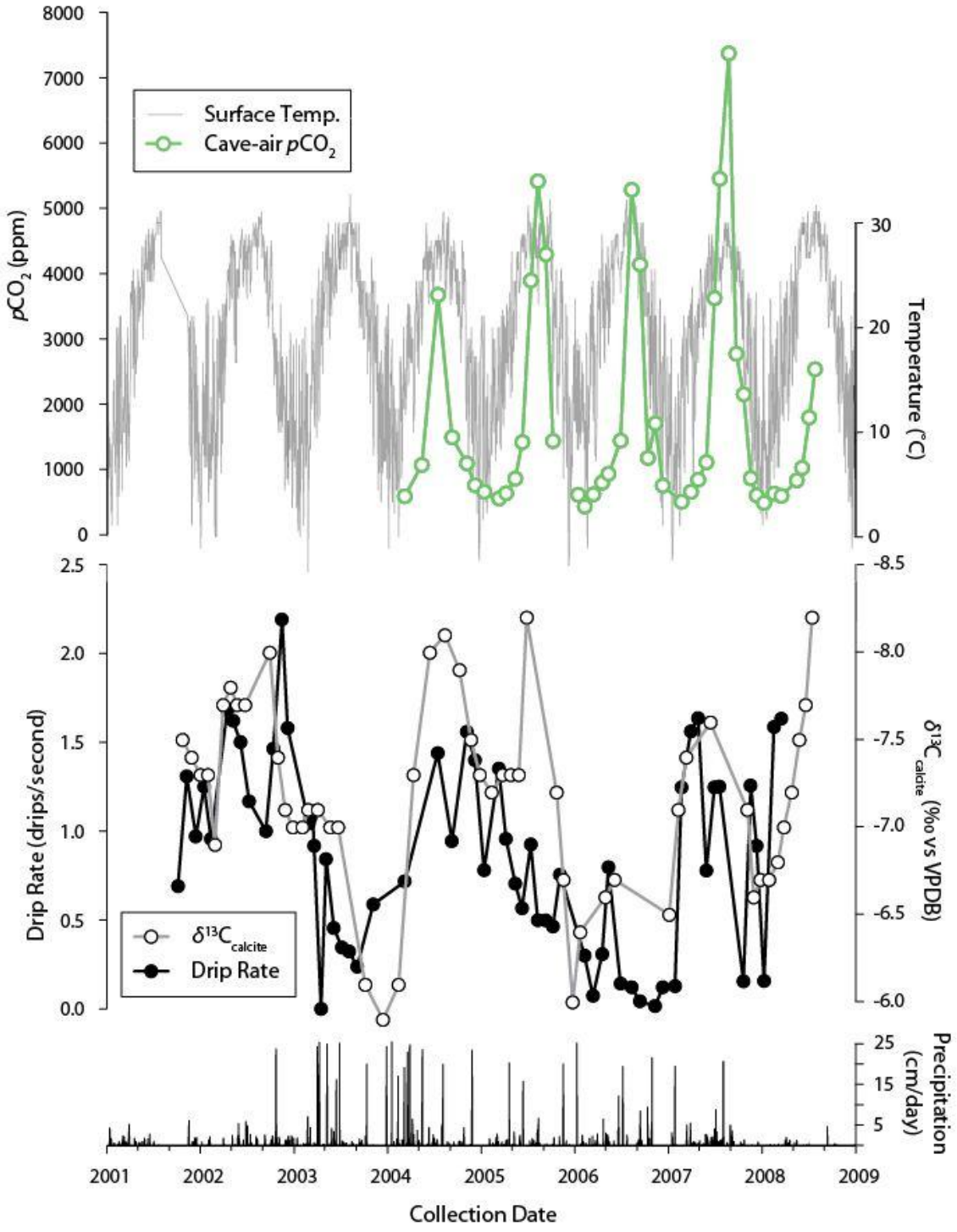

Figure 18. Drip-rate and $\delta^{13}C_{cc}$ covariation adapted from Feng et al. (in prep). The axis for carbon isotope values is reversed. Results indicate that $\delta^{13}C_{cc}$ values were modulated by drip-rate under low pCO_2 conditions. The highest magnitude changes in $\delta^{13}C_{cc}$ occurred when pCO_2 and drip-rate were at a minimum (e.g. January 2006 and January 2008)

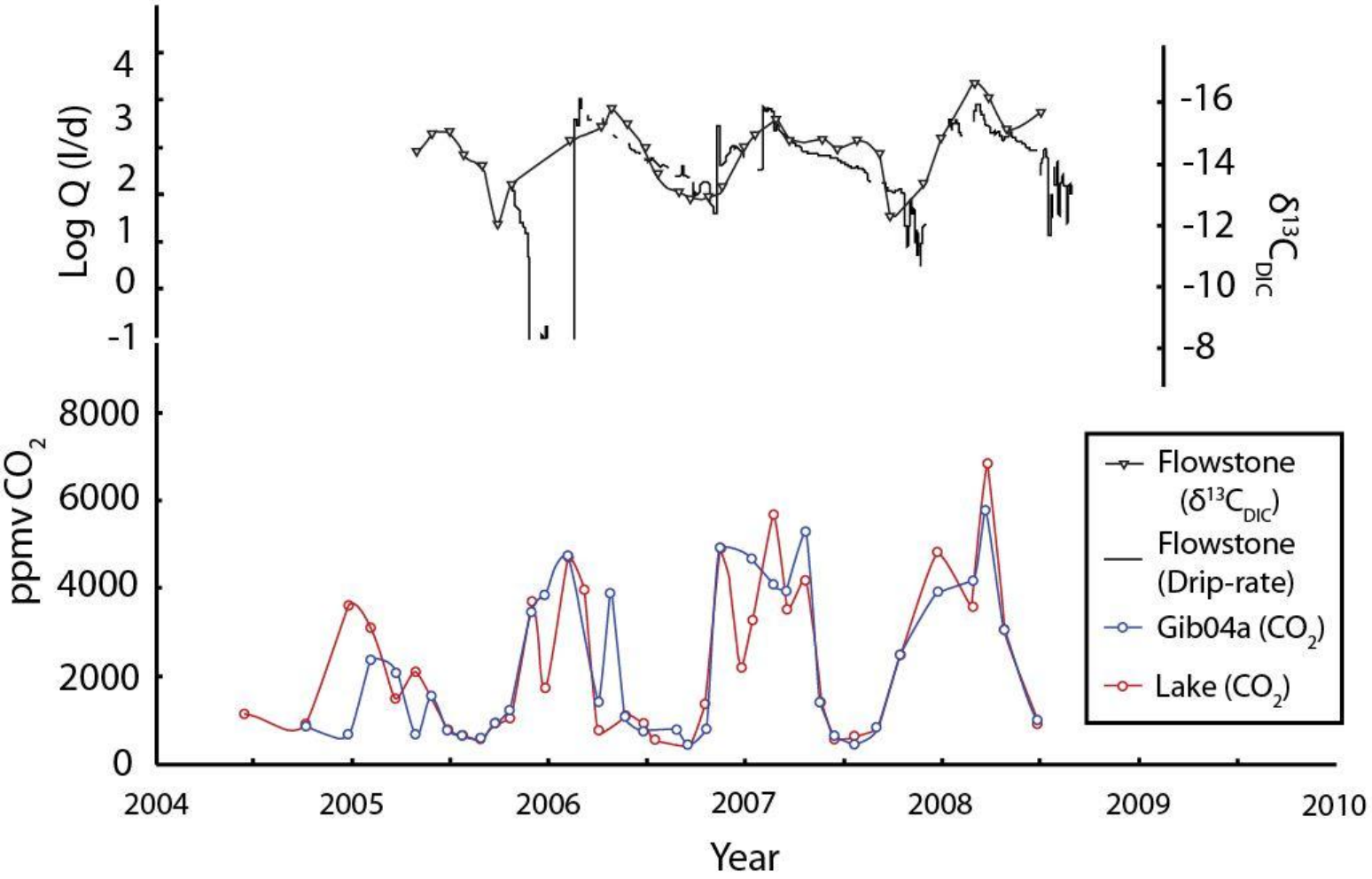

Figure 19. Drip-rate and $\delta^{13}C_{cc}$ covariation adapted from Mattey et al. (2010) at the Flowstone drip site. Features Gib04a and Flowstone are located ~4m apart within the same chamber of St. Michaels Cave, Gibraltar, and are therefore subject to the same pCO_2 conditions. The Lake site is at a considerably deeper interval within the cave.

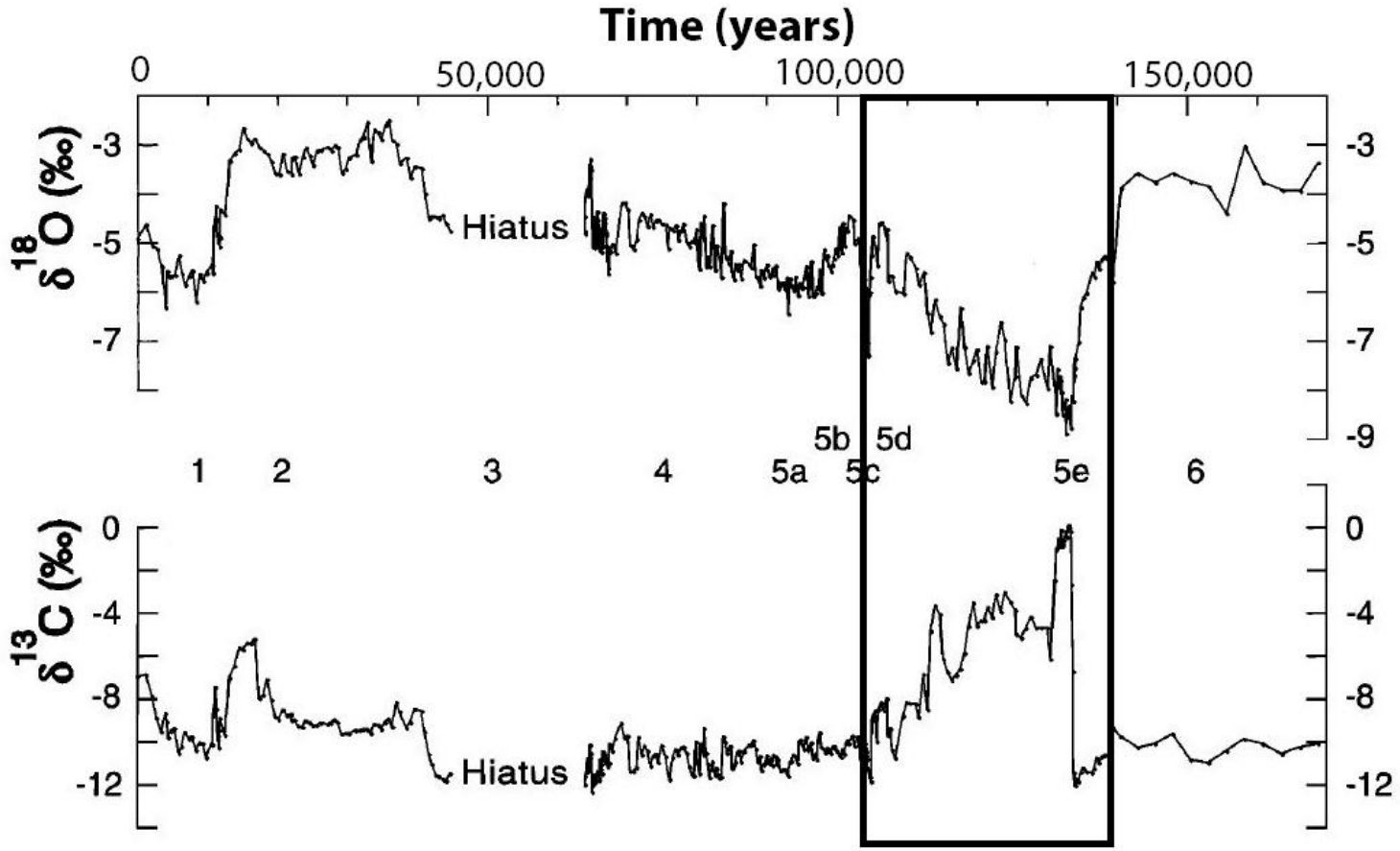

Figure 20. Speleothem isotope record from Jerusalem West Cave, Israel modified from Frumkin et al. (2000). The large excursions at stage 5e has been interpreted an indication of more arid conditions at this time. The correlated and anti-phased $\delta^{13}C$ and $\delta^{18}O$ values across this event are consistent with variations we would expect from increased aridity. Background $\delta^{13}C$ values may also define a vegetation baseline.

Table 2. Natural Bridge Caverns mean annual soil pCO_2, soil CO_2 $\delta^{13}C$, and calculated soil-respired CO_2 $\delta^{13}C$ values with depth (‰ vs. VPDB). For each case, we averaged the values of the two deepest wells when evaluating data in a time-series

Gas Wells (well number)	$\delta^{13}C_s$	$\delta^{13}C_r$	pCO_2 (ppm)	Depth (cm)
Mixed C_3-C_4 Grasses				
NBG4	-12.5 ± 1.8	-19.1 ± 1.1	1447 ± 824	6
NBG3	-13.0 ± 1.5	-19.4 ± 0.8	1619 ± 882	12
NBG2	-13.6 ± 1.4	-19.8 ± 0.7	2362 ± 1628	18
NBG1	-13.7 ± 1.5	-19.7 ± 0.8	2680 ± 1844	24
Streambed (mixed vegetation)				
NBSB4	-14.9 ± 0.7	-21.8 ± 0.9	1611 ± 1273	11
NBSB1	-15.8 ± 0.6	-21.9 ± 0.6	2608 ± 1457	19.5
NBSB3	-16.3 ± 0.7	-22.0 ± 0.5	3382 ± 1850	23
NBSB2	-16.7 ± 0.4	-22.0 ± 0.2	4371 ± 2442	33
Live oak sapling and juniper stump				
NBS4	-14.7 ± 2.2	-25.8 ± 2.0	983 ± 575	10
NBS3	-16.7 ± 1.7	-26.0 ± 1.1	1414 ± 860	15
NBS2	-17.5 ± 1.3	-25.5 ± 0.8	1859 ± 1264	22
NBS1	-18.8 ± 2.9	-25.1 ± 0.6	1965 ± 1556	29
Ashe juniper tree				
NBJ1	-16.2 ± 1.1	-24.5 ± 1.3	1332 ± 546	10
NBJ5	-17.4 ± 0.8	-24.2 ± 0.7	2200 ± 1044	15
NBJ4	-17.9 ± 0.8	-23.8 ± 0.6	3674 ± 2023	21
NBJ3	-18.6 ± 0.5	-23.9 ± 0.6	4810 ± 1887	34

Table 3. Cave drip site summary descriptions.

Site Name (Abbreviation)	Approx. distance from entrance (m)	Flow path (Indirect/Direct)	Approx. pCO_2 range (ppm)	Surface Vegetation
Natural Bridge				
Entrance Drip (NBED)	190	Indirect	400 – 8000	Ashe juniper (dominant), live oak, prickly pear, C_3-C_4 grasses
Castle Tabletop (NBCT)	235	Indirect	400 – 8000	Ashe juniper (dominant), live oak, prickly pear, C_3-C_4 grasses
Chandelier (NBCH)	250	Direct	400 – 8000	Ashe juniper (dominant), live oak, prickly pear, C_3-C_4 grasses
Inner Space				
Stone of Time (direct) ($ISST_{direct}$)	270	Direct	400 – 6500	C_3-C_4 grasses (dominant), impervious cover
Stone of Time (indirect) ($ISST_{indirect}$)	270	Indirect	400 – 6500	C_3-C_4 grasses (dominant), impervious cover
Lake of the Moon (ISLM)	460	Direct	400 – 10000	Live oak (dominant), prickly pear, C_3-C_4 grasses and a single ashe juniper tree

Table 4. Natural Bridge Caverns and Inner Space Cavern drip water $\delta^{13}C_{DIC}$, and calculated equilibrium CO_2 $\delta^{13}C$ values (‰ vs. VPDB).

Drip Site	Collection Date	$\delta^{13}C_{DIC}$	Equilibrium CO_2 $\delta^{13}C$	Water temperature (˚C)
NBCT (indirect)				
	7/5/2011	-10.9 ± 0.4	-	-
	8/19/2011	-11.0 ± 0.5	-18.4	22.8
	9/10/2011	-10.7 ± 0.3	-18.0	23.3
	10/6/2011	-10.5 ± 0.6	-17.9	23.0
	11/20/2011	-8.7 ± 0.4	-16.1	23.1
	2/12/2012	-8.4 ± 0.2	-16.0	21.7
NBCH (direct)				
	7/5/2011	-10.9 ± 0.1	-	-
	8/19/2011	-10.8 ± 0.4	-18.3	22.8
	9/10/2011	-11.0 ± 0.2	-18.4	23.3
	10/6/2011	-10.9 ± 0.4	-18.3	23.0
	11/20/2011	-10.3 ± 0.1	-17.7	23.1
	12/23/2011	-10.8 ± 0.6	-18.2	22.5
	2/12/2012	-10.4 ± 0.2	-18.0	21.7
ISST (indirect)				
	2/12/2012	-8.1*	-16.1	21.1
	2/26/2012	-8.2 ± 0.1	-16.0	21.5

Table 4. Cont.

ISST (direct)				
	6/26/2011	-9.8 ± 0.1	-	-
	8/16/2011	-10.3 ± 0.3	-	-
	9/9/2011	-9.8 ± 0.1	-17.3	22.9
	10/9/2011	-10.4 ± 0.2	-17.9	22.2
	11/18/2011	-9.9 ± 0.1	-17.4	22.1
	12/23/2011	-9.6 ± 0.3	-17.2	21.4
	1/21/2012	-9.9 ± 0.3	-17.7	20.6
	2/12/2012	-9.6 ± 0.2	-17.3	21.1
	2/26/2012	-10.0 ± 0.1	-17.6	21.5
ISLM (direct)				
	2/26/2012	-12.7 ± 0.3	-20.3	21.5

*Only a single sample collected; all other samples were collected with 4 total replicates.

Table 5. Natural Bridge Caverns and Inner Space Cavern drip water $\delta^{13}C_{DIC}$ change with respect to time.

Drip Site	Collection Date	Time of total elapsed degassing (hours)	$\delta^{13}C_{DIC}$	pH (± 0.08)	Water temperature (˚C)
ISST (direct)					
	2/26/2012	0.0	-10.0 ± 0.1	7.81	21.6
	2/26/2012	0.5	-9.8 ± 0.1	-	-
	2/26/2012	1.22	-9.5 ± 0.1	-	-
	2/26/2012	1.58	-9.6 ± 0.1	8.19	21.8
	2/26/2012	2.03	-9.6 ± 0.0	8.23	21.5
	2/26/2012	2.60	-9.3 ± 0.1	8.12	22.1
	2/26/2012	3.10	-9.1 ± 0.0	8.21	22.2
	2/26/2012	3.57	-9.2 ± 0.2	8.14	21.5
	2/26/2012	4.42	-8.9 ± 0.0	8.24	21.5
NBCH (direct)					
	4/22/2012	0.0	-11.1 ± 0.3	7.72	21.9
	4/22/2012	0.5	-10.4 ± 0.2	8.20	22.7
	4/22/2012	1.0	-10.1 ± 0.2	8.20	21.7
	4/22/2012	1.6	-10.1 ± 0.2	8.29	22.0
	4/22/2012	2.0	-10.1 ± 0.4	8.24	8.24
	4/22/2012	2.5	-9.7 ± 0.2	8.29	8.29

Table 6. Natural Bridge Caverns and Inner Space Cavern $\delta^{13}C_{cc}$ values (‰ vs. VPDB).

Drip Site	Collection Date		$\delta^{13}C_{cc}$*	$\delta^{13}C_{DIC}$	$\Delta^{13}C_{m\text{-}e}$**
ISST (direct)					
	2/26/2012	Minimum	-8.7	-10.0 ± 0.1	+0.3
	2/26/2012	Maximum	-8.1	-10.0 ± 0.1	+0.9
NBCT (indirect)					
	2/23/2012	Minimum	-8.4	-8.4 ± 0.2	-0.9
	12/30/2011	Maximum	-7.4	-8.7 ± 0.4	+0.3
ISST (indirect)					
Feng et al. (in	12/25/2004	Minimum	-7.2	-7.3	-0.9
prep)	12/22/2005	Maximum	-6.0	-6.9	-0.1

*$\delta^{13}C_{cc}$ samples were collected nearest to the source of drip water impact on the plate.
**Calculated from the drip water value most closely associated with the collected plate calcite temporally.

Appendix A. Site Descriptions

Soil Gas Well Site Locations

Please refer to Figure 7 for a composite image depicting soil gas well locations.

Soil Gas Well Site Descriptions

Inner Space Cavern

At Inner Space Cavern both transient and permanently installed soil gas wells were sampled. The permanent wells are installed directly south of the Capital Area Rural Transportation System (CARTS) station parking lot (at 3620 South Austin Ave., Georgetown, TX; directly across I-35 from the Inner Space Cavern visitor's center). There are a total of 5 wells installed all within ~25-30 m of one another. The wells generally lie on a line running N-S from the parking lot. All wells have been marked with fluorescent orange flagging tape. We also noted prominent karst features near the soil gas wells. These features included: large limestone rock exposures, surface fractures, and streambeds and depressions that coincided with large fracture patterns and portions of the cave below.

Cactus 1 (C1) is the southernmost well and is located in a large patch of Texas prickly pear (*Opuntia engelmanii*) ~50 m due south from the parking lot (30˚36'34.3"N, 97˚41'05.8"W).

Cactus 2 (C2) is adjacent to and ~5 m north of well C1 (30˚36'34.5"N, 97˚41'05.7"W). This well is also situated in a patch of Texas prickly pear (*Opuntia engelmanii*).

Center 1 (Cen1) is ~10-15 m north of wells C1 and C2. It is located near a southern live oak tree (*Quercus virginiana;* 30˚36'34.8"N, 97˚41'05.8"W).

Center 2 (Cen 2) is ~1 m from Cen1 and is located closer to the trunk of the southern live oak tree (*Quercus virginiana*) where Cen 1 can be found.

North 1 (N1) is located ~10 m north of wells Cen 1 and Cen 2 . This well is situated in a variety of vegetation including cactus, low-lying shrubs and grasses, and live oak trees (30˚36'34.8"N, 97˚41'06.2"W).

Natural Bridge Caverns

At Natural Bridge Caverns permanent soil gas wells were installed SE of the visitor's center. The wells are located almost directly south of the entrance to the South Cave. Specifically, there is a small, roofed structure built to house one of the cave ventilation fans (we refer to as the 'fan house') south of the South Cave entrance, and the wells are installed in an approximate 30 m radius south of this structure. The wells are on the opposite side of a chain-link fence, which has an opening west of the fan house. The wells are clustered into groups of 4 wells (at different depths) at 4 different sites. All sites are marked with fluorescent orange flagging tape. We also noted prominent karst features near the soil gas wells. These features included: large limestone rock exposures, surface fractures, and streambeds and depressions that coincided with large fracture patterns and appeared to follow the entire extent of the North Cave.

Natural Bridge Grass (NBG) is located in a patch of mixed C_3-C_4 grasses and is the farthest site to the east. This site is also east of the fan house (on the south side of the fence), but to the west of a dry creek bed (runs ~N-S). The wells are also marked by a large piece of limestone at the center of the grass (29˚41'27.7"N, 98˚20'29.7"W).

Natural Bridge Juniper (NBJ) is located ~10-15 m west of the NBG site (29˚41'27.3"N, 98˚20'30.41"W). The site is directly in-line with the fan-house to the south and is installed at the base of an ashe juniper tree (*Juniperus asheii*).

Natural Bridge Stump (NBS) is located ~10 m west of NBJ and is closer to the fence. The wells are installed at an old juniper (*Juniperus asheii*) stump with a live oak sapling (*Quercus virginiana*) directly next to the stump (29˚41'27.6"N, 98˚20'31.1"W).

Natural Bridge Streambed (NBSB) is an additional site that is located in the streambed between the entrances to the North Cave and the South Cave. This site is separate from the other 3, and is ~50 m north of the fan house (30˚36'30.2"N, 97˚41'32.1"W).

Drip Site Locations

Please refer to Figures 6 and 7 for a cave map and composite image depicting drip site locations.

Drip Site Descriptions

Inner Space Cavern

We collected samples from 3 main drip sites within Inner Space Caverns. Two of these sites were established prior to this study and have been actively monitored for years.

Inner Space Cavern Flowing Stone of Time – Rear Drip ($ISST_{indirect}$) has been studied for over 12 years and is described in Guilfoyle (2006) and Musgrove (2000). This feature is located in the 'Discovery Room' of the cavern, and the site is on the backside of the feature. This site is also documented in Figure 13. We collected drip water and plate calcite samples from this site.

Inner Space Cavern Flowing Stone of Time – Top Drip ($ISST_{direct}$) is a drip site located at the top of the backside of the Flowing Stone of Time. We began monitoring this site in this study. The site is also depicted in Figure 13. We collected drip water and plate calcite samples from this site.

Inner Space Cavern Lake of the Moon (ISLM) is a drip site in the 'Lake of the Moon' chamber of the cavern. This site is described in Guilfoyle (2006) and Musgrove (2000). This

room is at the end of the concrete path within the cave. The drip is another ~15 m passed the end of the path. This site was also established prior to this study. We collected drip water and plate calcite samples from this site.

Natural Bridge Caverns

We collected samples from 3 main drip sites within Natural Bridge Caverns. Two of these sites were established for this study, while one site has been monitored consistently for years. All sites are located in a chamber of the North Cave referred to as the 'Castle of White Giants.'

Natural Bridge Caverns Castle Tabletop (NBCT) has been monitored for a significant period of time and is described by Guilfoyle (2006). The drip site sits atop a large, flat-topped (mushroom-shaped) stalagmite near a large bend in the concrete path at the back of the chamber. Access to the site requires plastic bags and gloves to avoid damaging calcite features. We collected drip water and plate calcite samples from this site.

Natural Bridge Caverns Chandelier (NBCH) is a site we began monitoring in this study. It is located near the base of the stairwell that exits the Castle of White Giants chamber, and farther along the path from NBCT. This site is past the chained-off area at the base of the stairwell, and is situated below the feature known as the 'Chandelier.' The drip site is within arm's reach and has the highest drip rate in this particular area. We collected drip water samples from this site.

Natural Bridge Entrance Drip (NBED) is a site near the concrete path at the entry to the Castle of White Giants chamber. The drip site is within arm's reach and is on a feature similar in morphology to NBCT, but is only ~1 m tall. This feature is the first of its kind encountered when entering the chamber.

Appendix B. Data Tables

All field and lab measurements are summarized in the following data tables. We also include any and all data used from the Banner Research Group Cave Database.

Appendix B1. Complete Natural Bridge Caverns and Inner Space Cavern soil gas data.

Gas Wells (well number)	Collection Date	$\delta^{13}C_s$ (‰ vs. VPDB)	Calculated $\delta^{13}C_r$ (‰ vs. VPDB)	pCO_2 (ppm)	Depth (cm)
Natural Bridge Caverns					
Mixed C_3-C_4 Grasses					
NBG4	7/5/2011	-13.4	-18.4	2913	6
	8/19/2011	-10.1	-18.0	539	6
	9/10/2011	-10.9	-19.5	576	6
	10/6/2011	-14.1	-19.9	952	6
	11/20/2011	-12.8	-18.4	1805	6
	12/23/2011	-14.3	-20.8	1433	6
NBG3					
	7/5/2011	-13.9	-20.1	1544	12
	8/19/2011	-11.2	-18.8	760	12
	9/10/2011	-11.7	-19.1	728	12
	10/6/2011	-14.6	-20.0	1218	12
	11/20/2011	-13.4	-18.6	2799	12
	12/23/2011	-14.8	-20.7	2050	12
NBG2					
	7/5/2011	-14.3	-19.0	5403	18
	8/19/2011	-12.0	-20.1	1060	18
	9/10/2011	-12.2	-19.5	985	18
	10/6/2011	-14.9	-20.1	1613	18
	11/20/2011	-13.9	-18.9	3439	18
	12/23/2011	-15.6	-21.0	3358	18

Appendix B1. Cont.

NBG1					
	7/5/2011	-14.3	-19.0	5952	24
	8/19/2011	-12.1	-19.9	1375	24
	9/10/2011	-12.5	-19.3	1261	24
	10/6/2011	-15.3	-20.5	2022	24
	11/20/2011	-13.6	-18.5	4206	24
	12/23/2011	-15.7	-21.0	3358	24
Streambed (mixed vegetation)					
NBSB4					
	7/5/2011	-14.8	-19.8	4390	11
	8/19/2011	-14.1	-22.2	977	11
	9/10/2011	-14.2	-22.6	950	11
	10/6/2011	-15.6	-21.4	2203	11
	11/20/2011	-15.3	-21.4	1899	11
	12/23/2011	-17.8	-22.5	1574	11
NBSB1					
	7/5/2011	-15.7	-20.6	5752	19.5
	8/19/2011	-15.1	-22.1	1368	19.5
	9/10/2011	-15.4	-22.2	1484	19.5
	10/6/2011	-16.6	-22.0	3377	19.5
	11/20/2011	-16.0	-21.4	3010	19.5
	12/23/2011	-16.5	-22.5	2246	19.5

Appendix B1. Cont.

NBSB3					
	7/5/2011	-16.3	-21.1	7535	23
	8/19/2011	-15.6	-22.0	1795	23
	9/10/2011	-15.9	-22.0	2000	23
	10/6/2011	-16.9	-22.1	4004	23
	11/20/2011	-16.4	-21.6	3999	23
	12/23/2011	-17.6	-23.1	3305	23
NBSB2					
	7/5/2011	-17.0	-21.7	9034	33
	8/19/2011	-16.2	-21.9	2619	33
	9/10/2011	-16.5	-22.1	2708	33
	10/6/2011	-17.2	-23.5	5455	33
	11/20/2011	-	-	-	33
	12/23/2011	-	-	-	33
Live oak sapling/juniper stump					
NBS4					
	7/5/2011	-17.7	-23.9	2328	10
	8/19/2011	-12.8	-29.1	977	10
	9/10/2011	-12.3	-24.9	576	10
	10/6/2011	-15.7	-25.2	952	10
	11/20/2011	-15.7	-24.0	1095	10
	12/23/2011	-17.7	-26.1	1574	10
					10
NBS3					
	7/5/2011	-18.5	-24.3	3106	15
	8/19/2011	-15.4	-27.2	1368	15

Appendix B1. Cont.

NBS3 (cont.)					
	9/10/2011	-15.0	-27.0	728	15
	10/6/2011	-16.9	-23.7	1218	15
	11/20/2011	-17.9	-24.9	1763	15
	12/23/2011	-19.7	-26.2	2443	15
NBS2					
	7/5/2011	-18.9	-24.2	4451	22
	8/19/2011	-16.7	-25.9	1795	22
	9/10/2011	-16.4	-26.1	985	22
	10/6/2011	-17.6	-25.0	1613	22
	11/20/2011	-	-	-	22
	12/23/2011	-20.0	-26.0	3101	22
NBS1					
	7/5/2011	-18.8	-24.0	5330	29
	8/19/2011	-17.3	-25.2	2619	29
	9/10/2011	-17.2	-25.5	1261	29
	10/6/2011	-18.0	-24.8	2022	29
	11/20/2011	-19.3	-25.0	3476	29
	12/23/2011	-20.7	-26.1	4506	29
Ashe juniper tree					
NBJ1					
	7/5/2011	-18.1	-24.1	2565	10
	8/19/2011	-15.6	-23.8	1104	10
	9/10/2011	-14.8	-24.7	840	10

Appendix B1. Cont.

NBJ1	10/6/2011	-16.3	-23.5	1484	10
	11/20/2011	-17.2	-24.2	1630	10
	12/23/2011	-17.2	-27.7	954	10
NBJ5					
	7/5/2011	-18.6	-24.5	3037	15
	8/19/2011	-17.1	-23.6	1907	15
	9/10/2011	-16.8	-25.0	1246	15
	10/6/2011	-18.1	-23.5	3858	15
	11/20/2011	-	-	-	15
	12/23/2011	-	-	-	15
NBJ4					
	7/5/2011	-19.3	-24.3	6068	21
	8/19/2011	-17.3	-23.2	2482	21
	9/10/2011	-17.2	-24.5	1528	21
	10/6/2011	-18.5	-23.9	4033	21
	11/20/2011	-17.9	-24.2	4418	21
	12/23/2011	-18.4	-23.3	6855	21
NBJ3					
	7/5/2011	-19.5	-24.6	6284	34
	8/19/2011	-18.0	-23.2	4410	34
	9/10/2011	-18.5	-24.6	2656	34
	10/6/2011	-18.5	-23.6	5402	34
	11/20/2011	-	-	-	34

Appendix B1. Cont.

NBJ3 (cont.)					
	12/23/2011	-18.9	-23.8	7850	34
Inner Space Caverns					
Cactus 1 (prickly pear)					
C1	6/26/2011	-15.1	-19.9	5375	-
	8/16/2011	-11.3	-17.6	571	-
	9/9/2011	-12.8	-25.1	614	-
	10/9/2011	-17.7	-24.3	2020	-
	11/18/2011	-14.6	-23.7	905	-
	12/23/2011	-17.5	-23.5	2535	-
Cactus 2 (prickly pear)					
C2	6/26/2011	-17.4	-21.9	13720	-
	8/16/2011	-17.0	-22.6	2875	-
	9/9/2011	-16.7	-24.3	1398	-
	10/9/2011	-16.8	-24.6	1341	-
	11/18/2011	-18.6	-25.0	2287	-
	12/23/2011	-16.8	-21.6	7020	-
Live Oak 1					
Cen1					
	6/26/2011	-19.4	-24.0	17554	-
	8/16/2011	-13.2	-23.0	741	-
	9/9/2011	-12.8	-31.7	517	-
	10/9/2011	-20.8	-27.9	2144	-
	11/18/2011	-18.5	-25.5	1827	-

Appendix B1. Cont.

Cen 1 (cont.)					
	12/23/2011	-	-	-	-
Live Oak 2					
Cen 2					
	6/26/2011	-	-	-	-
	8/16/2011	-17.4	-24.7	1548	-
	9/9/2011	-17.6	-28.0	987	-
	10/9/2011	-17.9	-20.7	998	-
	11/18/2011	-14.9	-24.2	896	-
	12/23/2011	-16.8	-25.4	1161	-
					-
Mixed Trees and Shrubs					
N1					
	6/26/2011	-	-	-	-
	8/16/2011	-17.7	-23.1	3772	-
	9/9/2011	-18.7	-25.8	1792	-
	10/9/2011	-19.1	-25.7	2249	-
	11/18/2011	-19.0	-25.0	2963	-
	12/23/2011	-20.5	-25.3	11003	-

Appendix B2. Complete Natural Bridge Caverns and Inner Space Cavern drip water data.

Drip Site	Collection Date	$\delta^{13}C_{DIC}$ (‰ vs.VPDB)	Equilibrium CO_2 $\delta^{13}C$	pH (± 0.08)	Alkalinity (meq/L)	Cave-air pCO_2 (ppm)*	Water temperature (˚C)
Natural Bridge Caverns							
NBCT (indirect)	7/5/2011	-10.9 ± 0.4	-	-	-		-
	8/19/2011	-11.0 ± 0.5	-18.4	7.51	-	5659 - 6691	22.8
	9/10/2011	-10.7 ± 0.3	-18.0	7.71	-	3516 – 3729	23.3
	10/6/2011	-10.5 ± 0.6	-17.9	7.89	2.9	1703 – 1919	23.0
	11/20/2011	-8.7 ± 0.4	-16.1	8.25	2.7	610 – 639	23.1
	12/23/2011	-	-	8.03	4.2	797**	22.5
	2/12/2012	-8.4 ± 0.2	-16.0	8.13	3.5	450 - 540	21.7
NBCH (direct)	7/5/2011	-10.9 ± 0.1	-	-	-		-
	8/19/2011	-10.8 ± 0.4	-18.3	7.53	-	5659 - 6691	22.8
	9/10/2011	-11.0 ± 0.2	-18.4	7.68	3.2	3516 – 3729	23.3
	10/6/2011	-10.9 ± 0.4	-18.3	7.73	3.2	1703 – 1919	23.0
	11/20/2011	-10.3 ± 0.1	-17.7	7.97	3.1	610 – 639	23.1
	12/23/2011	-10.8 ± 0.6	-18.2	7.82	4.8	797**	22.5
	2/12/2012	-10.4 ± 0.2	-18.0	7.84	4.0	450 - 540	21.7
Inner Space Caverns							
ISST (indirect)	2/12/2012	-8.1*	-16.1	8.04	-	580 – 540	21.1
	2/26/2012	-8.2 ± 0.1	-16.0	8.14	-	540 - 550	21.5

Appendix B2. Cont.

ISST (direct)							
	6/26/2011	-9.8 ± 0.1	-	-	-	-	-
	8/16/2011	-10.3 ± 0.3	-	-	-	-	-
	9/9/2011	-9.8 ± 0.1	-17.3	8.00	2.8	1023 – 1489	22.9
	10/9/2011	-10.4 ± 0.2	-17.9	7.90	2.9	1059 – 1109	22.2
	11/18/2011	-9.9 ± 0.1	-17.4	7.85	3.5	565 – 724	22.1
	12/23/2011	-9.6 ± 0.3	-17.2	7.95	4.8	463**	21.4
	1/21/2012	-9.9 ± 0.3	-17.7	7.88	5.3	512 – 554	20.6
	2/12/2012	-9.6 ± 0.2	-17.3	7.83	3.1	580 – 540	21.1
	2/26/2012	-10.0 ± 0.1	-17.6	7.84	4.6	540 - 550	21.5
ISLM (direct)							
	2/26/2012	-12.7 ± 0.3	-20.3	-	-	850**	21.5

*Cave-air pCO_2 ranges span the course of the collection day, tracking CO_2 change from arrival to departure at the field site.
**Indicates only one measurement was taken.

Appendix B3. Complete Natural Bridge Caverns and Inner Space Cavern calcite data.

Drip Site	Collection Date	Sample location (on-plate)	$\delta^{13}C_{cc}$* (‰ vs.VPDB)	$\delta^{13}C_{DIC}$ (‰ vs.VPDB)	$\varepsilon^{13}C_{calcite\text{-}DIC}$** (‰ vs.VPDB)	$\Delta^{13}C_{m\text{-}e}$** (‰ vs.VPDB)
ISST						
(direct)***	3/10/2012	center	-8.7	-10.0 ± 0.1	1.3	+0.3
	3/10/2012	center	-8.1	-10.0 ± 0.1	1.9	+0.9
	3/10/2012	edge	-8.0	-10.0 ± 0.1	2.0	+1.0
	3/10/2012	edge	-7.9	-10.0 ± 0.1	2.1	+1.1
	3/10/2012	edge	-7.3	-10.0 ± 0.1	2.7	+1.7
	3/10/2012	edge	-5.0	-10.0 ± 0.1	5.0	+4.0
NBCT						
(indirect)	12/1/2011	center	-7.5	-8.7 ± 0.4	1.2	+0.2
	12/30/2011	center	-7.4	-8.7 ± 0.4	1.3	+0.3
	12/30/2011	edge	-7.4	-8.7 ± 0.4	1.3	+0.3
	1/27/2012	center	-8.2	-8.4 ± 0.2	0.2	-0.8
	1/27/2012	edge	-8.2	-8.4 ± 0.2	0.2	-0.8
	2/23/2012	center	-8.3	-8.4 ± 0.2	0.1	-0.9
	2/23/2012	center	-8.3	-8.4 ± 0.2	0.1	-0.9
	2/23/2012	edge	-8.4	-8.4 ± 0.2	0.0	-1.0

*$\delta^{13}C_{cc}$ samples were collected nearest to the source of drip water impact on the plate.

**Calculated from the drip water value most closely associated with the collected plate calcite temporally.

***Samples were collected plates placed on the Lexan® flow channel. The data corresponds to the first plate (immediately underlying the dripsite) of the three. Subsequent plates did not accumulate enough calcite for analysis. Improvements on the apparatus will allow for increased accumulation on these plates.

Appendix B4. Temperature data measured at ISST and NBCT from the Banner Research Group Cave Database (as of 2011).

Drip Site	Measurement Date	Type of measurement	Temperature (˚C)
ISST	10/5/2001	air	21.3
ISST	11/8/2001	air	21
ISST	12/14/2001	air	21
ISST	1/15/2002	air	20.4
ISST	2/11/2002	air	19.7
ISST	4/16/2002	air	20.3
ISST	5/9/2002	air	20.9
ISST	6/6/2002	air	20.9
ISST	7/10/2002	air	21.3
ISST	8/7/2002	air	21.3
ISST	9/13/2002	air	21.3
ISST	10/12/2002	air	16.9
ISST	11/15/2002	air	15.4
ISST	12/7/2002	air	20.3
ISST	1/16/2003	air	15.1
ISST	2/20/2003	air	14.8
ISST	2/21/2003	air	14.2
ISST	2/28/2003	air	14.8
ISST	3/6/2003	air	20.4
ISST	3/14/2003	air	14.6
ISST	3/20/2003	air	15
ISST	4/17/2003	air	15.8
ISST	5/6/2003	air	16.3
ISST	6/5/2003	air	16.6
ISST	7/7/2003	air	16.9
ISST	8/4/2003	air	17
ISST	9/4/2003	air	17.4
ISST	11/6/2003	air	20.9
ISST	3/8/2004	air	20.6
ISST	5/13/2004	air	20.3
ISST	7/15/2004	air	21.6
ISST	9/8/2004	air	21.5
ISST	11/5/2004	air	20.1
ISST	12/7/2004	air	21
ISST	1/12/2005	air	17.4
ISST	4/7/2005	air	21.6
ISST	8/9/2005	air	21.1
ISST	9/9/2005	air	26.4

Appendix B4. Cont.

ISST	10/7/2005	air	21.1
ISST	12/1/2005	air	
ISST	1/13/2006	air	21.2
ISST	2/8/2006	air	20.3
ISST	3/13/2006	air	19.7
ISST	4/17/2006	air	24
ISST	5/12/2006	air	21.5
ISST	6/28/2006	air	22.7
ISST	8/10/2006	air	20.6
ISST	9/12/2006	air	21.5
ISST	10/13/2006	air	21.4
ISST	11/10/2006	air	21.4
ISST	3/30/2007	air	21.7
ISST	1/9/2008	air	20.3
ISST	2/17/2008	air	20.6
ISST	3/16/2008	air	20.7
ISST	5/15/2008	air	20.9
ISST	6/5/2008	air	20.8
ISST	7/3/2008	air	21.3
ISST	7/25/2008	air	21.4
ISST	9/6/2008	air	21.2
ISST	12/14/2008	air	20.4
ISST	2/15/2009	air	18
ISST	3/17/2009	air	19.3
ISST	4/26/2009	air	20
ISST	5/17/2009	air	20
ISST	6/17/2009	air	20
ISST	7/17/2009	air	20.9
ISST	8/30/2009	air	21
ISST	9/16/2009	air	21.5
ISST	9/27/2009	air	21.1
ISST	10/25/2009	air	20.7
ISST	11/15/2009	air	20.5
ISST	12/9/2009	air	20
ISST	12/18/2009	air	19.6
ISST	1/23/2010	air	19.6
ISST	3/27/2010	air	19.1
ISST	4/30/2010	air	19.8
ISST	5/30/2010	air	20.6
ISST	6/29/2010	air	20.9
ISST	7/14/2010	air	21.4
ISST	7/14/2010	air	21.3

Appendix B4. Cont.

ISST	7/14/2010	air	21.3
ISST	7/14/2010	air	21.7
ISST	7/14/2010	air	21.4
ISST	7/15/2010	air	21.3
ISST	7/15/2010	air	21.2
ISST	7/15/2010	air	21.7
ISST	7/15/2010	air	21.5
ISST	7/15/2010	air	21.8
ISST	7/15/2010	air	21.3
ISST	7/15/2010	air	21.3
ISST	7/29/2010	air	20.8
ISST	8/31/2010	air	21.1
ISST	9/26/2010	air	21
ISST	11/4/2010	air	20.1
ISST	11/30/2010	air	19.8
ISST	12/16/2010	air	20.4
ISST	1/29/2011	air	19
ISST	2/27/2011	air	20.1
ISST	5/15/2011	air	19.8
ISST	7/14/2011	air	22.2
ISST	9/11/2011	air	21.3
ISST	10/9/2011	air	20.7
ISST	5/31/2000	water	
ISST	6/30/2000	water	
ISST	8/1/2000	water	21.2
ISST	9/8/2000	water	
ISST	10/6/2000	water	20.5
ISST	11/3/2000	water	20.9
ISST	12/8/2000	water	19.7
ISST	1/23/2001	water	21.7
ISST	2/28/2001	water	20.4
ISST	4/3/2001	water	19.6
ISST	5/8/2001	water	21.8
ISST	6/7/2001	water	20.9
ISST	7/12/2001	water	21.4
ISST	8/16/2001	water	22.5
ISST	9/13/2001	water	21.7
ISST	10/5/2001	water	20.6
ISST	11/8/2001	water	21
ISST	12/14/2001	water	21.5
ISST	1/15/2002	water	19.8
ISST	2/11/2002	water	19.7

Appendix B4. Cont.

ISST	4/16/2002	water	20.2
ISST	5/9/2002	water	20.7
ISST	6/6/2002	water	21.2
ISST	7/10/2002	water	20.8
ISST	8/7/2002	water	21.6
ISST	9/13/2002	water	21
ISST	10/12/2002	water	21.4
ISST	11/15/2002	water	20.3
ISST	12/7/2002	water	20
ISST	1/16/2003	water	19.3
ISST	2/20/2003	water	19.3
ISST	2/21/2003	water	
ISST	2/28/2003	water	
ISST	3/6/2003	water	18.6
ISST	3/14/2003	water	19.5
ISST	3/20/2003	water	19.2
ISST	4/17/2003	water	19.6
ISST	5/6/2003	water	19.9
ISST	6/5/2003	water	20.2
ISST	7/7/2003	water	20.2
ISST	8/4/2003	water	20.3
ISST	9/4/2003	water	20.2
ISST	11/6/2003	water	19.6
ISST	1/19/2004	water	18.7
ISST	3/8/2004	water	18.8
ISST	5/13/2004	water	19.4
ISST	7/15/2004	water	19.8
ISST	9/8/2004	water	20
ISST	11/5/2004	water	19.4
ISST	12/7/2004	water	19.4
ISST	1/12/2005	water	19
ISST	3/10/2005	water	18.8
ISST	4/7/2005	water	18.8
ISST	5/13/2005	water	20
ISST	6/9/2005	water	20.7
ISST	7/13/2005	water	21.5
ISST	8/9/2005	water	21
ISST	9/9/2005	water	21.2
ISST	10/7/2005	water	20.8
ISST	11/4/2005	water	20
ISST	12/1/2005	water	20.4
ISST	1/13/2006	water	19.8

Appendix B4. Cont.

ISST	2/8/2006	water	19.4
ISST	3/13/2006	water	19.7
ISST	4/17/2006	water	21.2
ISST	5/12/2006	water	20.9
ISST	6/28/2006	water	22.3
ISST	8/10/2006	water	20.9
ISST	9/12/2006	water	
ISST	10/13/2006	water	22.1
ISST	1/27/2007	water	14.9
ISST	2/21/2007	water	19.4
ISST	3/30/2007	water	20.2
ISST	4/27/2007	water	20
ISST	5/29/2007	water	21.7
ISST	6/29/2007	water	20.8
ISST	7/19/2007	water	21.3
ISST	8/24/2007	water	24.1
ISST	9/22/2007	water	21.1
ISST	11/18/2007	water	21.1
ISST	12/11/2007	water	21.6
ISST	1/9/2008	water	20
ISST	2/17/2008	water	20.4
ISST	3/16/2008	water	20.4
ISST	5/15/2008	water	20.5
ISST	6/5/2008	water	21.4
ISST	7/3/2008	water	21.4
ISST	7/25/2008	water	21.2
ISST	9/6/2008	water	21.3
ISST	3/17/2009	water	20.5
ISST	4/26/2009	water	20.3
ISST	5/17/2009	water	20.5
ISST	6/17/2009	water	21.2
ISST	7/17/2009	water	20.8
ISST	8/30/2009	water	24.6
ISST	9/16/2009	water	23.3
ISST	9/27/2009	water	20.6
ISST	10/25/2009	water	22.5
ISST	11/15/2009	water	23.1
ISST	12/18/2009	water	20
ISST	1/23/2010	water	21
ISST	3/27/2010	water	19.8
ISST	4/30/2010	water	22.1
ISST	5/30/2010	Water	23.3

Appendix B4. Cont.

ISST	6/29/2010	water	20.8
ISST	7/14/2010	water	20.5
ISST	7/14/2010	water	20.3
ISST	7/14/2010	water	20.4
ISST	7/14/2010	water	20.5
ISST	7/14/2010	water	21.8
ISST	7/15/2010	water	20.2
ISST	7/15/2010	water	20.7
ISST	7/15/2010	water	20.8
ISST	7/15/2010	water	20.8
ISST	7/15/2010	water	20.2
ISST	7/15/2010	water	20.4
ISST	7/15/2010	water	20.7
ISST	7/29/2010	water	21.1
ISST	8/31/2010	water	21.9
ISST	9/26/2010	water	22
ISST	11/30/2010	water	20.6
ISST	2/27/2011	water	20.4
NBCT	7/17/2003	air	18.8
NBCT	2/7/2004	air	21.7
NBCT	6/9/2004	air	20.8
NBCT	8/23/2004	air	23.5
NBCT	10/23/2004	air	20.9
NBCT	12/28/2004	air	18.5
NBCT	9/18/2005	air	22.8
NBCT	12/3/2005	air	
NBCT	1/7/2006	air	21.8
NBCT	9/24/2006	air	22.3
NBCT	10/22/2006	air	21.8
NBCT	3/24/2007	air	20.6
NBCT	12/19/2007	air	22.5
NBCT	12/19/2007	air	22.5
NBCT	1/7/2008	air	21.6
NBCT	2/16/2008	air	21.2
NBCT	3/8/2008	air	21.5
NBCT	4/6/2008	air	21.8
NBCT	5/6/2008	air	22.4
NBCT	6/10/2008	air	22.6
NBCT	7/8/2008	air	22.9
NBCT	7/22/2008	air	22.7
NBCT	9/14/2008	air	22.9
NBCT	10/20/2008	air	22.8

Appendix B4. Cont.

NBCT	11/23/2008	air	21.8
NBCT	1/15/2009	air	20.7
NBCT	2/7/2009	air	20.9
NBCT	3/8/2009	air	21.2
NBCT	4/11/2009	air	21
NBCT	5/5/2009	air	21.3
NBCT	6/23/2009	air	22.5
NBCT	7/18/2009	air	22.4
NBCT	8/19/2009	air	22.7
NBCT	9/21/2009	air	22.5
NBCT	10/19/2009	air	22.5
NBCT	11/8/2009	air	22.2
NBCT	12/15/2009	air	21.2
NBCT	1/24/2010	air	20.3
NBCT	2/21/2010	air	20.5
NBCT	3/21/2010	air	20.1
NBCT	4/16/2010	air	20.6
NBCT	5/13/2010	air	21.3
NBCT	6/17/2010	air	22.5
NBCT	8/28/2010	air	21.9
NBCT	10/23/2010	air	22.2
NBCT	11/21/2010	air	22.1
NBCT	1/17/2011	air	20.8
NBCT	2/20/2011	air	20.9
NBCT	5/1/2011	air	21.3
NBCT	6/27/2011	air	23.2
NBCT	7/31/2011	air	22.2
NBCT	9/10/2011	air	23.3
NBCT	10/5/2011	air	22.4
NBCT	11/5/2011	air	21.7
NBCT	12/18/2011	air	21
NBCT	1/11/2012	air	21.1
NBCT	5/16/2001	water	22
NBCT	6/28/2001	water	
NBCT	7/31/2001	water	
NBCT	8/31/2001	water	23
NBCT	11/30/2001	water	22.4
NBCT	12/18/2001	water	22.1
NBCT	3/22/2002	water	21.9
NBCT	6/5/2002	water	22.8
NBCT	7/9/2002	water	
NBCT	8/30/2002	water	23.6

Appendix B4. Cont.

NBCT	10/4/2002	water	23.7
NBCT	11/8/2002	water	22.2
NBCT	2/6/2003	water	21.8
NBCT	3/4/2003	water	21
NBCT	4/1/2003	water	21.4
NBCT	5/15/2003	water	22.2
NBCT	6/19/2003	water	22.1
NBCT	7/17/2003	water	22.3
NBCT	8/14/2003	water	23
NBCT	10/16/2003	water	22.3
NBCT	12/17/2003	water	21.3
NBCT	2/7/2004	water	20.9
NBCT	4/7/2004	water	21.2
NBCT	6/9/2004	water	22
NBCT	8/23/2004	water	22.6
NBCT	10/23/2004	water	21.9
NBCT	12/28/2004	water	20.8
NBCT	2/12/2005	water	20.2
NBCT	4/2/2005	water	21.3
NBCT	5/24/2005	water	
NBCT	6/22/2005	water	22.9
NBCT	7/26/2005	water	23.5
NBCT	9/18/2005	water	24.2
NBCT	12/3/2005	water	22
NBCT	1/7/2006	water	21.6
NBCT	2/18/2006	water	20.5
NBCT	4/30/2006	water	21.8
NBCT	6/12/2006	water	22.3
NBCT	7/18/2006	water	24.1
NBCT	8/26/2006	water	23.3
NBCT	9/24/2006	water	22.2
NBCT	10/22/2006	water	22.1
NBCT	12/3/2006	water	21
NBCT	2/10/2007	water	17.1
NBCT	3/24/2007	water	21.7
NBCT	4/23/2007	water	21
NBCT	5/15/2007	water	21.5
NBCT	6/14/2007	water	22.9
NBCT	7/17/2007	water	22.7
NBCT	9/19/2007	water	24.1
NBCT	10/13/2007	water	24.1
NBCT	11/20/2007	water	23.1

Appendix B4. Cont.

NBCT	12/19/2007	water	22.2
NBCT	1/7/2008	water	21.9
NBCT	2/16/2008	water	21
NBCT	3/8/2008	water	21.7
NBCT	4/6/2008	water	22.6
NBCT	5/6/2008	water	21.7
NBCT	6/10/2008	water	23.2
NBCT	7/8/2008	water	23.8
NBCT	7/22/2008	water	27
NBCT	9/14/2008	water	23.6
NBCT	10/20/2008	water	22.8
NBCT	11/23/2008	water	22.8
NBCT	1/15/2009	water	20.2
NBCT	2/7/2009	water	21.1
NBCT	3/8/2009	water	21.5
NBCT	4/11/2009	water	22.2
NBCT	5/5/2009	water	21.9
NBCT	6/23/2009	water	23.7
NBCT	7/18/2009	water	23
NBCT	8/19/2009	water	23.1
NBCT	9/21/2009	water	22.6
NBCT	10/19/2009	water	22.6
NBCT	11/8/2009	water	22
NBCT	12/15/2009	water	21.1
NBCT	1/24/2010	water	20.9
NBCT	2/21/2010	water	21.1
NBCT	3/21/2010	water	20.3
NBCT	4/16/2010	water	20.9
NBCT	5/13/2010	water	21.6
NBCT	5/13/2010	water	23.3
NBCT	6/17/2010	water	22.3
NBCT	8/28/2010	water	23
NBCT	11/21/2010	water	22.1
NBCT	1/17/2011	water	21
NBCT	2/20/2011	water	21.1
NBCT	4/10/2011	water	21.8
NBCT	5/1/2011	water	24.1
NBCT	6/27/2011	water	22.6
NBCT	7/31/2011	water	23.8
NBCT	9/10/2011	water	22.7
NBCT	10/5/2011	water	22.4
NBCT	11/5/2011	water	21.8

References

Amundson R., Stern L., Baisden T., and Wang Y. (1998) The isotopic composition of soil and soil-respired CO_2. *Geoderma* **82**, 83-114.

Atkinson T. (1977) Diffuse flow and conduit flow in limestone terrain in the Mendip Hills, Somerset (Great Britain). *Journal of Hydrology* **35**, 93-110.

Ayliffe L., Cerling T., Robinson T., West A., Sponheimer M., Passey B., Hammer J., Roeder B., Dearing M., and Ehleringer J. (2004) Turnover of carbon isotopes in tail hair and breath CO_2 of horses fed an isotopically varied diet. *Oecologia* **139**, 11-22.

Badeck F., Tcherkez G., Nogués S., Piel C., and Ghashghaie J. (2005) Post-photosynthetic fractionation of stable carbon isotopes between plant organs – a widespread phenomenon. *Rapid Communications in Mass Spectrometry* **19**, 1381-1391.

Bai E., Boutton T., Wu X., Liu F., and Archer S. (2009) Landscape-scale vegetation dyanmics inferred from spatial patterns of soil $\delta^{13}C$ in a subtropical savanna parkland. *Journal of Geophysical Research* **114**, G01019, doi:10.1029/2008JG000839

Bai E., Boutton T., Liu F., Wu X., and Archer S. (2012) Spatial patterns of soil $\delta^{13}C$ reveal grassland-to-woodland successional processes. *Organic Geochemistry* **42**, 1512-1518.

Banner J., Guilfoyle A., James E., Stern L., and Musgrove M. (2007) Seasonal variations in modern speleothem calcite growth in central Texas, U.S.A. *Journal of Sedimentary Research* **77**, 615-622.

Bar-Matthews M., Ayalon A., Kaufman A., and Wasserburg G. (1999) The Eastern Mediterranean paleoclimate as a reflection of regional events: Soreq cave, Israel. *Earth and Planetary Science Letters* **166**, 85-95.

Bar-Matthews M., Ayalon A., Gilmour M., Matthews A., and Hawkesworth C. (2003) Sea-land oxygen isotopic relationships from planktonic foraminifera and speleothems in the Easter Mediterranean region and their implication for paleorainfall during interglacial intervals. *Geochimica et Cosmochimica Acta* **67,** 17, 3181-3199.

Baskaran M. and Krishnamurthy R. (1993) Speleothems as proxy for the carbon isotope composition of atmospheric CO_2. *Geophysical Research Letters* **20**, 24, 2905-2908.

Blyth A., Baker A., Thomas L., and van Calsteren P. (2011) A 2000-year lipid biomarker record preserved in a stalagmite from north-west Scotland. *Journal of Quaternary Science*, **26** 326-334.

Boström B., Comstedt D., and Ekblad, A. (2007) Isotope fractionation and ^{13}C enrichment in soil profiles during the decomposition of soil organic matter. *Oecologia* **153**, 89-98.

Boutton T., Archer S., Midwood A., Zitzer S., and Bol R. (1998) $\delta^{13}C$ values of soil organic carbon and their use in documenting vegetation change in a subtropical savanna ecosystem. *Geoderma* **82**, 5-41.

Bowling D., Pataki D., and Randerson, J.. (2008) Carbon isotopes in terrestrial ecosystem pools and CO_2 fluxes. *The New Phytologist* **178**, 24-40.

Breecker D., Payne A., Quade J., Banner J., Ball C., Meyer K. (submitted) The sources and sinks of CO_2 in caves under mixed woodland and grassland vegetation. *Geochimica et Cosmochimica Acta*.

Breecker D. and Sharp Z (2008) A field and laboratory method for monitoring the concentration and isotopic composition of soil CO_2. *Rapid Communications in Mass Spectrometry* **22**, 449-454.

Cerling T. (1984) The stable isotopic composition of modern soil carbonate and its relationship to climate. *Earth and Planetary Science Letters* **71**, 229-240.

Cerling T., Solomon D., Quade J., and Bowman J. (1991) On the isotopic composition of carbon in soil carbon dioxide. *Geochimica et Cosmochimica Acta* **55**, 3403-3405.

Clark J., Grimm E., Lynch J., and Mueller P. (2001) Effects of Holocene climate change on the C_4 grassland/woodland boundary in the Northern Plains, USA. *Ecology*, **82**, 620-636.

Cowan B. (2010) Temporal and spatial variability of cave-air carbon dioxide in central Texas, USA. *M.S. Thesis*, University of Texas, Austin.

Crow S., Sulzman E., Rugh W., Bowden R., and Lajtha K. (2006) Isotopic analysis of respired CO_2 during decomposition of separated soil organic matter pools. *Soil Biology and Biochemistry* **38**, 3279-3291.

Davidson R. (1995) The stable isotopic composition and measurement of carbon in soil CO_2. *Geochimica et Cosmochimica Acta* **59**, 2-6.

Davidson E. and Janssens I. (2006) Temperature sensitivity of soil carbon decomposition and feedbacks to climate change. *Nature* **440**, 165-173.

Dorale J., Gonzalez L., Reagan M., Pickett D., Murrell M., and Baker R. (1992) A high-resolution record of Holocene climate change in speleothem calcite from Cold Water Cave, Northeast Iowa. *Science* **258**, 5088, 1626-1630.

Dorale, J. (1998) Climate and vegetation history of the midcontinent from 75 to 25 ka: A speleothem record from Crevice Cave, Missouri, USA. *Science* **282**, 1871-1874.

Dorsey M. and Slagle D. (1987) Hydrologic and geologic data for the Edwards Aquifer recharge zone near Georgetown, Williamson County, Texas, 1986-87. *U.S. Geological Survey Open-File Report 87-691*.

Edwards R., Chen J., and Wasserburg G. (1986) ^{238}U-^{234}U-^{230}Th-^{232}Th systematics and the precise measurement of time over the past 500,000 years. *Earth and Planetary Science Letters*, **81** 175-192.

Ehleringer J., Cerling T., and Helliker B. (1997) C_4 photosynthesis, atmospheric CO_2, and climate. *Oecologia* **112**, 285-299.

Ehleringer J. and Monson R. (1993) Evolutionary and ecological aspects of photosynthetic pathway variation. *Annual Review of Ecology and Systematics* **24**, 411-439.

Elliot W. and Veni G. (1994) The caves and karst of Texas: A guidebook for the 1994 convention of the National Speleological Society with emphasis on the southwestern Edwards Plateau: Brackettville, Texas, June 19-24, 1994. *National Speleological Society*, Huntsville, Ala.

Fairchild I., Borsato A., Tooth A., Frisia S., Hawkesworth C., Huang Y., McDermott F., and Spiro B. (2000) Controls on trace element (Sr-Mg) compositions of carbonate cave waters: implications for speleothem climatic records. *Chemical Geology*, **166**, 255-269.

Fairchild I., Smith C., Baker A., Fuller L., Spötl C., Mattey D., McDermott F., and E.I.M.F. (2006) Modification and preservation of environmental signals in speleothems. *Earth-Science Reviews* **75**, 105-153.

Farquhar G., Ehleringer J., and Hubick K. (1989) Carbon isotope discrimination and photosynthesis. *Annual Reviews of Plant Physiology and Plant Molecular Biology* **40**, 503-537.

Feng W., Banner J., Guilfoyle A., Musgrove M., and James E. (2012) Oxygen isotopic fractionation between drip water and speleothem calcite: A 10-year monitoring study, central Texas, USA. *Chemical Geology* **304-305**, 53-67.

Feng W., Banner J., and Guilfoyle A. (in prep.) Seasonal $^{13}C/^{12}C$ variations of speleothem calcite and some associated drip water: Evidence from a 10 year monitoring study from a cave in central Texas, USA, and implications for paleoclimatic studies.

Frisia S., Fairchild I., Fohlmeister J., Miorandi R., Spötl C., Borsato A. (2011) Carbon mass-balance modelling and carbon isotope exchange processes in dynamic caves. *Geochimica et Cosmochimica Acta* **75**, 380-400.

Frumkin A., Ford D., and Schwarcz H. (2000) Paleoclimate and vegetation of the last glacial cycles in Jerusalem from a speleothem record. *Global Biogeochemical Cycles*, **14** 863-870.

Gascoyne M. (1992) Palaeoclimate determination from cave calcite deposits. *Quaternary Science Reviews* **11**, 609-632.

Genty D., Vokal B., Obelic B., and Massault M. (1998) Bomb ^{14}C time history recorded in two modern stalagmites – importance for soil organic matter dynamics and bomb ^{14}C distribution over continents. *Earth and Planetary Science Letters*, **160** 795-809.

Genty D., Blamart D., Plagnes G., Causse C., Bakalowicz M., Zouari K., Chkir N., Hellstrom J., Wainer K., and Bourge F. (2006) Timing and dynamics of the last deglaciation from European and North African $\delta^{13}C$ stalagmite profiles – comparison with Chinese and South Hemisphere stalagmites. *Quaternary Science Reviews*, **25**, 2118-2142.

Guilfoyle A. (2006) Temporal and spatial controls on cave water and speleothem calcite isotopic and elemental chemistry. *M.S. Thesis*, University of Texas, Austin.

Hanson P., Edwards N., Garten C., and Andrews J. (2000) Separating root and soil microbial contributions to soil respiration : A review of methods and observations. *Biogeochemistry* **48**, 115-146.

Hendy C. and Wilson A. (1968) Palaeoclimatic data from speleothems. *Nature* **219**, 48-51.

Hendy C. (1971) The isotopic geochemistry of speleothems – I. The calculation of the effects of different modes of formation on the isotopic composition of speleothems and their applicability as palaeoclimatic indicators. *Geochimica et Cosmochimica Acta* **35**, 801-824.

Jackson R., Moore, L., Hoffmann W., Pockman W., and Linder C. (1999) Ecosystem rooting depth determined with caves and DNA. *Proceedings of the National Academy of Sciences* **96**, 11387-11392.

James E. and Banner J. (2008) A global model for seasonal preservation bias in speleothem proxy records. *Geological Society of America Abstracts with Programs*, **40**, 6, 197.

Jessup K., Barnes P., and Boutton T. (2003) Vegetation dynamics in a Quercus-Juniperus savanna: An isotopic assessment. *Journal of Vegetation Science*, **14**, 841-852.

Kastning E. (1983) Geomorphology and hydrogeology of the Edwards Plateau karst, central Texas. *Ph.D. Dissertation*, University of Texas, Austin.

Lambert, W. and Aharon P. (2011) Controls on dissolved inorganic carbon and $\delta^{13}C$ in cave waters from DeSoto Caverns: Implications for speleothem $\delta^{13}C$ assessments. *Geochimica et Cosmochimica Acta* **75**, 753-768.

Maclay R. and Small T. (1983) Hydrostratigraphic subdivisions and fault barriers of the Edwards Aquifer, South-Central Texas, USA. *Journal of Hydrology* **61**, 127-146.

Mattey D., Fairchild I., Atkinson T., Latin J. Ainsworth M., and Durell R. (2010) Seasonal microclimate control of calcite fabrics, stable isotopes and trace elements in modern speleothem from St Michaels Cave, Gibraltar. *Geological Society, London, Special Publications* **336**, 323-344.

McDermott F. (2004) Palaeo-climate reconstruction from stable isotope variations in speleothems: A review. *Quaternary Science Reviews* **23**, 901-918.

Mickler P., Banner J., Stern L., Asmerom Y., Edwards R., and Ito E. (2004) Stable isotope variations in modern tropical speleothems: Evaluating equilibrium vs. kinetic isotope effects. *Geochimica et Cosmochimica Acta* **68**, 4381-4393.

Mickler P., Stern L., and Banner J. (2006) Large kinetic isotope effects in modern speleothems. *Geological Society of America Bulletin* **118**, 65-81.

Mook W., Bommerson J., and Staverman W. (1974) Carbon isotope fractionation between dissolved bicarbonate and gaseous carbon dioxide. *Earth and Planetary Science Letters* **22**, 169-176.

Mook W. (2000) Environmental isotopes in the hydrological cycle principles and applications, Volume I: Introduction - Theory, Methods, Review. *IHP-V Technical Documents in Hydrology*, **1** 39. UNESCO/IAEA.

Musgrove M. (2000) Temporal Links between climate and hydrology: Insights from central Texas cave deposits and groundwater. *Ph.D. Dissertation*, University of Texas, Austin.

Musgrove M., Banner J., Mack L., Combs D., James E., Cheng H., and Edwards R. (2001) Geochronology of late Pleistocene to Holocene speleothems from central Texas : Implications for regional paleoclimate. *Geological Society of America Bulletin*, **113** 1532-1543.

Overpeck J., Webb R., and Webb T. (1992) Mapping eastern North American vegetation change of the past 18 ka: No-analogs and the future. *Geology*, **20** 1071-1074.

Palmer A. (1991) Origin and morphology of limestone caves. *Geological Society Of America Bulletin,* **103**, 1, 1-21.

Polag D., Scholz D., Mühlinghaus C., Spötl C., Schröder-Ritzrau A., Segl M., and Mangini A. (2010) Stable isotope fractionation in speleothems: Laboratory experiments. *Chemical Geology* **279**, 31-39.

Richards D. and Dorale J. (2003) Uranium-series chronology and environmental applications of speleothems. *Reviews in Mineralogy and Geochemistry*, **52** 407-460.

Romanek C., Grossman E., and Moore J. (1992) Carbon isotopic fractionation in synthetic aragonite and calcite: Effects of temperature and precipitation rate. *Geochimica et Cosmochimica Acta*, **56** 419-430.

Rosholt J. and Antal P. (1962) Evaluation of the ^{231}Pa/U-^{230}Th/U method for dating Peistocene carbonate rocks. *U.S. Geological Survey Professional Paper 450*, E108-E111.

Rushdi A., Clark P., Mix A., Ersek V., Simoneit B., Cheng H., and Edwards R. (2011) Composition and sources of lipid compounds in speleothem calcite from southwestern Oregon and their paleoenvironmental implications. *Environmental Earth Sciences*, **62** 1245-1261.

Sage R. (2004) The evolution of C_4 photosynthesis. *New Phytologist*, **161** 341-370.

Sinclair D. (2011) Two mathematical models of Mg and Sr partitioning into solution during incongruent calcite dissolution: Implications for dripwater and speleothem studies *Chemical Geology* **283**, 119-133.

Sinclair D., Banner J., Taylor F., Partin J., Jenson J., Mylroie J., Goddard E., Quinn T., Jocson J., and Miklavič B. (2012) Magnesium and strontium systematics in tropical speleothems from the Western Pacific. *Chemical Geology* **294-295**, 1-17.

Small T., Hanson J., and Hauwert N. (1996) Geologic framework and hydrogeologic characteristics of the Edwards Aquifer outcrop (Barton Springs segment), northeastern Hays and southwestern Travis counties, Texas. *U.S. Geological Survey Water-Resources Investigations Report 96-4306*.

Small T. and Hanson J. (1994) Geologic framework and hydrogeologic characteristics of the Edwards Aquifer outcrop, Comal County, Texas. *U.S. Geological Survey Water-Resources Investigations 94-4117*.

Spötl C., Fairchild I., and Tooth A. (2005) Cave air control on dripwater geochemistry, Obir Caves (Austria): Implications for speleothem deposition in dynamically ventilated caves. *Geochimica et Cosmochimica Acta*, **69** 2451-2468.

Spötl C., Scholz D., and Mangini A. (2008) A terrestrial U/Th-dated stable isotope record of the Penultimate Interglacial. *Earth and Planetary Science Letters* **276**, 283-292.

Sulzman E., Brant J., Bowden R., and Lajtha K. (2005) Contribution of aboveground litter, belowground litter, and rhizosphere respiration to total soil CO_2 efflux in an old growth coniferous forest. *Biogeochemistry* **73**, 231-256.

Teeri J. and Stowe L. (1976) Climatic patterns and distribution of C_4 grasses in North America. *Oecologia* **23**, 1-12.

Thompson P. (1973) Procedures for extraction and isotopic analysis of uranium and thorium from speleothem. Technical Memorandum 73-9, Department of Geology, McMaster University, Hamilton, Ontario.

Tremaine D., Froelich P., and Wang Y. (2011) Speleothem calcite farmed *in situ*: Modern calibration of $\delta^{18}O$ and $\delta^{13}C$ paleoclimate proxies in a continuously-monitored natural cave system. *Geochimica et Cosmochimica Acta* **75**, 4929-4950.

Trumbore S. (2006) Carbon respired by terrestrial ecosystems – recent progress and challenges. *Global Change Biology* **2**, 141-153.

Veizer J., Ala D., Azmy K., Bruckschen P., Buhl D., Bruhn F., Carden G., Diener A., Ebneth S., Godderis Y., Jasper T., Korte C., Pawellek F., Podlaha O., and Strauss H. (1999) $^{87}Sr/^{86}Sr$, $\delta^{13}C$ and $\delta^{18}O$ evolution of Phanerozoic seawater. *Chemical Geology*, **161** 59-88.

Vogel J., Grootes P., and Mook W. (1970) Isotopic fractionation between gaseous and dissolved carbon dioxide. *Zeitschrift Für Physik a Hadrons and Nuclei*, **230**, 225-238.

Wang Y., Cheng H., Edwards R., An Z., Wu J., Shen C., and Dorale J. (2001) A high-resolution absolute-dated late Pleistocene Monsoon record from Hulu Cave, China. *Science* **294**, 2345-2348.

Wang Y., Cheng H., Edwards R., Kong X., Shao X., Chen S., Wu J., Jiang X., Wang X., and An Z. (2008) Millennial- and orbital-scale changes in the East Asian monsoon over the past 224,000 years. *Nature* **451**, 1090-1093.

White W. and White E. (2005) Ground water flux distribution between matrix, fractures, and conduits: constraints on modeling. *Speleogenesis and Evolution of Karst Aquifers*, **3**, 2-6.

Wingate L., Ogée J., Burlett R., Bosc A., Devaux M., Grace J., Loustau D., and Gessler A. (2010) Photosynthetic carbon isotope discrimination and its relationship to the carbon isotope signals of stem, soil and ecosystem respiration. *The New phytologist* **188**, 576-89.

Wong C., Banner J., & Musgrove M. (2011) Seasonal dripwater Mg/Ca and Sr/Ca variations driven by cave ventilation: Implications for and modeling of speleothem paleoclimate records. *Geochimica et Cosmochimica Acta* **75**, 3514-3529.

Wong C. and Banner J. (2010) Response of cave air CO_2 and drip water to brush clearing in central Texas: Implications for recharge and soil CO_2 dynamics. *Journal of Geophysical Research* **115**, G04018, doi:10.1029/2010JG001301

Zhang J., Quay P., and Wilbur D. (1995) Carbon isotope fractionation during gas-water exchange and dissolution of CO_2. *Geochimica et Cosmochimica Acta* **59**, 107-114.

Vita

Kyle William Meyer was born in Watsonville, CA in 1986, but was raised in Juneau, AK. Kyle attended the University of California, Davis where he became interested in paleoclimate studies under the supervision of Dr. Isabel Montañez. The experiences of his youth, particularly observing the retreat of the Mendenhall Glacier over a decade, only reinforced his interest in understanding and being involved with climate science. With the mentorship of Dr. Montañez, Kyle received his B.S. in Geology and enrolled at the University of Texas at Austin. With the guidance from his advisors Dr. Daniel Breecker and Dr. Jay Banner, Kyle now aims to pursue a Ph.D. with the University of Michigan, where he hopes to develop new techniques and methods in glaciochemistry and isotope geochemistry.

Permanent email: kwmeyer.mailhub@gmail.com

This thesis was typed by the author, Kyle William Meyer.